# Aggregation of Conjugated Polyelectrolytes in Dilute Solutions and Transmission Spectroscopy Based on Metal Nanoslit Arrays

by

**Palwinder Kaur**

BS (H.S.), Punjab University, India, 1999

MS (H.S.), Punjab University, India, 2001

Submitted to the Graduate Faculty of

Arts and Sciences in partial fulfillment

of the requirements for the degree of

Doctor of Philosophy

University of Pittsburgh
2007

**UNIVERSITY OF PITTSBURGH**

**FACULTY OF ARTS AND SCIENCES**

This thesis was presented

by

**Palwinder Kaur**

It was defended on

July 19th 2007

And approved by

Dr. Sunil Saxena, Asst. Professor, Department of Chemistry, University of Pittsburgh

Dr. Steve Weber, Professor, Department of Chemistry, University of Pittsburgh

Dr. Sachin Velankar, Asst. Professor, Department of Chemical Engineering, University of Pittsburgh

Dr. David Waldeck, Professor, Department of Chemistry, University of Pittsburgh
Dissertation Director

# *DEDICATION*

***This thesis is dedicated to my family for their unconditional support through all these trying years.***

# Aggregation of Conjugated Polyelectrolytes in Dilute Solutions and Transmission Spectroscopy Based on Metal Nanoslit Arrays

Palwinder Kaur, Ph.D.

University of Pittsburgh

## ABSTRACT

This thesis consists of two parts. The first part describes the work done on understanding the affect of different solution conditions and association with different macromolecules on optical properties of polyphenylethynylene (**PP1**) and polyphenylphenylene (**PP2**) based conjugated polyelectrolytes. Conjugated polymers are of great scientific interest because of their promise for applications. The photophysical studies performed on these polyelectrolytes has provided important insight in to the structural changes in different solution conditions. These studies are useful if the potential of these polyelectroytes in complex biological fluids are to be realized as biosensors since the optical properties are greatly affected by solution conditions. Second part of the thesis investigates the chemical modification of metallic nanoaperture arrays and their potential for biochemical sensing using surface plasmon resonance. Surface plasmon resonance (SPR) spectroscopy is widely used in chemical and biological sensing. The SPR technique senses the integral changes in the dielectric ambient near a metal surface that supports surface plasmon waves. There has been a growing interest in SPR sensing of biochemicals using a nanostructured metal layer because they can also operate in the transmission configuration, thereby simplifying the optical arrangement and requiring small amounts of analyte.Optical transmission through metal nano-slit arrays has been investigated. Chemical modification of these nanoslit arrays by alkanethiols has shown to red shift the main transmission peak by 11 nm. Analysis of the plasmonic fields and charge distributions shows that the strong confinement of optical fields in the narrow slit region allows sensitive transduction of surface modification into a shift of surface plasmon resonance wavelength. Further, potential of these nano-slit arrays for biosensing has been investigated. Preliminary data shows that these nano-slit arrays have the potential for biological and chemical sensing.

# TABLE OF CONTENTS

# List of Tables

# List of Figures

# List of Schemes

# Acknowledgements

I wish to acknowledge an immeasurable debt of gratitude to a few individuals for their support and encouragement during my graduate studies. I owe my most sincere gratitude to my advisor, Dr. D. H. Waldeck. No words can fully convey my respect and appreciation for him. Dave's wisdom, knowledge and commitment inspired and motivated me through out these graduate years. He was always there to help and guide me, no matter how many times in a day I bothered him. My graduate studies would not have been the same without the academic challenges that Dave provided in his research group. His carefulness and critical analysis has helped me shape up as better scientist. It was only due to his valuable guidance, cheerful enthusiasm and ever-friendly nature that I was able to complete my research work and I am forever indebted to him for this.

During this work I have collaborated with many colleagues for whom I have great regard, and I wish to extend my warmest thanks to all those who have helped me with my work. I would specially like to thank Dr. Min Liu with whom I did my first project. She was the one who taught me a lot about polymers and spectroscopy. I would like to thank Hongjun Yue and Minyang Wu with whom I worked on polymer project. Without them this project would have been incomplete. I wish to thank Laura and Jennifer who worked with me on the polymer project. I wish to thank my colleague Subhasis Chakrabarti for helping me with the TCSPC apparatus and Amit Paul for many invaluable discussions. I would also like to thank Kathy Davis for proof reading my documents many times.

I wish to extend my warmest thanks to all those who have helped me with NIRT project, specially Dr. H. K. Kim and his research group. I would also like to thank Daniel Lemont and Matt Kofke and Lei Wang for their invaluable help on NIRT project.

I also want to express my appreciation to the machine shop staff - Dennis, Jeff and Tom – who helped me from time to time and also to the electronic shop personnel Dave, Bob, Jim and Chuck who helped me with troubleshooting fluorimeter at various occasions.

I owe my loving thanks to my parents for their constant support and encouragement in all my professional endeavors. I wish to express my deepest gratitude to my husband Deepak for his unconditional love and support through out these years. Without his encouragement and understanding it would have been difficult to realize my dreams. Finally, I would like to thank my brother, Jagdeep Gill and sister Dilraj Gill for their unconditional love and support.

# CHAPTER 1 INTRODUCTION TO CONJUGATED POLYELECTROLYTE STUDIES

## 1.1 BRIEF RETROSPECTIVE

Because they exhibit high fluorescence quantum yields and tunable photophysical properties[1-8] conjugated polymers are of great scientific interest and have promise for applications, such as bio-chemical sensors,[9-17] LEDs,[18-20] lasers[21] etc. One class of conjugated polymers which is being extensively studied is polyphenylethynylene (PPE) polymers. Over the past decade a number of reports concerned with the synthesis and photophysical characterization of PPEs have been published.[22] Many research groups have studied the affects of solvent, temperature and concentration on the photophysical properties of these PPE based conjugated polymers, e.g. PPE based polymers aggregate in “bad solvent” conditions. Most recently, interest has shifted to studying conjugated polyelectrolytes[12,23-25] because of their potential as bio-chemical sensors, since they can interact electrostatically with other charged species and have extraordinarily high sensitivity to fluorescence quenchers. A number of groups have demonstrated the sensitivity of these PPE polyelectrolytes towards analytes, but the mechanism of sensing and the selectivity they display is often unclear, or inconclusive. For practical applications as biosensors it is very important to fully understand the optical properties of these polymers in different environments.

## 1.2 PHOTOPHYSICAL PROPERTIES OF CONJUGATED POLYMERS IN SOLUTIONS

### 1.2.1 PPE based conjugated polymers

Over the past decade a number of reports concerned with the synthesis and photophysical characterizations of PPEs in solution have been published.[22,26-30] Bunz et al. showed that the addition of non-solvent (methanol) to a chloroform solution of dialkyl PPEs leads to the development of a new red-shifted band in the absorption spectrum, which is similar to the absorption observed in the solid state (see Figure 1.1).[29,31] Bunz attributed these changes in the optical spectra to aggregate formation in the poor solvent, methanol, and he proposes that the interaction of the π- systems by π-stacking causes the bathochromic shift. This interpretation is corroborated by concentration studies. The optical spectra at low concentration are similar to those observed in good solvent, whereas those at higher concentration are similar to that seen in the solid state or in a poor solvent, indicating the PPEs are aggregated at higher concentration.

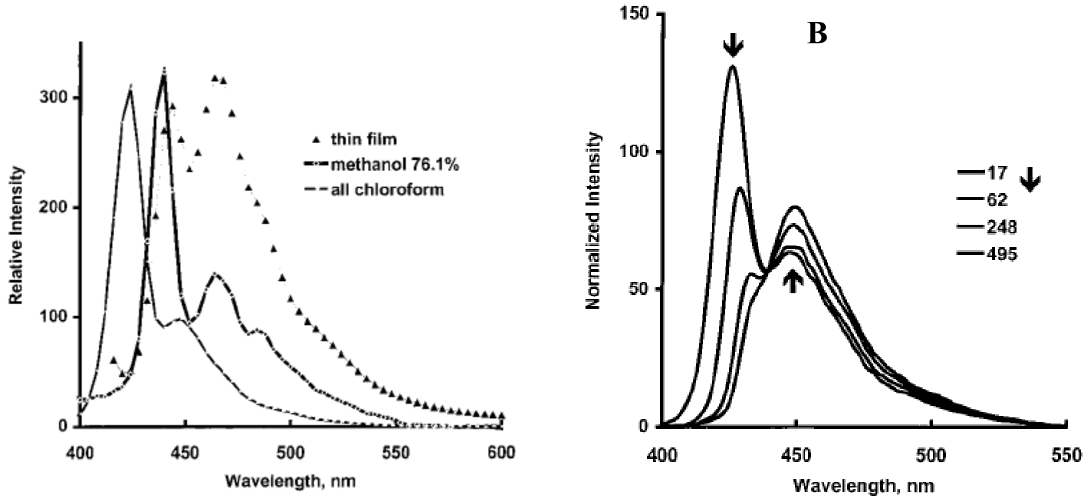

***Figure 1.1*** *Emission spectrum of dialkyl PPE based conjugated polymer as thin film and as solution in methanol/chloroform. (**B**) Emission spectrum of dialkyl PPE based conjugated polymer as function of concentration in chloroform (arrow shows increasing concentration in mg/ml). Reproduced from references 29.*

X-ray diffraction, powder diffraction and electron microscopy has been exploited to understand the structure of these polymers in solid films, and it has been shown that they can form both lamellar and interdigitated structures. X-ray diffraction studies have shown that interdigitated structures are formed by dialkoxy-PPEs in which every benzene ring carries one solubilizing group or if two solubilizing groups of substantially different length are used in an alternating fashion. Lamellar structure has been shown to be formed by simple dialkoxy PPEs. Despite these structural differences in the films, the UV-Vis and fluorescence spectra appears to be the same.

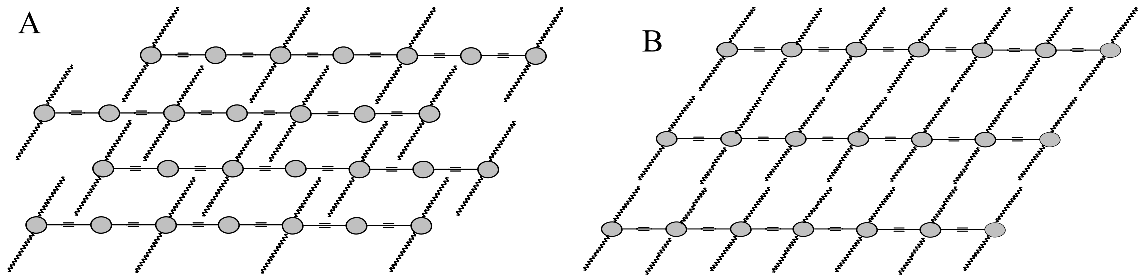

***Scheme 1.1*** *Interdigitated (A) and lamellar (B) structure of PPEs.*

Besides their solvatochromic behavior these PPE based conjugated polymers also show thermochromicity. Chu et al.[27,28,32] observed that on decreasing the temperature (25° C to – 108° C) for PPE-$OC_6H_{13}$ in good solvent (THF) the emission spectrum shifted red and the vibronic structure became more pronounced (Figure 1.2). These effects have been attributed to planarization of the chromophores and reduced molecular motion at low temperature. Interesting behavior was observed for PPE-$OC_6H_{13}$ in a mixture of good solvent and poor solvent (methanol). As PPE-$OC_6H_{13}$ in a mixture of THF and the poor solvent is cooled, the emission spectrum shifts red and a new peak starts to appear at -30° C. In addition, the absorption spectrum also develops a sharp red shifted peak. These changes are attributed to aggregation induced by planarization of the backbone facilitating π- π stacking at low temperature. These concentration and temperature changes for the spectra of PPE based conjugated polymers are consistently explained by 'planarization' and aggregation, hence π- π stacking of the backbone.

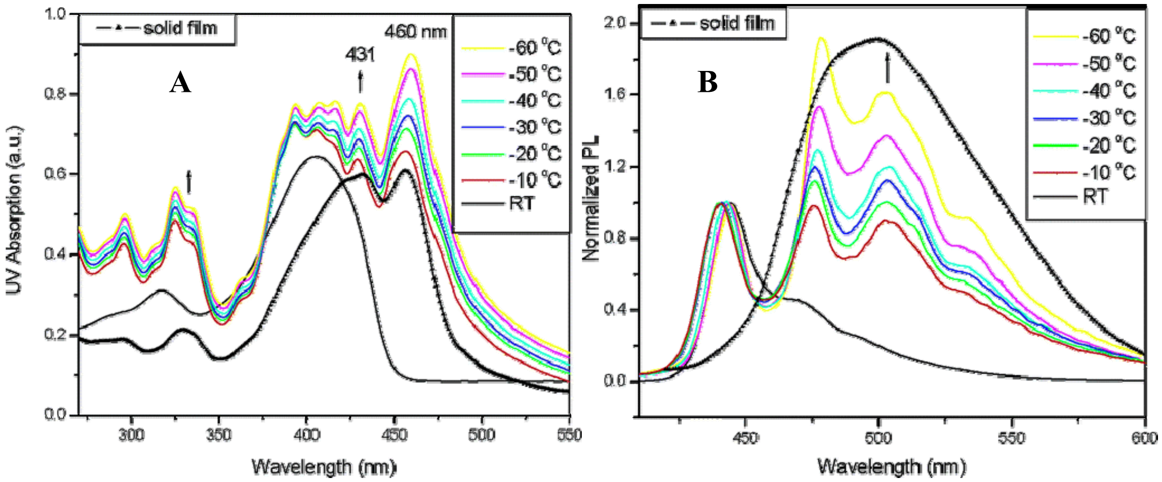

***Figure 1.2*** *Absorption* ***(A)*** *and emission spectra* ***(B)*** *of PPE polymer in a mixture solvent ($2.16 \times 10^{-5}$ M) of methanol and THF (methanol/THF = 20:1 by volume) at various temperatures. The spectrum of the film (▲) is also shown for direct comparison. Reproduced from reference 32.*

More recently, interest has shifted to PPE based conjugated polyelectrolytes.[23] These PPEs are water soluble, undergo fluorescence quenching with a series of cationic quenchers and have a potential for biological and chemical sensing. A number of research groups have studied the fluorescence quenching of these polyelectrolytes by addition of heavy metal ions,[12,24,25] surfactants[33,34] and with change in pH.[35,36]

Anionic PPEs are soluble in water but can form aggregates upon change in the environmental conditions. These aggregates are characterized by the appearance of a sharp red shifted peak in absorption and a broad red shifted emission, similar to what is observed for neutral PPE based polymers in bad solvent.[27,28] Schanze et al.[36] showed that PPE with sulfonate terminated side chains (PPE-$SO_3^-$) has its fluorescence quantum yield reduced by changing the solvent from methanol to water. The spectral changes observed were similar to that found for PPE in poor solvent, so Schanze et al. attributed them to formation of aggregates of PPE-$SO_3^-$. Figure 1.3 shows the absorption and emission spectra of PPE-$SO_3^-$ in water and methanol.

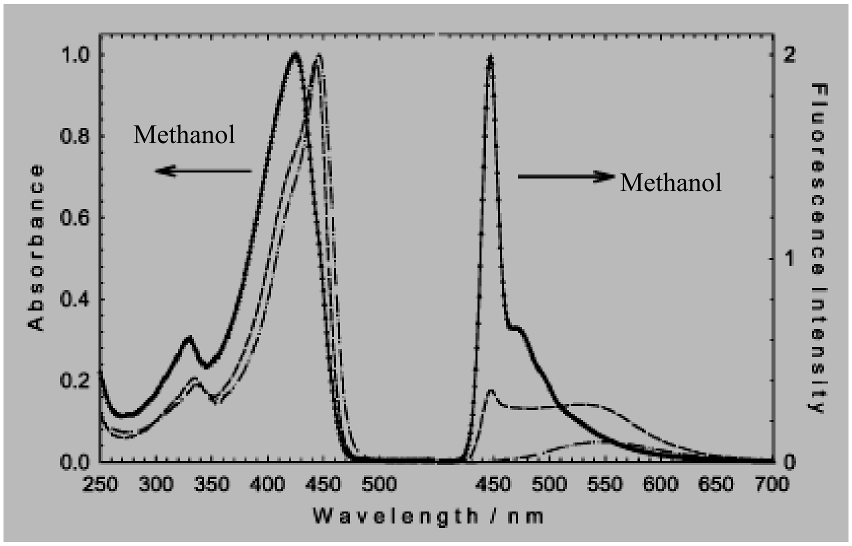

***Figure 1.3*** *Absorption (left) and fluorescence (right) spectra of PPE-$SO_3$ in MeOH (Δ), (1:1) $H_2O$/MeOH (---), and $H_2O$ (— - —). Fluorescence spectra are area normalized to reflect relative quantum yields. This figure is taken from reference 37.*

Recently Kim et al.[12,24] (Figure 1.4) studied the addition of metal ions such as $Pb^{2+}$, $Hg^{2+}$, $Ca^{2+}$, $Mg^{2+}$ etc. to solutions of PPE with carboxylate-terminated side chains (PPE-$CO_2^-$) and to a model compound. They observed that the polyelectrolyte had its fluorescence more efficiently quenched than the corresponding model compound. Further the polyelectrolyte was most sensitive to the presence of mercury ion, among all the metal cations to which it was exposed. They also showed that proper use of buffer dramatically influences the binding constants of conjugated polymers to metal ions in aqueous solution, which is important for experiments performed with conjugated polymers on biological samples. Similar quenching behavior was observed by Jiang et al.[37] for PPE-CO$_2^-$ with a lower charge density, as compared to the one used by Kim, on addition of Ca$^{2+}$ ions. It was proposed that since Ca$^{2+}$ is a closed-shell ion and cannot act as an electron or energy acceptor, the fluorescence quenching observed on addition of Ca$^{2+}$ arises from aggregation of the polymer chains. These studies showed that the optical properties of these polyelectrolytes can be modulated by addition of heavy metal ions as well as Ca$^{2+}$.

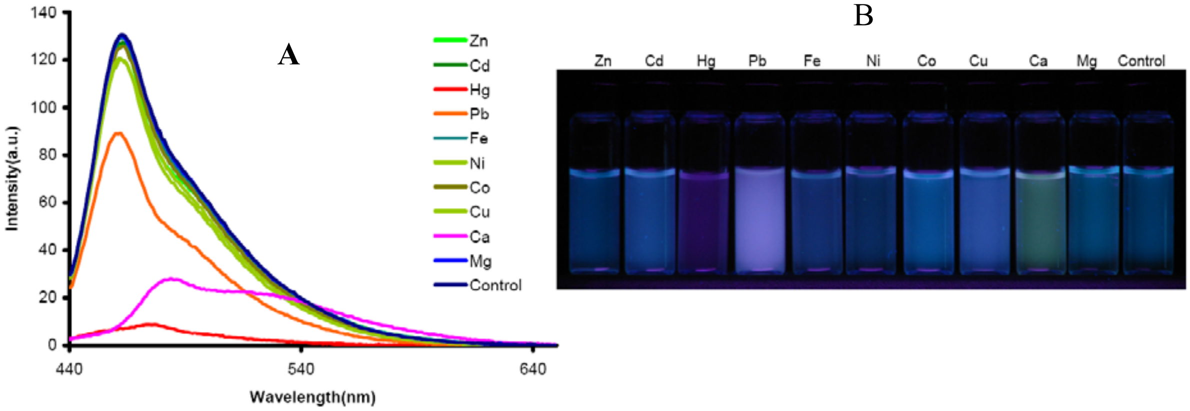

***Figure 1.4(A)*** *Emission spectra of solutions of PPE-CO$_2^-$ by addition of 20 μL of a 0.4 mM solution of metal ions. Spectra show significant red shift with Ca ions and quenching with Hg ions. (**B**) Fluorescence of PPE-CO$_2^-$ in the presence of metal ions. This figure is taken from 12.*

Besides the solvent and metal ion studies, Pinto et al.[36] reported the formation of interchain aggregates for PPE-PO$_3^-$ on decreasing the pH (Figure 1.5). It was shown that as the pH decreased the polymer strands were neutralized and aggregates were formed due to the absence of electrostatic repulsive forces between strands. These conclusions were based on the the absorption and emission spectrum. As the pH decreased from 12 to 9.5, the absorption spectra slightly shifted red and the fluorescence was quenched but the peak at 438 nm could still be observed. On further decrease in the pH a new red-shifted peak appeared in absorption spectrum and the emission became very broad and excimer like. They attributed these changes to planarization and subsequent aggregation of polymer strands on decreasing the pH from 12 to 7.5. Fan et al.[35] later explored the effect of pH and ionic strength on PPE-$N(C_2H_5)_3^+$. They showed that addition of salt in a neutral environment causes planarization of the PPE-$N(C_2H_5)_3^+$ backbone but no aggregation whereas addition of salt in an alkaline environment significantly promotes interchain aggregation and planarization of the backbone. The absorbance shifted red and no new red shifted peak was observed until pH 10. These changes were attributed to planarization of polymer strands. A red shifted peak was also observed at pH 10 in the presence of 0.1 M NaCl and at pH 14 in the absence of any salt. They hypothesized that untill pH 10, the polymer chains planarize and on further increase in the pH leads to polymer aggregation.

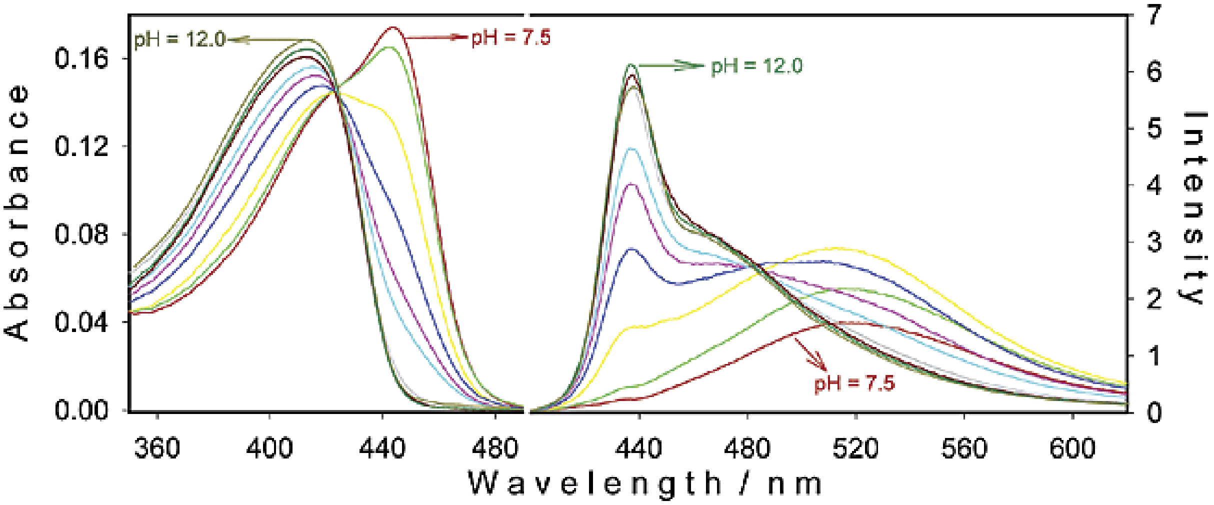

***Figure 1.5*** *Absorption spectra of PPE-$PO_3^-$ in aqueous solution as a function of pH. (right) Fluorescence spectra of PPE-$PO_3^-$ in aqueous solution as a function of pH. [PPE-$PO_3^-$] = 1 µM in phosphate buffer at 1 mM, pH range from 7.5 to 12.0 in 0.5 pH unit interval. This figure is taken from reference 36.*

These PPE based polyelectrolytes have also been shown to undergo spectral changes in surfactant solutions.[33,34] Thuneman et al[34] found that the emission spectrum shifts red from 430 nm to 515 nm on addition of surfactant to PPE-$CO_2^-$ and showed that the shifts depend on the nature of counterions in solution. These shifts have been interpreted using hard soft acid base theory (HSAB theory) because the spectra shift more to higher wavelength when the counterion becomes more polarizable. Based on their results they hypothesized that the counterions influence the effective conjugation length of the polymeric backbone; hard counterions decrease it and soft counterions increase it. Later Lavigne et al[38] investigated the dependence of the optical properties of water soluble sugar substituted PPE based polymer. They concluded that addition of surfactant essentially breaks the aggregates of the polymer but no proof of aggregation and deaggregation was provided.

All the above mentioned studies provide useful insight in to the photophysical properties of PPE based polyelectrolytes. It is clear from all these studies that fluorescence quenching in PPE based polyelectrolytes occurs upon addition of heavy metal ions, changing pH, or solvent changes. The appearance of a red shifted peak in the absorption spectrum and broad excimer like emission band is strongly suggestive of aggregate formation.The changes in the optical properties are interpreted in terms of either planarization and/or interchain aggregation. Although these studies provide useful information about the optical properties, little direct or structural data on the solution phase aggregates are given.  In addition, little effort has been made to study aggregate formation and subsequent fluorescence quenching induced by simple salts (such as NaCl, KCl etc.), which could be quite important for understanding the behavior of these materials in complex fluid environments.

### 1.2.2 PPP based conjugated polymers

Polyphenylphenylene based conjugated polymers are another class of polyelectrolytes which have gained some attention in the recent past.[39-44] These polyelectrolytes are not as extensively studied as PPE materials and have been shown to behave in an opposite manner as compared to the latter.[45] Small-angle X-ray scattering data of aqueous solutions of sulfonated poly(p-phenylene)s have shown that polymer strands aggregate in the form of cylindrical micelles, in which the phenylene backbone is oriented parallel to the long axis of the micelles.[43] Figure 1.6 shows the WAXS profile for PPP-$SO_3^-$ from a cast film with the film surface parallel to the X-ray beam. It was shown that the diameter and aggregation number of the micelles is controlled by the charge density and alkyl side chains. The hydrophobic backbones and the dodecyl chains tend to minimize the interactions with the water molecules and therefore favor micellization whereas the repulsive interaction of the charges opposes micellization. Figure 1.6c shows the proposed model of the aggregation of PPP based conjugated polymers.

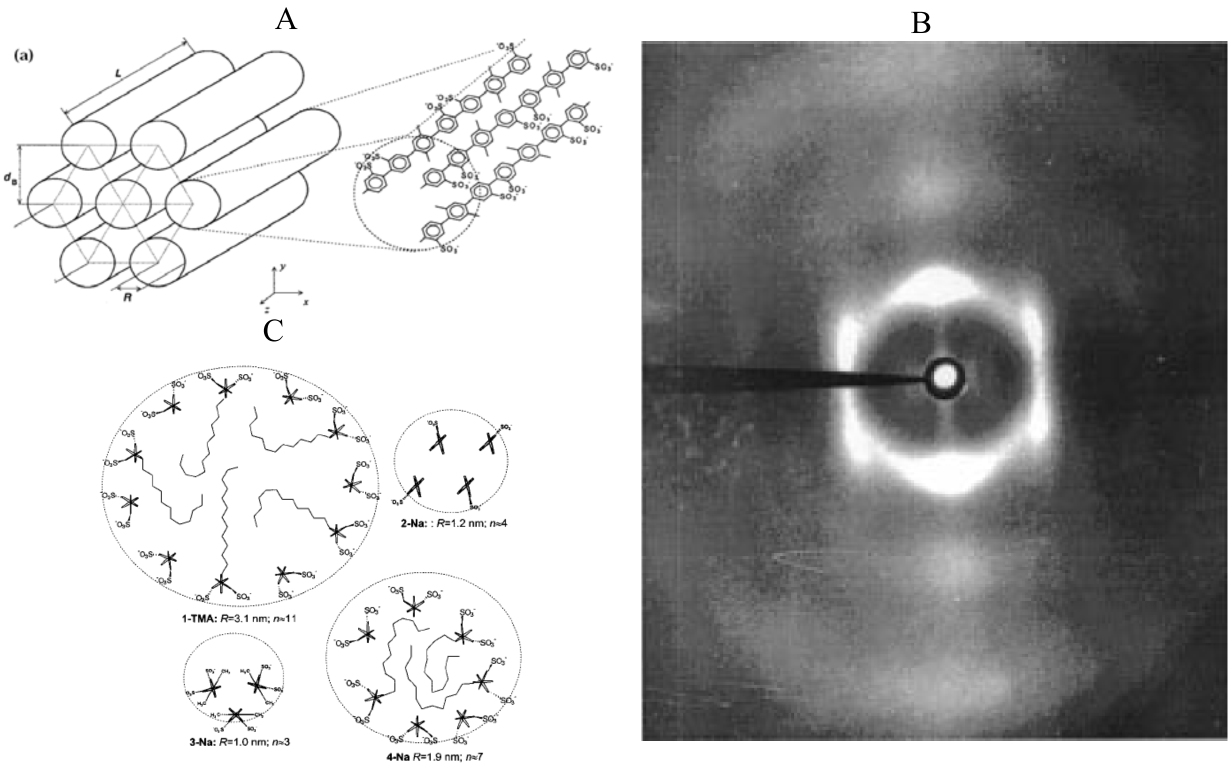

***Figure 1.6 (A)*** *Model of the hexagonal column at superstructure of a sulfonated poly(p-phenylene) forming strands of radial aggregation number arad ) 3. The Bragg spacing dB is observed as layer reflection from cast films.* ***(B)*** *WAXS profile for* ***3-Na*** *from a cast film exposed with the film surface parallel to the X-ray beam.* ***(C)*** *Proposed model of the aggregation in the form of srands. This figure is taken from reference 46.*

Later Bockstaller et al.[39] showed the hierarchical structure formation of PPP based polyeletrolytes in aqueous solution. It was proposed that single micelles exist below the concentration of 0.02 g/L. At concentrations of 0.02 g/L, the cylinders start to associate into clusters of ellipsoidal shape and above that a nematic phase appears, which transforms into hexagonal packing of cylinders above 8 g/L. The proposed structures were corroborated by small angle X-ray scattering, photon correlation spectroscopy and polarization microscopy data. Figure 1.7 shows the schematic representation of hierarchical structure formation of PPP in aqueous solution.

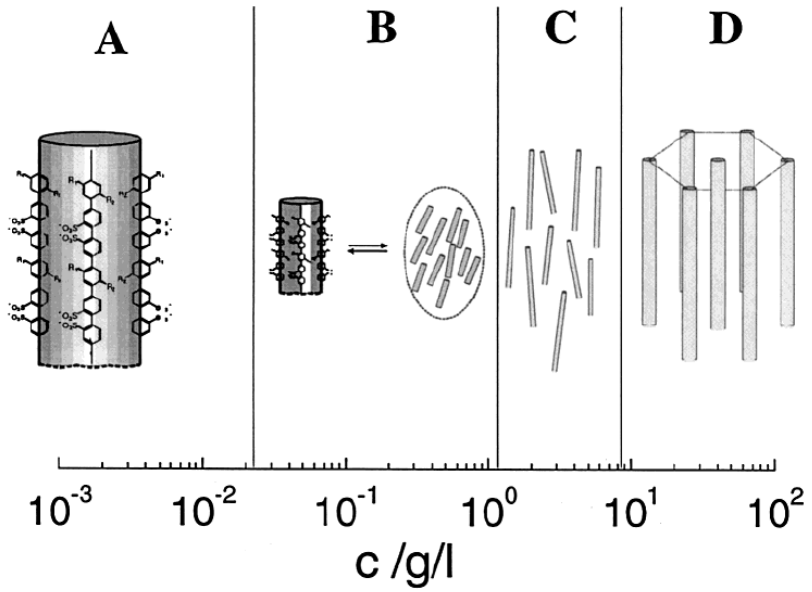

***Figure 1.7*** *Chemical structure of the polyelectrolyte and schematic representation of the hierarchical structure formed by PPP in aqueous solution as its concentration increases. PPP first forms cylindrical micelles* ***(A)*** *in which the hydrophobic side chains are oriented toward the interior. With increasing concentration, these micelles associate to form ellipsoidal clusters with internal lyotropic order* ***(B)****, a nematic phase* ***(C)****, and end up in a triangular lattice* ***(D)****.This f igure is taken from reference 40.*

Recently Valiyaveettil et al[47-50] have made an effort towards understanding the optical properties of phenylene based conjugated polymers. They investigated the affects of solvent on the optical properties of sulfonate and alkyl substituted phenylene conjugated polymers and showed that the emission intensity initially increased on addition of the non-solvent, THF to the aqueous polymer solution. On further increase in the percentage of THF beyond 65% by volume, the emission intensity decreased. They attributed this phenomenon to the formation of polymer aggregates and their subsequent precipitation from the solution. These studies were corroborated by dynamic light scattering which showed an increase in the size of the aggregates from 80-800 nm with an increase in the amount of THF in the polymer solution.  These studies provide important structural information about the aggregation of polyphenyl based conjugated systems and its dependence on solution properties. But so far no studies have been performed to see the affect of ionic strength and surfactants on these polyelectrolytes and no effort has been made to compare their optical properties to that of PPE based polyelectrolytes on addition of simple salts such as NaCl etc.

The work described in this thesis examines the photophysical properties and the biosensing abilities of polyphenylethynylene (PPE) and polyphenylphenylene (PPP) based conjugated polyelectrolytes. Chapter 2 and 3 illustrate how the photophysical properties of PPP-$SO_3^-$ (represented as **PP1**) and PPE-$SO_3^-$ (represented as **PP2**) polyelectrolytes (Scheme 1.2) are affected by changes in the solution environment such as addition of salt (NaCl), surfactant, change in temperature, concentration, etc. PPE-$SO_3^-$ aggregates in the presence of simple salts such as NaCl and this causes the fluorescence quantum yield to decrease. Although PPP-$SO_3^-$ also aggregates, its quantum yield increases in the presence of salt. Detailed analysis of the experimental data reveal that PPE based polymers form aggregates with a lower radiative rate whereas PPP-$SO_3^-$ forms aggregate structures with a higher radiative rate.

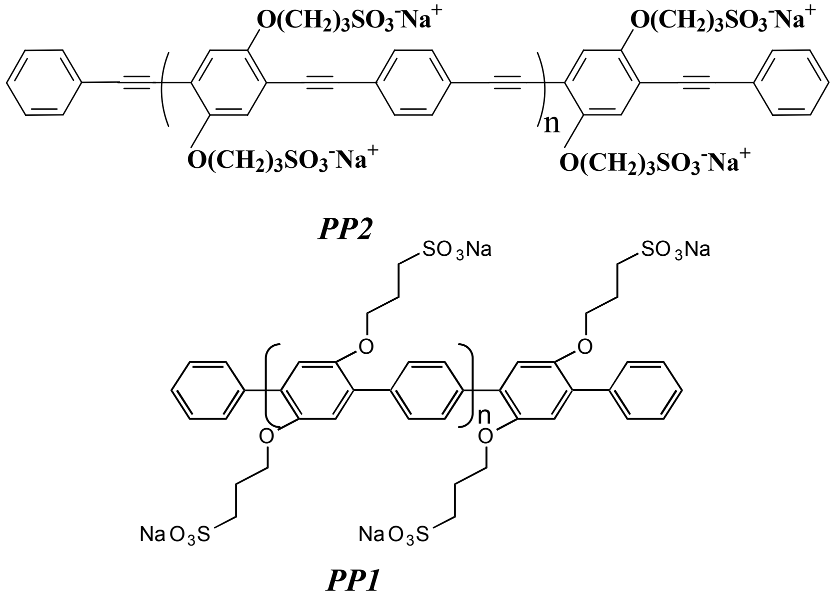

***Scheme 1.2*** *Chemical structure of* ***PP1*** *and* ***PP2****.*

## 1.3 CONJUGATED POLYMERS AS BIOSENSORS

Because of their unique combination of properties conjugated polyelectrolytes have been studied as materials with potential utility in the biosensor field[9-17]. The fluorescence intensity of these polymers can be made to respond to very minute quantities of analytes. The sensitivity of these materials arises from extremely rapid exciton diffusion along the conjugated polyelectrolyte chain to the quencher binding site, which significantly increases the effective “quenching radius” of the quencher. Excitons are created by absorption of a photon and then they migrate along the polymer backbone. Analyte binding produces a trapping site whereby the excitation is effectively deactivated, typically by electron or energy transfer. Such behavior has been referred to in the literature as the “molecular wire effect”.[16-18]

A number of conjugated polymer materials are fluorescent (PPV, PPP, polythiophenes, and others) and have been demonstrated to perform as sensing agents for chemical and biological molecules. An important development is the use of anionic functionalities on the polymer backbone to make the materials water soluble and useful for biological sensing. The fluorescence quenching for most conjugated polyelectrolytes can be described best by the Stern-Volmer equation[51]

$$\frac{F_0}{F} = 1 + K_{sv}[Q]$$

with $F_0$ being the fluorescence intensity of the conjugated polymer by itself and $F$ being the fluorescence intensity of the conjugated polymer after addition of a given concentration of quencher $[Q]$. $K_{sv}$ is the Stern-Volmer constant and can be extracted from the slope of the graph that plots $F_0/F$ versus quencher concentration.

Receptor specific interactions were first demonstrated by Chen et al.[52] Shown in figure 1.8 is the scheme for a novel, fluorescent biosensor, based on a luminescent polyelectrolyte, proposed by Chen. They demonstrated that the luminescence of MBL-PPV is readily quenched when mixed in solution with biotin-methyl-viologen, which was prepared by covalently attaching the viologen unit to biotin by a short flexible tether. They further demonstrated that the addition of avidin, which has four biotin binding sites, causes the fluorescence of the polyelectrolyte to increase. In a control experiment, they demonstrated that the addition of avidin to a solution of MEH-PPV and methyl-viologen (without biotin) does not affect the quenching of the PPV. They also showed that the fluorescence of the quenched polyelectrolyte does not increase on addition of choleratoxin protein which lacks a biotin binding site. These results demonstrate that fluorescence is reversed because of receptor specific interactions. Later Fan et al[53] demonstrated the utility of PPV based polyelectrolyte to detect the protein cytochrome c, a heme protein that acts as an electron carrier in the respiratory chain of aerobic organisms. These polyelectrolytes have also been exploited for detection of various chemical species and some explosive materials[54]. Chen et al[55,56] reported the dependence of quenching of PPV based conjugated polelectrolyte by methyl viologen on addition of surfactant. They showed that the Stern-Volmer constant decreased on addition of surfactant. They hypothesized that the surfactant changes the polymer itself, its microenvironment and its accessibility towards various reagents. Later Kim et al[12] showed the dependence of Stern-Volmer constant on the buffer used. They showed that the Stern-Volmer constant was different for different buffer solutions, emphasizing the importance of buffer choice for such studies.

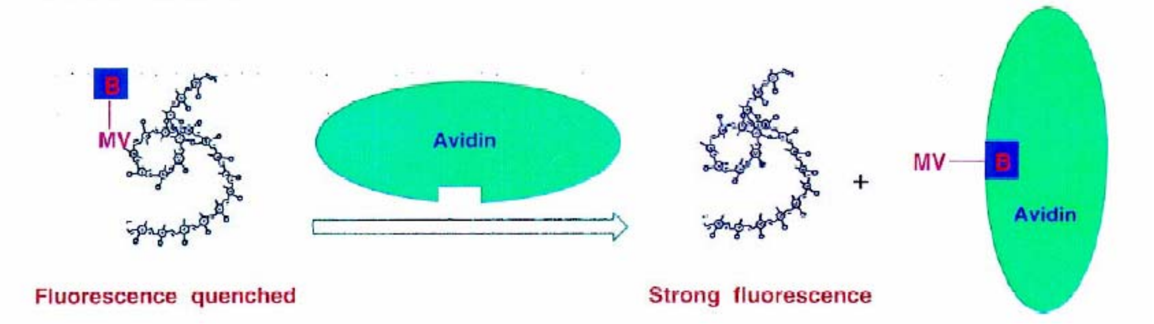

***Figure 1.8*** *Specific binding of avidin to biotin modified PPV based polyelectrolyte.This figure is taken from references 57.*

In the past few years conjugated polyelectrolytes with cationic functionalities have been exploited for DNA detection[9,13,58-60]. Gaylord et al[9] exploited the light-harvesting properties of cationic conjugated polymers to sensitize the emission of a dye on a specific peptide nucleic acid (PNA) sequence for the purpose of homogeneous,''real-time'' DNA detection(figure 1.9). In their studies they used a cationic conjugated polyelectrolyte containing iodide counter ions. A PNA probe corresponding to the CAGTCCAGTGATACG base sequence with fluorescein at the 5' end (PNA-C*) was added to the polyelectrolyte; since PNA is neutral it does not have any electrostatic interactions with the polyelectrolyte. Addition of a complementary DNA strand quenched the fluorescence of the polyelectrolyte due to the fact that there were attractive electrostatic interactions between the DNA strand and the cationic polyelectrolyte and also there was base pairing between the DNA strand and the PNA-C* probe. The base pairing between the DNA and the PNA-C* probe is believed to bring the PNA-C* probe close enough to the polyelectrolyte that energy transfer occurs from the polyelectrolyte to the fluorescein dye. They proposed that this kind of strategy could eliminate the need for multiple probes.

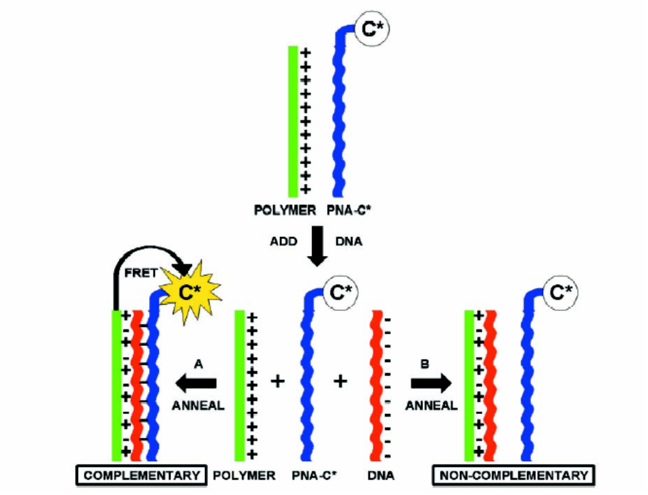

***Figure 1.9*** *Schematic representation for the use of a water-soluble CP with a specific PNA-C* optical reporter probe to detect a complementary ssDNA sequence. This figure is taken from reference 9.*

Although workers have demonstrated the use of these conjugated polyelectrolytes for specific sensing purposes, the important problem of non-specific interactions remains. Recently Kim et al.[61] investigated the non-specific interactions between conjugated polyelectrolytes and proteins. The fluorescence quenching of PPE-$CO_2^-$ polyelectrolyte was studied in the presence of different charged and uncharged proteins. Except for the negatively charged BSA protein all other proteins (charged or neutral) quenched the fluorescence of the polymer. These results showed that although these polyelectrolytes provide an attractive proposition for being used as biosensors, one has to take into account the non-specific interactions. For proteins bound in complex biological fluids this issue will be especially important because the optical and fluorescent properties of most of the conjugated polyelectrolytes are likely to be modulated by complex biological fluids, hence the practical application of conjugated polyelectrolytes to bio-sensing will be difficult to realize. Therefore it is important to understand the mechanism of quenching in these polyelectrolytes on addition of different analytes.

Chapter 4 and 5 explores the fluorescence quenching mechanism of the polymers with ‘model’ analytes. Chapter 4 explores the fluorescence quenching mechanism of the polyelectrolyte **PP1** by studying the fluorescence emission of **PP1** as a function of the analyte concentrations (figure 1.10). A comparison of the different analytes confirms that the quenching mechanism is dominated by the electrostatic binding between the macromolecular analyte and the polyelectrolyte and electron transfer or energy transfer is not necessary. Chapter 5 explores the fluorescence quenching mechanism for **PP2** in the presence of various analytes such as ferric cyt-c, PAMAM 3G, PEG, ODTMA etc. The experimental data demonstrate that the interaction of these analytes induces aggregation in **PP2.** Experiments with PAMAM-3G and DEM3.5G show that both electrostatic and hydrophobic interactions are important for inducing aggregation in **PP2**, however these interactions are not sufficient to quench the fluorescence of **PP2** as effectively as ferric cyt-c where the presence of an energy transfer center makes the fluorescence quenching very efficient.

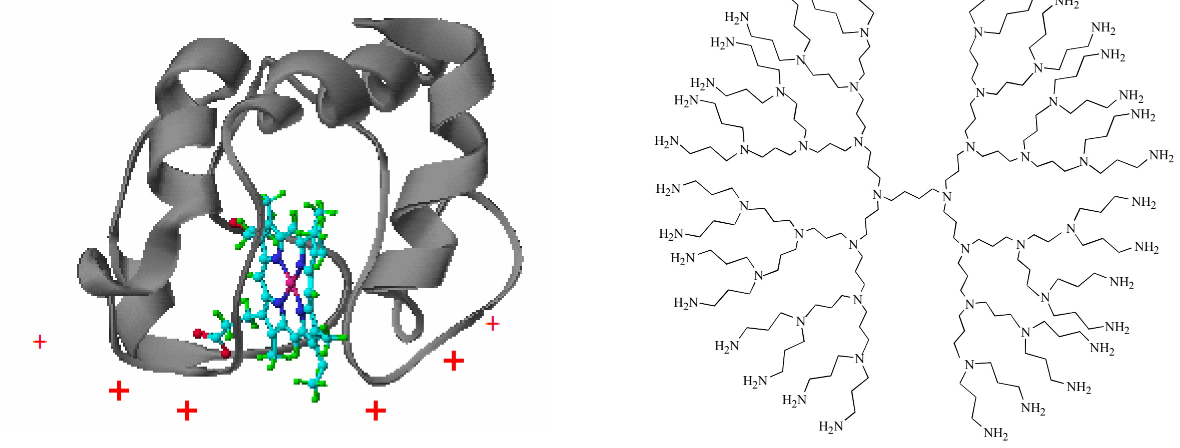

**Ferric Cyt-c**

**PAMAM 3G**

***Figure 1.10*** *Analytes used in the fluorescence quenching studies of* $\boldsymbol{PPP\text{-}SO_3^-}$**.**

Chapter 3 clearly shows the dependence of the optical properties on the ionic strength of solution as well as the concentration of **PP1**. Harrison et al[10] showed the dependence of the Stern-Volmer constant on the concentration of a cationic PPE based polymer. They showed that the Stern-Volmer constant decreased by a factor of 175 upon increasing the concentration of the polyelectrolyte from 1.0 μM to 10 μM. This large decrease in the sensitivity was ascribed to increased polymer aggregation at higher polymer concentration. Since the sensitivity is affected by the change in concentration, it might also be affected by change in the ionic strength since PPE based conjugated polyelectrolytes aggregate at higher ionic strength. Therefore it is important to find the optimum conditions where sensitivity of the polymer is highest. Chapter 5 explores the affect of changes in the solution condition on Stern-Volmer constant. The experimental data demonstrated that when **PP2** is in a relatively unaggregated form, it is more readily quenched.

## 1.4 REFERENCES

(1) Bunz, U. H. F.; Imhof, J. M.; Bly, R. K.; Bangcuyo, C. G.; Rozanski, L.; Bout, D. A. V. *Macromolecules* **2005**, *38*, 5892-5896.

(2) Jones, R. M.; Bergstedt, T. S.; McBranch, D. W.; Whitten, D. G. *J Am Chem Soc* **2001**, *123*, 6726-7.

(3) Levitsky, I. A.; Kim, J.; Swager, T. M. *J. Am. Chem. Soc* **1999**, 1466-1472.

(4) Perahia, D.; Traiphol, R.; Bunz, U. H. F.; *Macromolecules* **2001**, *34*, 151-155.

(5) Rothberg, L. J.; Yan, M.; Galvin, M. E.; Kwock, E. W.; Miller, T. M.; Papadimitrakopoulos, F. *Synthetic Metals* **1996**, *80*, 41-58.

(6) Skotheim, T. E.; Elsenbaumer, R. L.; Reyolds, J. R. *Eds. Handbook of Conducting Polymers* **1998**, *Marcel Decker: New York.*

(7) Wilson, J. N.; Bunz, U. H. F. *J. Am. Chem. Soc* **2005**, *127*, 4124-4125.

(8) Zhou, C. Z.; Liu, T.; Xu, J. M.; Chen, Z. K. *Macromolecules* **2003**, *36*, 1457-1464.

(9) Gaylord, B. S.; Heeger, A. J.; Bazan, G. C. *Proc. Nat. Acad. Sci.* **2002**, *99*, 10954-10957.

(10) Harrison, B. S.; M.B.;, R.; Reyolds, J. R.; Scahnze, K. S., , . *J.Am. Chem. Soc.* **2000**, *122*, 8561.

(11) Heeger, A. J.; Diaz-Garcia., M. A. *Curr. Opin. Solid State Mater.* **1983**, *3*, 16.

(12) Kim, I.-B.; Dunkhorst, A.; Gilbert, J.; Bunz, U. H. F. *Macromolecules* **2005**, *38*, 4560-4562.

(13) Kushon, S. A.; Ley, K. D.; Bradford, K.; Jones, R. M.; McBranch, D.; Whitten, D. *Langmuir* **2002**, *18*, 7245-7249.

(14) Liu, M.; Kaur, P.; Waldeck, D. H.; Xue, C.; Liu, H. *Langmuir* **2005**, *21*, 1687-1690.

(15) McQuade, D. T.; Hegedus, A. H.; Swagger, T. *J.Am.Chem.Soc.* **2000**, *122*, 12389.

(16) Rininsland, F.; Xia, W.; Wittenburg, S.; Shi, X.; Stankewicz, C.; Achyuthan, K.; McBranch, D.; Whitten, D. *Proc. Nat. Acad. Sci.* **2004**, *101*, 15295-15300.

(17) Schanze, K. S.; Pinto, M. R. *Proc. Nat. Aca. Sci.* **2004**, *101*, 7505-7510.

(18) Ho, P. K. H.; Kim, J. S.; Burroughes, J. H.; Becker, H. L.; Li, S. F. Y.; Brown, T. M.; Cacialli, F.; Friend, R. H. *Nature* **2000**, *404*, 481-484.

(19) Sirringhaus, H.; Tessler., N.; Friend, R. H. *Science* **1998**, *280*, 1741-1744.

(20) Zhang, C.; Broun, D.; Heeger, A. J. *J. Appl. Phys.* **1993**, *73*, 5177.

(21) Hide, F.; Diaz-Garcia, M. A.; Schwartz, B. J.; Andersson, M. R.; Pei, Q.; Heeger, A. J. *Science* **1996**, *273*, 1833-1836.

(22) Bunz, U. H. F. *Chem. Rev.* **2000**, *100*, 1605-1644.

(23) Haskins-Glusac, K.; Pinto, M. R.; Tan, C.; Schanze, K. S. *J. Am. Chem. Soc.* **2004**, *126*, 14964-14971.

(24) Kim, I.-B.; Bunz, U. H. F. *J. Am. Chem. Soc.* **2006**, *128*, 2818-2819.

(25) Kim, I.-B.; Phillips, R.; Bunz, U. H. F. *Macromolecules* **2007**, *40*, 814-817.

(26) Breitenkamp, R. B.; Tew, G. N. *Macromolecules* **2004**, *37*, 1163-1165.

(27) Chu, Q.; Pang, Y. *Macromolecules,* **2003**, *36*, 4614-4618.

(28) Chu, Q.; Pang, Y.; Ding, L.; Karasz, F. E. *Macromolecules* **2002**, *35*, 7569-7574.

(29) Halkyard, C. E.; Rampey, M. E.; Kloppenburg, L.; Studer-Martinez, S. L.; Bunz, U. H. F. *Macromolecules* **1998**, *31*, 8655-8659.

(30) Miteva, T.; Palmer, L.; Kloppenburg, L.; Neher, D.; Bunz, U., H. F. *Macromolecules* **2000**, *33*, 652-654.

(31) Fiesel, R.; Halkyard, C. E.; Rampey, M. E.; Kloppenburg, L.; Studer-Martinez, S. L.; Scherf, U.; Bunz, U. H. F. *Macromolecular Rapid Communications* **1999**, *20*, 107-111.

(32) Chu, Q.; Pang, Y. *Macromolecules* **2005**, *38*, 517-520.

(33) Thunemann, A. F. *Adv. Mater.* **1999**, *11*, 127-130.

(34) Thunemann, A. F.; Ruppelt, D. *Langmuir* **2001**, *17*, 5098-5102.

(35) Fan, Q.; Zhou, Y.; Lu, X. M.; Hou, H. M.; Huang, W. *Macromolecules,* **2005**, *38*, 2927-2936.

(36) Pinto, M.; Kristal, B. M.; Schanze, K. S. *Langmuir* **2003**, *19*, 6523-6533.

(37) Jiang, H.; Zhao, X.; Schanze, K. S. *Langmuir* **2006**, *22*, 5541-5543.

(38) Lavigne, J. J.; Broughton D. L. ; Wilson, J. N.; Erdogan, B.; Bunz, U. H. F. *Macromolecules* **2003**, *36*, 7409-7412.

(39) Bockstaller, M.; Kohler, W.; Wegenr, G.; Fytas, G. *Macromolecules* **2001**, *34*, 6353-6358.

(40) Bockstaller, M.; Kohler, W.; Wegenr, G.; Vlassopoulos, D.; Fytas, G. *Macromolecules* **2001**, *34*, 6359-6366.

(41) Futterer, T.; Hellweg, T.; Findenegg, G. H.; Frahn, J.; Schluter, A. D. *Macromolecules* **2005**, *38*, 7443-7450.

(42) Liu, T.; Rulkens, R.; Wegenr, G.; Chu, B. *Macromolecules* **1998**, *31*, 6119-6128

(43) Rulkens, R.; Wegenr, G.; Thurn-Albrecht, T. *Langmuir* **1999**, *15* 4022-4025.

(44) Vanhee, S.; Rulkens, R.; Lehmann, U.; Rosenauer, C.; Schulze, M.; Kohler, W.; Wegenr, G. *Macromolecules* **1996**, *29*, 5136--5142.

(45) *Manuscript in preparation*.

(46) Rulkens, R.; Wegner, G.; Albrecht-Thurn, T. *Langmuir* **1999**, *15*, 4022.

(47) Bhaskar, C.; Lai, Y.-H.; Valiyaveettil, S. *Macromolecules* **2001**, *34*, 6255

(48) Ravindranath, R.; Ajikumar, P. K.; Advincula, R. C.; Knoll, W.; Valiyaveettil, S. *Langmuir* **2006**, *22*, 9002

(49) Ravindranath, R.; Vijila, C.; Ajikumar, P. K.; Hussain, F. S. J.; Ng, K. L.; Wang, H.; Jin, C. S.; Knoll, W.; Valiyaveettil, S. *J. Phys. Chem. B* **2006**, *110*, 25958

(50) Vetrichelvan, M.; Hairong, L.; Ravindranath, R.; Valiyaveettil, S. *J. Poly. Sci. Part. A* **2006**, *44*, 3763.

(51) Lakowicz, J. R. *Principles of Fluorescence Spectroscopy* **1983**, Plenum Press, New York.

(52) Chen, L.; McBranch, D. W.; Wang, H.-L.; Helgeson, R.; Wudl, F.; Whitten, D. G. *Proc. Natl. Acad. Sci. U.S.A.* **1999**, *96*, 12287

(53) Fan, C. F.; Plaxco, K. W.; Heeger, A. J. *J.Am. Chem. Soc.* **2002**, *124*, 5642-5643.

(54) Haskins-Glusac, K.; Pinto, M. R.; .T.;, C.; Schanze, K. S. *J.Am.Chem.Soc.* **2004;**, *126*, 14964.

(55) Chen, L.; Xue, C.; McBranch, D. W.; Whitten, D. *J Am Chem Soc.* **2000**, *122*, 9302.

(56) Chen, L.; McBranch, D. W.; Wang, R.; Whitten, D. *Chem Phys. Lett.* **2000**, *330*, 27.

(57) Chen, L.; McBranch, D. W.; Wang, H.-L.; Helgeson, R.; Wudl, F.; Whitten, D. G. *Proc. Natl. Acad. Sci. U.S.A.* **1999**, *96*, 12287.

(58) Kushon, S.; Bradford, K.; Marin, V.; Suhrada, B.; Armitage, B. A.; McBrach, D.; Whitten, D. G. *Langmuir* **2003**, *10*.

(59) Lin, B.; Bazan, G. C. *J.Am.Chem.Soc.* **2004**, *126*, 1942.

(60) Wang, S.; Gaylord, B. S.; Bazan, G. C. *J.Am.Chem.Soc.* **2004**, *126*, 5446.

(61) Kim, I. B.; Dunkhorst, A.; Bunz, U., H. F. *Langmuir* **005**, *21*, 7985-7989.

# CHAPTER 2 SOLVATION AND AGGREGATION OF POLYPHENYLETHYNYLENE BASED ANIONIC POLYELECTROLYTES IN DILUTE SOLUTIONS

*This work has been published as Palwinder Kaur, Hongjun Yue, Mingyan Wu, Min Liu, Jennifer Treece, David H. Waldeck, Cuihua Xue, and  Haiying Liu, J. Phys. Chem. B.; (2007); ASAP.*

## 2.1 ABSTRACT

The absorption and fluorescence properties of a polyphenylethynylene based conjugated polyelectrolyte with sulfonate solubilizing groups (**PP2**) are shown to change dramatically with solution conditions because of the equilibrium between unaggregated and aggregated forms of the polymer. The fluorescence of **PP2** is strongly quenched on addition of counterions such as $Na^+$, $K^+$, $Li^+$ and $TBA^+$, an effect which arises from the creation of salt stabilized aggregates. The formation of aggregates has been further corroborated by concentration and temperature studies in water and comparisons to DMSO solvent, in which the polymer does not aggregate. In aqueous solutions, the addition of the cationic surfactant, octadecyltrimethyl ammonium, causes the polymer aggregrates to dissociate and creates polymer/surfactant aggregrates that have spectral properties like that of the unaggregated polymer.

## 2.2 INTRODUCTION

Conjugated polymers are of great interest because of their tunable photophysical properties[1-8] and their promise in application[9], such as bio-chemical sensors,[10-18] lasers[19], LEDs[20-22] etc.

One class of conjugated polymers which is being studied extensively is polyphenylethynylene (PPE) based conjugated polymers. Over the past decade a number of reports concerned with the synthesis and photophysical characterization of PPEs in solution has been published.[23-28] These polymers have shown to change their optical properties with solvent. Bunz et al[24,29] has shown that addition of non-solvent (methanol) to a chloroform solution of for dialkyl PPEs leads to the development of a new red-shifted band in the absorption spectrum which is similar to the absorption observed in the solid state. In addition, the fluorescence emission from these dialkyl PPE solutions is broad and red shifted, similar to that seen for the solid state. Bunz attributed these changes in the optical spectra to aggregate formation in the poor solvent, methanol and proposes that the interaction of the π- systems by π-stacking causes the bathochromic shift. This interpretation is corroborated by concentration studies.[29] The optical spectra at low concentration are similar to those observed in good solvent and at higher concentration; the spectra are similar to that seen in the solid state or in the poor solvent, indicating the PPEs are aggregated at higher concentration.

Besides solvatochromic behavior these PPE based conjugated polymers also show thermochromicity. Pang et al[26,27] observed that on changing the temperature (25° C to – 108° C) for PPE-$OC_6H_{13}$ in good solvent (THF) the emission spectrum shifted red and the vibronic structure became more pronounced. These effects have been attributed to planarization of chromophores and reduced molecular motion at low temperature. Interesting behavior was observed for PPE-$OC_6H_{13}$ in mixture of solvent and poor solvent (THF and methanol). As PPE-$OC_6H_{13}$ in a mixture of THF and the poor solvent is cooled, the emission spectrum shifts red and a new peak starts to appear at -30$^o$ C and the absorption spectrum also develops a sharp red shifted peak. These changes are attributed to aggregation induced by planarization of the backbone facilitating π- π stacking at low temperature. These concentration and temperature changes for the spectra of PPE based conjugated polymers are consistently explained by 'planarization' and aggregation, hence π- π stacking of the backbone.

More recently interest has shifted to PPE based conjugated polyelectrolytes.[30] These PPEs are water soluble, undergo fluorescence quenching with a series of cationic quenchers and have a potential for biological and chemical sensing.[10-18] A number of research groups have studied the fluorescence quenching of these polyelectrolytes by addition of heavy metal ions,[31-33] surfactants[34,35] and with change in pH,[36,37] however little effort has focused on aggregate formation and subsequent fluorescence quenching induced by simple salts (such as NaCl, KCl etc.). To develop these PPE based polyelectrolytes into practical sensors, it is important to understand their photophysical behavior in different environments such as ionic strength and addition of surfactant.

Anionic PPEs soluble in water but can form aggregates upon change in the environmental conditions. These aggregates are characterized by the appearance of a sharp red shifted peak in absorption and a broad red shifted emission, similar to what is observed for neutral PPE based polymers in bad solvent..[26,27]Schanze et al[38] showed that PPE with sulfonate terminated side chains (PPE-$SO_3^-$) has its fluorescence quantum yield reduced by changing the solvent from methanol to water. The spectral changes observed were similar to that found for PPE in poor solvent, so Scahnze attributed them to formation of aggregates of PPE-$SO_3^-$. Recently Bunz et al[31,32] studied the addition of metal ions such as $Pb^{2+}$, $Hg^{2+}$, $Ca^{2+}$, $Mg^{2+}$ etc. to solutions of carboxy terminated side chains on a PPE backbone (PPE-$CO_2^-$). Similar quenching behavior was observed by Schanze et al[39] for PPE-$CO_2^-$ with a lower charge density, as compared to the one used by Bunz, on addition of $Ca^{2+}$ ions. It was proposed that since $Ca^{2+}$ is a closed-shell ion and cannot act as an electron or energy acceptor, the fluorescence quenching observed on addition of $Ca^{2+}$ arises from aggregation of the polymer chains. Beside the solvent and metal ion studies, Schanze et al[37] reported the formation of interchain aggregates for PPE-$PO_3^-$ on decreasing the pH. Huang et al [36] later showed the effect of pH and ionic strength on PPE-$N(C_2H_5)_3^+$ and reported that addition of salt in an neutral environment only creates planarization of the PPE-$N(C_2H_5)_3^+$ backbone whereas addition of salt in an alkaline environment significantly promotes interchain aggregation.

These PPE based polyelectrolytes have also been shown to undergo spectral changes in surfactant solutions.[34,35,40] The emission spectrum shifts red on addition of surfactant to PPE-$CO_2^-$ and the shifts has been interpreted using hard soft acid base theory (HSAB theory) showing that spectra shift to higher wavelength when the counterion becomes more polarizable.

It is clear from all these studies that either planarization or interchain aggregation is responsible for fluorescence quenching in PPE based polyelectrolytes on addition of heavy metal ions, changing pH, or solvent changes. This work explores the fluorescence quenching behavior in simple electrolytes in order to disentangle effctes of aggregates from other effects of metal ions. And explain the effect of addition of surfactant (ODTMA) to PPE based polyelectrolyte.

This work reports the effect of addition of simple ionic salts such as NaCl, KCl, surfactants etc. on optical properties of (poly[2,5-bis(3-sulfonatopropoxy)-1,4-phenylethynylene-alt-1,4-polyphenylene ethynylene],identified as **PP2**. These studies show that the **PP2's** fluorescence is quenched on addition of ionic salts and this quenching is accompanied by the appearance of a sharp red shifted peak in the absorption spectrum due to formation of polymer aggregates. The fluorescence is enhanced on heating the polymer solution and on addition of surfactant due to breaking of **PP2** aggregates. Further to develop a fundamental understanding of the types of aggregates formed FCS studies have been done on **PP2** to get an insight in to the size of these aggregates. These studies show that the solution properties (solvent, temperature, ionic strength and surfactant) control the spectral properties of a conjugated polyelectrolyte by manipulating the equilibria between aggregated and unaggregated forms of the polymer.

## 2.3 EXPERIMENTAL

Material: Poly[2,5-bis(3-sulfonatopropoxy)-1,4-phenylethynylene-alt-1,4-polyphenylene ethynylene] (identified as **PP2**) is a polyelectrolyte with two negative charges per repeat unit and was prepared in a manner similar to that reported in the literature.[41] ODTMA (octadecyltrimethyl ammonium bromide), PEG (polyethylene glycol), TBAF (tetra butyl ammonium fluoroborate), TEAF (tetraethyl ammonium fluoroborate) and AF (ammonium fluoroborate) were bought from Sigma-Aldrich. Size exclusion chromatography[42] was used to determine the molecular weight and it was found that molecular weight of **PP2** in DMSO (a good solvent) is 38,100 Da with a polydispersity of 3.04.

The experimental polymer solutions were highly diluted; for example, the highest concentration of **PP2** was $3.9 \times 10^{-6}$ M in polymer repeat units (all concentrations reported in paper are in terms of polymer repeat unit). At these concentrations the effect of the polymer on solution properties, such as viscosity, can be neglected. For studies in electrolyte solutions, the concentration of background electrolyte was always much higher than the concentration of polyelectrolyte and the ionic strength was determined by the background electrolyte. In the current experiment, the nature of the electrolyte and the ionic strength of electrolyte were varied from $5 \times 10^{-4}$ M to 0.1 M.

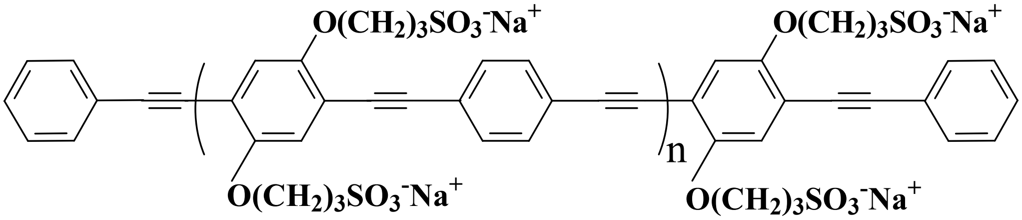

***Figure 2.1** Chemical structure of **PP2***

Steady state spectroscopy: Steady-state absorption spectra were measured on an Agilent 8453 spectrometer and the steady-state emission spectra were measured on a Spex Fluorolog 0.22 m double spectrometer.

Time dependent fluorescence spectroscopy: The time-resolved fluorescence data were collected using the time-correlated single photon counting method.[18] The instrument response function was measured using a sample of colloidal $BaSO_4$. The samples were excited at 438 nm using a diode laser (PIL043, A.L.S. GmbH) and the emission was collected at different wavelengths. The fluorescence decay curves were fit by a convolution and compare method using IBH-DAS6 analysis software. Other details of the TCSPC apparatus can be found in ref [43].

Fluorescence Correlation Spectroscopy (FCS): FCS is a non-invasive single molecule method which obtains dynamic and kinetic information by following the fluctuation trajectory of fluorescence about the equilibrium state.[44-48] FCS was performed on a home made FCS instrument based on a Zeiss IM35 inverted microscope. Details of the instrumentation will be provided elsewhere.[49] The sample was excited at 438 nm through an objective lens (Olympus UPlanfluor 40X/1.30 Oil) and the fluorescence was collected by the same lens. The concentrations of the polymer solutions were controlled to be 5.2 × $10^{-8}$ M and 2.5× $10^{-6}$ M. To avoid photobleaching and optical trapping, the laser power was kept low, 24 μW, as measured at the front of the objective lens. Each measurement lasted 2 to 5 min, during which the time trajectory of fluorescence was monitored and only those having stable fluorescence intensity were kept. The corresponding autocorrelation function G(t) was fit by equation (1)

$$G(t) = \frac{1}{\overline{N}}\left(1 + \frac{t}{\tau_D}\right)^{-1}\left(1 + \frac{\omega_{xy}^2\, t}{\omega_z^{\,2}\, \tau_D}\right)^{-1/2} \tag{2.1}$$

to extract the correlation time $\tau_D$. $\overline{N}$ is the average number of fluorescent molecules in the focal volume; $\omega_{xy}$ is the radius of the focal spot in the transverse direction, and $\omega_z$ is the Rayleigh range of the excitation beam (see reference [50] for details relating to equation 1). The correlation time $\tau_D$ is related to the translational diffusion coefficient $D$ of the fluorophore by

$$\tau_D = \frac{\omega_{xy}^2}{4D} \tag{2.2}$$

The apparatus was calibrated and tested using a 10 nM Rhodamine 6G aqueous solution, assuming the diffusion coefficient $D = 4.27\times10^{-6}$ $cm^2$ $s^{-1}$. The Stokes-Einstein approximation, equation (3) was used to extract the hydrodynamic radius $R_H$ from the measured diffusion coefficient

$$D = \frac{k_B T}{6\pi\eta R_H} \tag{2.3}$$

where $\eta$ is the shear viscosity, $T$ is the temperature and $k_B$ is Boltzmann's constant.

*Zeta Potential measurements:* The electrophoretic mobility measurements were performed at $25^0$C with an electrical field strength of 15V/cm by using a "Zeta Plus" zeta-potential analyzer from Brookhaven Instrument Co.

## 2.4 RESULTS AND DISCUSSION

### 2.4.1 Solvent and Concentration Effects

Figure 2.2 A shows the electronic absorption and the emission spectra of **PP2** in water and DMSO at $2.0\times10^{-6}$ M. In DMSO the fluorescence band is narrow, displays vibronic structure and has a small Stokes shift. These spectra are similar to that reported in the literature for neutral dialkyl and dialkoxy PPE as well as anionic PPE-$SO_3^-$ based conjugated polymers in good solvents [24,26,27,38]. This correspondence suggests that the electronic properties are governed mainly by the backbone, rather than the side chains. In contrast, the aqueous polymer solutions display a broad and red shifted emission band. This broad fluorescence band has been attributed to an excimer like state that dominates the photophysical properties of aggregated polymers and arises from $\pi$-stacking of phenylene rings.[37,38] The absorption spectrum also changed on changing the solvent. In water the absorption spectrum has a very well defined red peak at 439 nm whereas in DMSO this red shifted peak disappears and overall the spectrum shifts blue. These findings are similar to that reported by Schanze[38] and suggests that water is a poor solvent, in which the **PP2** aggregates, and DMSO is a good solvent, in which **PP2** does not aggregate.

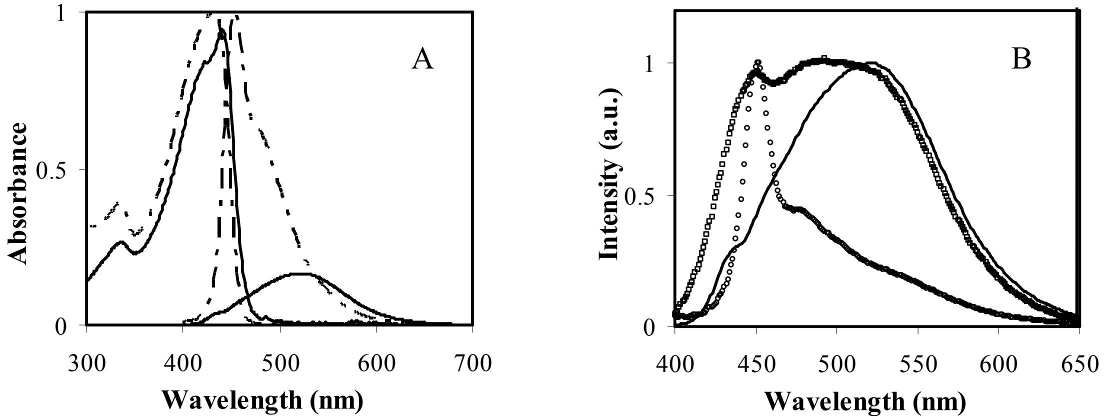

***Figure 2.2 A)*** *Normalized absorption and emission spectra for **PP2** in DMSO (— — —) and water (——) **(B)** Emission spectra for **PP2** in water at different concentrations (2.0×10-6(——), 8.8×10-8(□), 1.0×10-8 (○) M).*

The concentration dependence of **PP2** in water was studied in detail. Figure 2.2B shows the emission spectra for **PP2** at three different concentrations. The spectrum at the highest concentration (2.0x10$^{-6}$ M) is the same as that shown in panel A. As the concentration of polymer is lowered an emission band on the blue edge of the spectrum 'grows in'. At the lowest concentration (8.8x10$^{-8}$ M) the emission spectrum resembles that obtained for **PP2** in DMSO, indicating that the polymer is unaggregated at these low concentrations.[24] At intermediate concentration (1.1x10$^{-8}$ M) the spectrum displays features of both aggregated and unaggregated forms of polymer.

Figure 2.3 shows the emission and absorption spectra of **PP2** as the temperature is varied. Heating of the aqueous **PP2** solutions to 90° C causes the band on the red edge of the absorption spectrum to disappear; the spectrum becomes more like that observed for **PP2** in DMSO. In addition, the fluorescence spectra show that a band on the blue edge of the emission 'grows in' with increasing temperature. Although a significant amount of the broad red-shifted emission remains, the band on the blue edge is similar to that observed for **PP2** in DMSO. Upon cooling the **PP2** solution to room temperature (45 minutes cooling time) the emission maxima do not shift, however the amplitude of the broad band emission increases slightly in amplitude. After nine hours at room temperature, the absorption spectrum shows a red shifted shoulder and the amplitude of the broad red shifted band increases. These studies indicate that **PP2** aggregates are dissociated upon heating but that the reaggregation at room temperature occurs slowly.

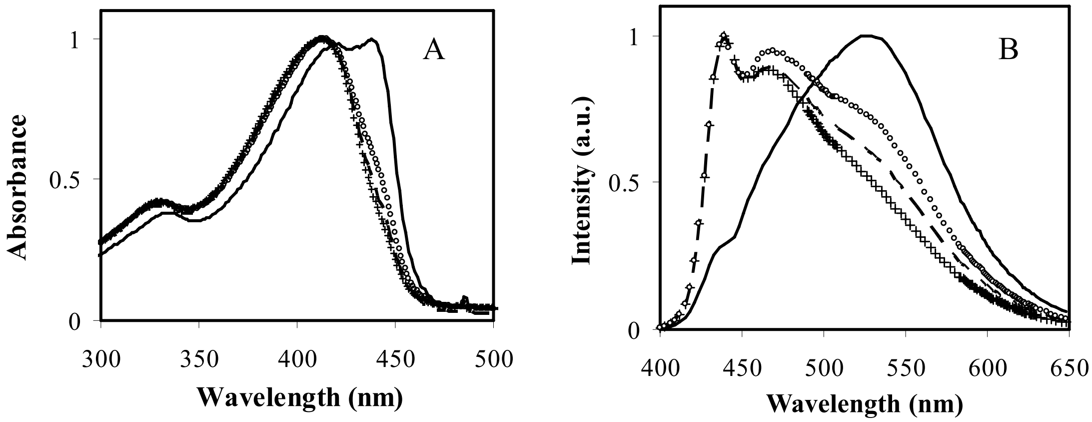

***Figure 2.3 A)*** *Absorption spectra of* ***PP2*** *(2.0×10$^{-6}$ M) in water at room temperature (—), 90°C (++), Cooled to room temperature from 90°C (— —) and 9 hrs later (○).****3B)****Emission spectra of* ***PP2*** *in water at room temperature (—), 90°C (++), Cooled to room temperature from 90°C (— — ) and 9 hrs later (○).*

Lifetime data for **PP2** was collected in water and DMSO at 2.0x10$^{-6}$ M. As in previous studies[38] the fluorescence decay profile of **PP2** in DMSO was wavelength independent and nearly exponential. The major lifetime component in a biexponential fit to the data was 535 ps and the fluorescence decay has a correlation time, $<\tau_F>$[38], of 327 ps. This nonexponentiality contrasts with earlier reports of Schanze that the emission is exponential, however it does not display a wavelength dependence and may result from polydispersity in the polymer sample. In water the fluorescence decay profile must be fit by a sum of three or more exponentials and it displays a strong wavelength dependence; $<\tau_F>$ ranges from 878 ps to 2.4 ns as the emission wavelength changes from 480 nm to 600 nm. Although both solvents display some inhomogeneity in the fluorescence decay law, the inhomogeneity in aqueous solutions appears to be more pronounced. The wavelength dependence of the fluorescence decay law in water is consistent with the presence of both aggregated and unaggregated forms that possess different emissive states.[37,38]

*FCS Studies:* FCS studies demonstrate the aggregation of **PP2** in water. Figure 2.4 shows the measured autocorrelation functions for **PP2** at two concentrations ($5.2 \times 10^{-8}$ M to $2.5\times 10^{-6}$ M) and fits of the data by equation (1). The decrease in amplitude of the autocorrelation function for the higher concentration data arises because more fluorophores appear in the excitation volume, see equation (1). The correlation time $\tau_D$ for the autocorrelation function increases by approximately 400-fold with the concentration increase. At low concentration $\tau_D$=563 μs, D=$5.9\text{x}10^{-7}\text{cm}^2/\text{s}$ and using a spherical model one gets a hydrodynamic radius of $R_H$ = 4.2 nm (using equation 1 with $\eta$= 0.89 cP and $\omega_{xy}$= 0.39 μm). If one uses a rigid rod model instead of spherical model, the hydrodynamic radius of **PP2** at low concentration is 26.2 nm.(Please see supplemental information for details of model). At high concentration a much larger hydrodynamic radius, $R_H$=1.5 μm, was obtained. Corresponding FCS studies were performed on **PP2** in DMSO at low ($\sim 10^{-9}$ M) and high ($\sim 10^{-7}$ M) concentration, and the hydrodynamic radius (5.1 nm) does not change with concentration. To conclude, no aggregation takes place in DMSO even at higher concentration, whereas aggregation occurs in water at higher concentration.

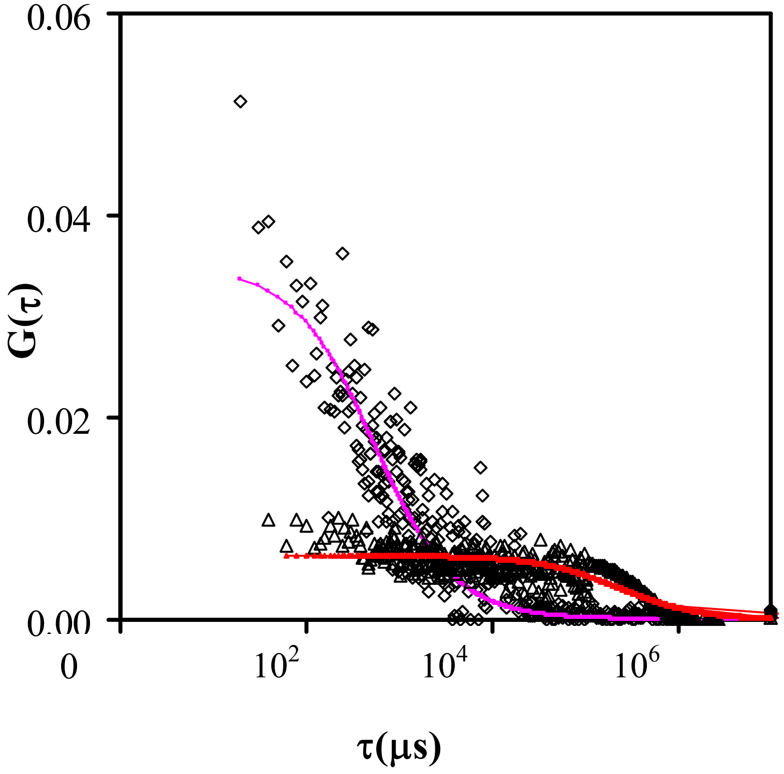

***Figure 2.4*** *Autocorrelation function for* ***PP2*** *in water at lower, $5.2\times10^{-8}$ M (◊) and higher, $2.5\times10^{-6}$ M(Δ).*

The much larger hydrodynamic radius for the polymer at high concentration is consistent with aggregates of the polymer. Using a spherical model and the hydrodynamic radius as a measure of the aggregate size, then a comparison to the 4.2 nm radius of a single monomer chain suggests that about $5\text{x}10^7$ polymer molecules constitute the aggregate. Calculations using the rigid rod model gives a number of about $6\text{x}10^5$. These data indicate the existence of unimolecular species at lower concentration and aggregates at higher concentration. To have a better understanding of how many molecules are in an aggregate, a better model to connect the diffusion coefficient and the particle size may be required.

The hydrodynamic radius $R_H$ of 4.2 nm is consistent with single polymer chains at low concentration. Using a molecular weight of 38100 g/mole, the contour length of the polymer is calculated to be 92 nm. Comparing this value to a Kuhn length of 30 nm, which is typical of polyphenylethynylene,[51] implies that a Gaussian chain model is not appropriate. Instead, we use the Kratky-Porod wormlike chain model,[51] and calculate a radius of gyration $R_G$ for **PP2** of 11.6 nm. Comparing this to our measured $R_H$ gives $R_G/R_H$ is 2.8. Studies for polymers with similar backbone have yielded a ratio of 2.[51]

These results demonstrate that **PP2** aggregates at higher concentration ($2.0 \times 10^{-6}$ M polymer repeat unit) in water, but appear to exist as single strands at lower concentrations in water. The aggregation of the polymer, as demonstrated by the FCS studies, correlates with the changes observed in the absorption and emission spectra of the aqueous polymer solutions. The 'aggregates' fluorescence spectra are broad and red shifted (see Figures 2.2) and the 'aggregates' spectrum is inhomogeneous, as revealed by the wavelength dependence of the fluorescence decay law. The 'aggregates' absorption spectra display a band on the red edge, which disappears under conditions of isolated polymer strands in solution. The temperature studies reveal that the aggregation is reversible, but with a very slow time constant.

### 2.4.2 Effect of Electrolyte on Aggregation

When **PP2** was dissolved in DMSO, the addition of inorganic salts ($LiNO_3$ and $NaClO_4$ were used) did not induce any significant changes in the absorption or fluorescence spectra and did not cause any fluorescence quenching, ranging from an ionic strength of 1mM to 100mM. In contrast, electrolyte had a profound effect on the spectral properties in aqueous solutions.

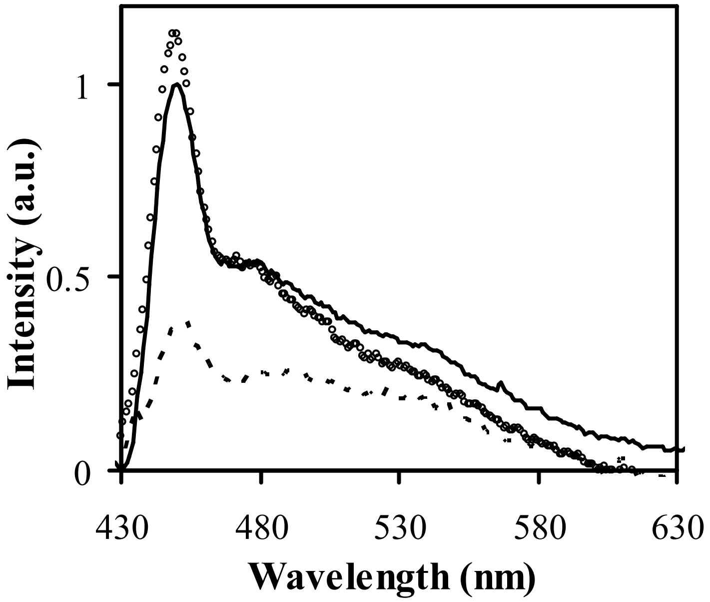

***Figure 2.5** Steady state fluorescence of **PP2** (5.2×10$^{-8}$ M) in water (——), with 50µM NaCl (○) and 100mM NaCl (----).Relative intensities are meaningful.*

Low concentration regime: Figure 2.5 shows the steady-state fluorescence spectrum for aqueous solutions of **PP2** (5.2x10$^{-8}$ M) at different NaCl concentrations. The addition of 50µM NaCl does not change the shape of the steady state emission spectrum; only 7% of the fluorescence was quenched. Similarly, using a spherical model, FCS studies give a hydrodynamic radius of $R_H$= 3.8 nm in a 50 µM NaCl solution, which is similar to the $R_H$= 4.2 nm in water at low concentration. In the 100mM NaCl solutions, the steady state fluorescence of **PP2** was quenched by 50% and the relative importance of the broad red shifted emission increased with respect to the sharp band at 451 nm. In addition, the FCS data for the 100mM NaCl solution showed a five fold increase in the hydrodynamic radius, indicating that aggregates of **PP2** form at higher NaCl concentration. Hence, the broad red-shifted emission correlates with increased aggregation, which is induced by the electrolyte. These observations imply that the **PP2** is not shielded effectively at low salt concentration and exists in a mostly unaggregated state, whereas the addition of excess salt better shields the charge on the **PP2** chains, reducing the interchain repulsion and increasing the aggregation.

FCS studies were also performed for **PP2** in DMSO with and without $NaNO_3$. The hydrodynamic radius remained the same for **PP2** in the presence and absence of $NaNO_3$ indicating no significant formation of aggregates upon addition of salt.

*High Concentration regime:* Although **PP2** is already aggregated in aqueous solutions with **PP2** concentrations of $2.0 \times 10^{-6}$ M, addition of electrolyte affects the spectral characteristics.

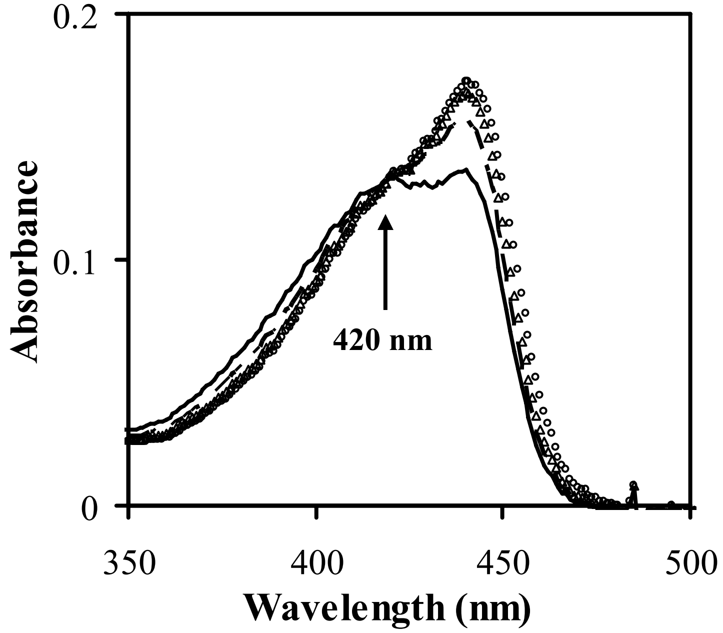

***Figure 2.6*** *Absorption spectra of* ***PP2*** *($2.0 \times 10^{-6}$ M) in water for NaCl solutions of different ionic strength; 0 mM(—), 2.5 mM(– –), 5 mM(Δ), 20 mM (○). The arrow indicates the isosbestic point.*

Figure 2.6 shows the absorption spectra of **PP2** in NaCl solutions for ionic strengths ranging from 0 mM to 20 mM. The absorption spectrum of **PP2** in water has absorption peaks at $\lambda_{max}$ at 439 nm and 421 nm. Upon increasing the ionic strength the red shifted peak grows in intensity and its position shifts by 2-3 nm on further addition of salt. An isosbestic point occurs near 420 nm, as if two distinct chromophoric states of the polymer (unaggregated and aggregated) are present.

By assuming a two species equilibrium reaction (**PP2**+$M^+ \leftrightarrow$ **PP2:**M), the absorption spectra were fit to obtain a stability constant, K. An example of the fitting results for **PP2** in NaCl solutions is in the supplemental information. Table 2.1 presents the stability constant K and gives the absorption peaks of the two 'species' for different electrolyte solutions. In this analysis, the percentage of the 'bluer aggregate species' decreased to 24% in 3 mM NaCl solution. These observations indicate the presence of different aggregates in the absence and presence of salt. We hypothesize that when salt is added, "self associated" aggregates of **PP2** are formed which presumably have ions incorporated in them. The formation of these aggregates is corroborated by FCS studies (a larger average size with salt) and also reflected by the growth of the red shifted peak in absorption spectrum

**Table 2.1 Spectral characteristics and model parameters for a two species model of PP2 in electrolyte solutions.**

| Salt | Isosbestic point(nm) | **PP2·M$^+$** $\lambda_{max}$ (nm) | Stability Constant (ln K) | Percentage of unaggregated **PP2** in 3 mM salt solution |
|---|---|---|---|---|
| LiCl | 419 | 445 | 3.30 | 32 |
| NaCl | 420 | 445 | 3.22 | 24 |
| KCl | 425 | 447 | 3.23 | 26 |
| AF | 421 | 444 | 3.64 | 16 |
| TEAF | 422 | 444 | 3.77 | 12 |
| TBAF | 425 | 454 | 3.58 | 18 |

The emission spectrum also changes with the addition of salt (figure 2.7A). Without NaCl added to the solution, **PP2** has a broad emission with a maximum at 525 nm and a shoulder near 435 nm. The shoulder at 435 nm disappears completely upon the addition of NaCl to the solution. Figure 2.7B shows how the relative fluorescence quantum yield of the **PP2** emission changes with increasing ionic strength, for three excitation wavelengths: 380 nm, 419 nm and 439 nm. The data show that the fluorescence intensity ratio of **PP2** in NaCl solution to that in water increases until 2.0 mM of NaCl (see the insert in 2.7B). The fluorescence decreases by almost 80% on further increase of ionic strength to 50 mM and becomes almost constant at an ionic strength >50mM. No difference in the fluorescence quenching efficiency was observed for different excitation wavelengths.

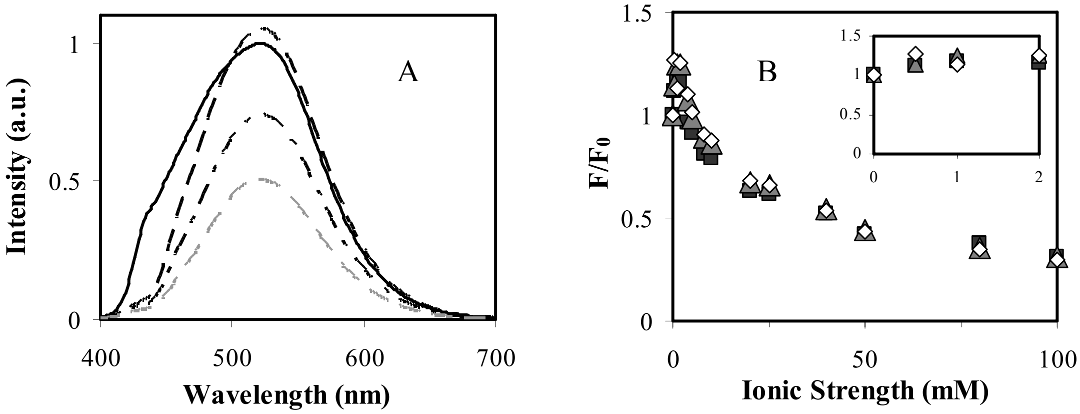

***Figure 2.7A** Fluorescence spectra of **PP2** ($2.0\times10^{-6}$ M) in water for NaCl solutions of different ionic strength; 0 mM(—), 2.5 mM(– –), 5 mM(— - —), 20 mM (— —) 7**B)** Fluorescence intensity ratio of **PP2** in ionic NaCl solution (F) to that in water ($F_0$) versus the ionic strength at three different excitations,380 nm(■), 419 nm(▲) and 439 nm(◊).*

The spectral and photophysical properties in other 1:1 small electrolytes were nearly identical to the behavior observed in NaCl solutions. For the inorganic cations, the isosbestic points and the red peak's spectral shift correlate with the radius of the cation [Li$^+$ (0.59 Å), Na$^+$ (1.02 Å) to K$^+$ (1.33 Å)]. The degree of fluorescence quenching changed somewhat with the nature of the electrolyte, however. The fluorescence quenching in NaCl and KCl solutions were very similar; the LiCl solutions had a slightly lower quenching. The fluorescence quenching in the organic salts TBAF, TEAF and AF was weaker than that observed for the inorganic cations. These data are provided in the supplemental information.

*Other observations*: In contrast to the significant effect of temperature on the polymer aggregation in water, temperature had little effect for **PP2** with NaCl in water. An aqueous solution of **PP2** with 20mM NaCl was heated to $90^0$ C. Although the fluoresence intensity increased by 10%, the absorption and emission spectra of **PP2** before and after heating were the same. This behavior contrasts sharply with that seen for **PP2** in deionized water. This observation suggests that the aggregates in the salt solution are more tightly bound; i.e. do not dissociate as readily upon heating as they do in water.

From these ionic strength studies, we infer that addition of counter ions shields the charge on the **PP2** backbone, reduces the interchain repulsions, and promotes the formation of tighter aggregates.

### 2.4.3 Effect of surfactant on Aggregation

*Low Concentration:* The emission and absorption spectrum of **PP2** in the low concentration regime ($1.1\text{x}10^{-8}$ M) was measured before and after addition of the cationic surfactant, ODTMA. Figure 8 shows the fluorescence spectrum for $1.1\text{x}10^{-8}$ M **PP2** in water and with 50 μM ODTMA; it does not change. In contrast, FCS experiments give a correlation time which is approximately three times larger for **PP2** in the ODTMA solution than for **PP2** in water. This correlation time gives a diffusion coefficient of $D=2.1 \times 10^{-7}$ $cm^2/s$ and a hydrodynamic radius of $R_H$= 11.7 nm using a spherical model (see equation 1). This significant change of hydrodynamic size, caused by ODTMA indicates complexation between the **PP2**, a polyanion, and the ODTMA, a cationic surfactant, to form heteroaggregates (**PP2:** ODTMA).

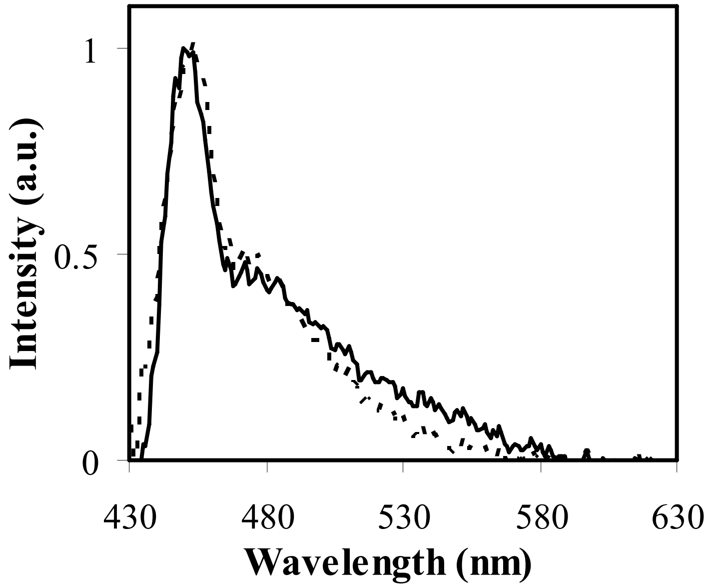

***Figure 2.8*** *Emission spectrum of* ***PP2*** *(*1.1x10$^{-8}$ M) *in water without (—) and with 50μM ODTMA (---)*

The association of ionic surfactants with polyelectrolytes has been reported previously for PPV and PPE. [34,35,53] These heteroaggregates of **PP2** and ODTMA are different from the homoaggregates (**PP2:PP2**) formed in water at high concentration and the aggregates formed on addition of electrolyte, which were discussed earlier. Presumably, they consist of individual **PP2** molecules associated with a number of different surfactant molecules. The hydrodynamic radius, using a spherical model, of 11.7 nm indicates a volume that is 20-25 times larger than that of a **PP2** molecule and suggests that about 165 ODTMA molecules are bound to the polymer. If all the charged groups on **PPE** are coordinated by ODTMA then for n=73, determined from average molecular weight, each **PPE** molecule should have 146 ODTMA molecules attached to it. Hence, the agreement is good.

*High Concentration:* Figure 2.9A shows the absorption spectrum for 2.0x10$^{-6}$ M (concentration in polymer repeat unit) **PP2** solutions of ODTMA. As the concentration of

ODTMA increases, the peak absorption at 439 nm, which is associated with the **PP2** aggregates, decreases in intensity until it disappears. In addition, the spectrum shifts blue by about 26 nm; the color of the **PP2** solution changs from yellow to light yellow. The blue shift is attributed to the decrease in conjugation because of breaking of the aggregates. In aggregates many polymers chains are stacked on each other increasing the effective conjugation length and hence red shift in absorption spectrum. No isosbestic point is observed on addition of ODTMA.

Figure 2.9B shows the dependence of the fluorescence spectrum on the ODTMA concentration. As the ODTMA concentration increases, a sharp peak at 451 nm grows in, similar to that observed at low concentrations and in DMSO. The intensity ratio of the shoulder and the sharp peak remain constant for ODTMA >0.01mM. This behavior should be contrasted with that obtained at low concentration. At low concentration, **PP2** is already unaggregated and addition of surfactant does not change the steady state spectrum. At higher concentration the **PP2** is homoaggregated and the addition of surfactant seems to dissociate these homoaggregates (**PP2:PP2**) and form heteroaggregates (**PP2**: ODTMA).

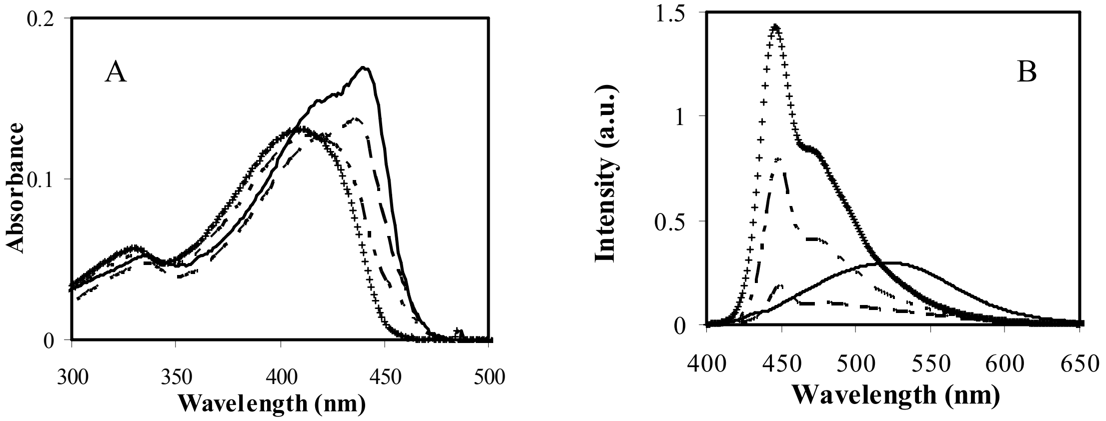

***Figure 2.9A)*** *Absorption spectrum of* ***PP2****(2.0×10$^{-6}$ M) in water at different ionic strength solutions of ODTMA; 0 mM(——), 0.005mM (— —),0.025 mM(— - - —) and 0.05 mM(+)* ***9B)*** *Emission spectrum of* ***PP2****(2.0×10$^{-6}$ M) in water at different ionic strength solutions of ODTMA. 0 mM(——), 0.005mM (— —),0.025 mM(— - - —) and 0.05 mM(+)*

The dissociation of the homoaggregates is further corroborated by lifetime measurements. The fluorescence lifetime,$<\tau_F>$, changes from 878 ps in water to 183 ps in the presence of 0.05mM ODTMA. In addition to the decrease in the $<\tau_F>$, the quantum yield in the presence of 0.05 mM ODTMA solution increases by three times over that in water. The decrease in $<\tau_F>$ and corresponding increase in quantum yield demonstrates that addition of ODTMA to **PP2** changes the nature of the emitting state to one with a higher radiative rate. The radiative rates for **PP2** with 0.05mM ODTMA were approximately 12 times higher than that found in water.

The formation of complexes between ODTMA and **PP2** (2.0x10$^{-6}$ M) was further investigated by measuring the zeta potential of **PP2** as a function of ODTMA concentration. Figure 2.10 shows how the zeta potential varies with the addition of surfactant. On addition of surfactant the zeta potential increases and becomes more and more positive as the concentration of surfactant is increased. The binding between **PP2** and ODTMA molecules causes charge neutralization, and a zeta potential of zero occurs when the **PP2** molecules are neutralized by

ODTMA molecules. At zero, the solution has 182 ODTMA molecules for each **PP2** molecule, which is in good agreement with 166 obtained from the FCS measurements at low concentration of **PP2**. At higher concentration of ODTMA the change in the sign of the zeta potential implies that excess surfactant molecules bind on a **PP2:**surfactant complex.[54]

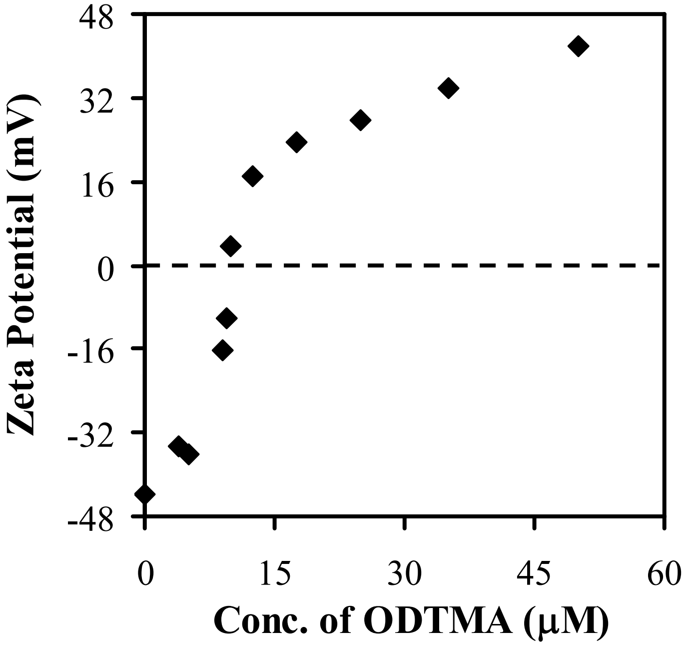

***Figure 2.10*** *Zeta potential vs concentration of ODTMA for **PP2** in water.*

These studies support the argument that the ODTMA forms heteroaggregates with **PP2** and dissociates the homoaggregates (**PP2:PP2**). Scheme 2.1 illustrates the type of aggregates formed on addition of ODTMA. In water **PP2** is in aggregated form, the **PP2** strands are wrapped on each other but on addition of ODTMA, these aggregates dissociate and each **PP2** molecule is surrounded by ODTMA molecules.

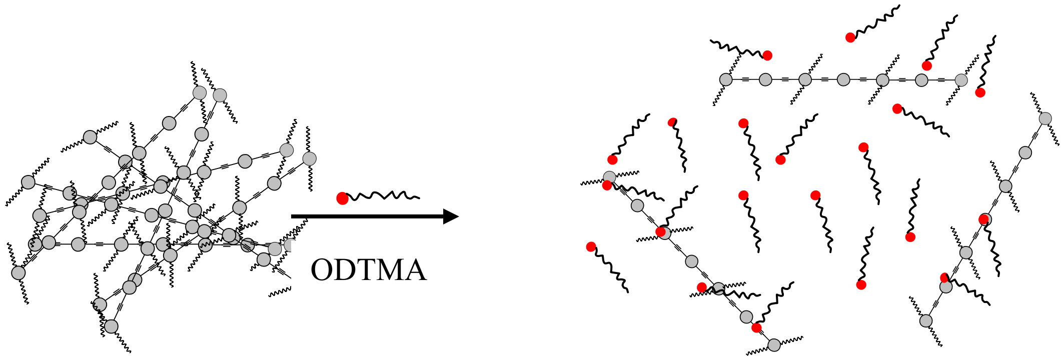

***Scheme 2.1*** *Formation of heteroaggregates on addition of ODTMA*

Steady-state spectra and FCS studies show that when **PP2** is at low enough concentration, the addition of surfactant does not change the photophysical properties of **PP2**. At higher concentration, the addition of surfactant changes the absorption and emission spectra so that they look similar to those observed for the unaggregated form of the **PP2**.

*PEG (Nonionic surfactant):* The absorption spectrum of **PP2** shifts red on addition of PEG, but no isosbestic point is observed. On addition of PEG the **PP2** fluorescence spectrum develops a sharp peak at 448 nm, however the broad red peak at 530 nm remains, even at large excess of PEG. Time resolved fluorescence studies show that the decay law of the excited state is nonexponential and exhibits a strong dependence on the emission wavelength. Lastly, the average lifetime is slower than that found for **PP2** with 0.05mM ODTMA indicating that PEG does not break the homoaggregates fully. The neutral surfactant does not interact strongly enough with the **PP2** in order to dissociate the homoaggregates.

## 2.5 SUMMARY AND CONCLUSION

It is evident that the solution properties affect the **PP2** aggregation and hence the optical properties and the excited state lifetime of **PP2**. **PP2** has an emission spectrum with evidence of vibronic structure in DMSO and in water with ODTMA surfactant. At low concentration in water the **PP2** spectrum is indicative of an unaggregated form. As the concentration of **PP2** in water increases the well-defined emission band disappears and a broad, red-shifted emission band appears. The large change in hydrodynamic radius of the fluorophore, as determined by FCS, correlates with these spectral changes and demonstrates the aggregation. In addition, the temperature studies show that aggregated **PP2** can be dissociated at high temperature.

At concentrations of $10^{-6}$ M **PP2** in water, the absorption spectrum displays a band on the red edge from the aggregate and the emission spectrum is dominated by the aggregated form, broad and red-shifted. The addition of small electrolyte ions to the solution perturbs these spectral characteristics and appears to stabilize the aggregates. In NaCl solutions the size of the aggregates, as determined by FCS, are larger than that found in water, and heating of the solutions to $90^{o}$ C does not dissociate the aggregates. The steady-state spectra of **PP2** display similar behavior for the different cations and anions that are studied, indicating that specific interactions such as ion pair formation may not be important.

Addition of ODTMA surfactant to **PP2** in water causes remarkable changes in the fluorescence and absorption spectra. Comparison with the spectra in DMSO, indicates that the ODTMA dissociates the homoaggregates of **PP2.** The zeta potential measurement and FCS studies at low **PP2** concentration demonstrate that ODTMA forms its own complexes with **PP2**. The fluorescence quantum yield of **PP2** in 0.05 mM ODTMA increases by approximately three times as compared to water. The decrease in the excited state lifetime and corresponding increase in quantum yield demonstrates that addition of ODTMA to **PP2** changes the nature of the emitting state to one with a higher radiative rate. The radiative rate for **PP2** with 0.05mM ODTMA is approximately 12 times higher than that found in water. The change in the radiative rate supports the conclusion that the emitting chromophore changes under different solution conditions, and supports the explanation that the aggregate emission is ‘excimer-like’.

These studies have important implications for the use of these materials in sensing. The above studies show that the photophysical properties of polyphenylethynylene are very sensitive to electrolyte concentration and surfactants. For example, the fluorescence intensity of **PP2** decreased with increasing ionic strength of inorganic and organic salts, because of the formation of aggregates.[55-58] If the aggregates and the unaggregated form have different sensitivities for the analyte, then the aggregation will need to be controlled for sensing applications. A number of workers have reported that the Stern-Volmer constant depends on the concentration of the conjugated polyelectrolyte.[37] Studies of the effect of ionic strength on Stern-Volmer constant are under way and will be published elsewhere.

## 2.6 ACKNOWLEDGEMENT

We acknowledge support from the U.S. National Science Foundation (CHE-0415457).

## 2.7 REFERENCES

(1) Bunz, U. H. F.; Imhof, J. M.; Bly, R. K.; Bangcuyo, C. G.; Rozanski, L.; Bout, D. A. V. *Macromolecules* **2005**, *38*, 5892-5896.

(2) Jones, R. M.; Bergstedt, T. S.; McBranch, D. W.; Whitten, D. G. *J Am Chem Soc* **2001**, *123*, 6726-7.

(3) Levitsky, I. A.; Kim, J.; Swager, T. M. *J. Am. Chem. Soc* **1999**, 1466-1472.

(4) Perahia, D.; Traiphol, R.; Bunz, U. H. F.; *Macromolecules* **2001**, *34*, 151-155.

(5) Rothberg, L. J.; Yan, M.; Galvin, M. E.; Kwock, E. W.; Miller, T. M.; Papadimitrakopoulos, F. *Synthetic Metals* **1996**, *80*, 41-58.

(6) Wilson, J. N.; Bunz, U. H. F. *J. Am. Chem. Soc* **2005**, *127*, 4124-4125.

(7) Zhou, C. Z.; Liu, T.; Xu, J. M.; Chen, Z. K. *Macromolecules* **2003**, *36*, 1457-1464.

(8) Skotheim, T. E.; Elsenbaumer, R. L.; Reyolds, J. R. *Eds. Handbook of Conducting Polymers* **1998**, *Marcel Decker: New York.*

(9) Moroni, M.; J., L. M.; Luzzati, S. *Macromolecules* **1999**, *32*, 562-571.

(10) Gaylord, B. S.; Heeger, A. J.; Bazan, G. C. *Proc. Nat. Acad. Sci.* **2002**, *99*, 10954-10957.

(11) Harrison, B. S.; M.B.;, R.; Reyolds, J. R.; Scahnze, K. S., , . *J.Am. Chem. Soc.* **2000**, *122*, 8561.

(12) Kushon, S. A.; Ley, K. D.; Bradford, K.; Jones, R. M.; McBranch, D.; Whitten, D. *Langmuir* **2002**, *18*, 7245-7249.

(13) McQuade, D. T.; Pullen, A. E.; Swager, T. M. *Chem Rev* **2000**, *100*, 2537-74.

(14) Rininsland, F.; Xia, W.; Wittenburg, S.; Shi, X.; Stankewicz, C.; Achyuthan, K.; McBranch, D.; Whitten, D. *Proc. Nat. Acad. Sci.* **2004**, *101*, 15295-15300.

(15) Schanze, K. S.; Pinto, M. R. *Proc. Nat. Aca. Sci.* **2004**, *101*, 7505-7510.

(16) Heeger, A. J.; Diaz-Garcia., M. A. *Curr. Opin. Solid State Mater.* **1983**, *3*, 16.

(17) Kim, I. B.; Dunkhorst, A.; Gilbert, J.; Bunz, U. H. F. *Macromolecules* **2005**, *38*, 4560-4562.

(18) Liu, M.; Kaur, P.; Waldeck, D. H.; Xue, C.; Liu, H. *Langmuir* **2005**, *21*, 1687-1690.

(19) Hide, F.; Diaz-Garcia, M. A.; Schwartz, B. J.; Andersson, M. R.; Pei, Q.; Heeger, A. J. *Science* **1996**, *273*, 1833-1836.

(20) Ho, P. K. H.; Kim, J. S.; Burroughes, J. H.; Becker, H. L.; Li, S. F. Y.; Brown, T. M.; Cacialli, F.; Friend, R. H. *Nature* **2000**, *404*, 481-484.

(21) Sirringhaus, H.; Tessler., N.; Friend, R. H. *Science* **1998**, *280*, 1741-1744.

(22) Zhang, C.; Broun, D.; Heeger, A. J. *J. Appl. Phys.* **1993**, *73*, 5177.

(23) Bunz, U. H. F. *Chem. Rev.* **2000**, *100*, 1605-1644.

(24) Halkyard, C. E.; Rampey, M. E.; Kloppenburg, L.; Studer-Martinez, S. L.; Bunz, U. H. F. *Macromolecules* **1998**, *31*, 8655-8659.

(25) Breitenkamp, R. B.; Tew, G. N. *Macromolecules* **2004**, *37*, 1163-1165.

(26) Chu, Q.; Pang, Y. *Macromolecules,* **2003**, *36*, 4614-4618.

(27) Chu, Q.; Pang, Y.; Ding, L.; Karasz, F. E. *Macromolecules* **2002**, *35*, 7569-7574.

(28) Miteva, T.; Palmer, L.; Kloppenburg, L.; Neher, D.; Bunz, U., H. F. *Macromolecules* **2000**, *33*, 652-654.

(29) Fiesel, R.; Halkyard, C. E.; Rampey, M. E.; Kloppenburg, L.; Studer-Martinez, S. L.; Scherf, U.; Bunz, U. H. F. *Macromolecular Rapid Communications* **1999**, *20*, 107-111.

(30) Haskins-Glusac, K.; Pinto, M. R.; Tan, C.; Schanze, K. S. *J. Am. Chem. Soc.* **2004**, *126*, 14964-14971.

(31) Kim, I.-B.; Bunz, U. H. F. *J. Am. Chem. Soc.* **2006**, *128*, 2818-2819.

(32) Kim, I.-B.; Dunkhorst, A.; Gilbert, J.; Bunz, U. H. F. *Macromolecules* **2005**, *38*, 4560-4562.

(33) Kim, I.-B.; Phillips, R.; Bunz, U. H. F. *Macromolecules* **2007**, *40*, 814-817.

(34) Thunemann, A. F.; Ruppelt, D. *Langmuir* **2001**, *17*, 5098-5102.

(35) Thunemann, A. F. *Adv. Mater.* **1999**, *11*, 127-130.

(36) Fan, Q.; Zhou, Y.; Lu, X. M.; Hou, H. M.; Huang, W. *Macromolecules,* **2005**, *38*, 2927-2936.

(37) Pinto, M.; Kristal, B. M.; Schanze, K. S. *Langmuir* **2003**, *19*, 6523-6533.

(38) Tan, C.; Pinto, M. R.; Schanze, K. S. *Chem Comm.* **2002**, 446-447.

(39) Jiang, H.; Zhao, X.; Schanze, K. S. *Langmuir* **2006**, *22*, 5541-5543.

(40) Lavigne, J. J.; Broughton D. L. ; Wilson, J. N.; Erdogan, B.; Bunz, U. H. F. *Macromolecules* **2003**, *36*, 7409-7412.

(41) Kim, S.; Jackiw, J.; Robinson, E.; Schanze, K. S.; Reynolds, J. R.; Baur, J.; Rubner, M. F.; Boils, D. *Macromolecules* **1998**, *31*, 964-974.

(42) *GPC studies were performed by American Polymer Std. OHIO*.

(43) Liu, M.; Waldeck, D. H.; Oliver, A. M.; Head, N. J.; Paddon-Row, M. N. *Journal of the American Chemical Society* **2004**, *126*, 10778-10786.

(44) Koppel, D. E. *Physical Review A* **1974**, *10*, 1938-1945.

(45) Magde, D.; Elson, E.; Webb, W. W. *Physical Review Letters* **1972**, *29*, 705-708.

(46) Pristinski, D.; Kozlovskaya, V.; Sukhishvili, S. A. *Journal of Chemical Physics* **2004**, *122*, 14907-14907.

(47) Van Rompaey, E.; Sanders, N.; Van Craenenbroeck, E.; Engelborghs, Y.; De Smedt, S. C.; Demeester, J. *Macromolecules* **2000**, *33*, 8280-8288.

(48) Leng, X. S., K.; Buffle, J. *J.Coll. Inter. Sci.* **2002**, *251*, 64.

(49) Yue, H.; Waldeck, D. H.; Xue, C.; Liu, H. *Manuscript in preparation*.

(50) Krichenvsky, O.; Bonnet, B. *Rep.Prog.Phys.* **2002**, *65*, 251-297.

(51) Cotts, P. M.; Swager, T. M.; Zhou, Q. *Macromolecules* **1996**, *29*, 7323-7328.

(53) Chen, L.; Xu, S.; McBranch, D.; Whitten, D. *J. Am. Chem. Soc* **2000**, *122*, 9302-9303.

(54) Yuan, L. L.-J., D.; Hiroyuki, N.; and Kenichi. N *J. Coll. Inter. Sci.* **2003**, *264*, 561-564.

(55) Bronich, T. K.; Kabanov, A. V.; Kabanov, V. A.; Yu, K.; Eisenberg, A. *Macromolecules* **1997**, *30*, 3519-3525.

(56) Kuhn, P. S. L., Y.; Barbosa, M.C. **1998**, 299, 51-56. *Chemical Physics Letters,* 1998, *299*, 51.

(57) Macknight, W. J.; Ponomarenko, E. A.; Tirrell, D. A. *Acc. Chem. Res.* **1998**, *31*, 781-788.

(58) Samori, P.; Severin, N.; Muellen, K.; Rabe, J. P. *Adv. Mat.* **2000**, *12*, 579-582.

## 2.8 SUPPLEMENTAL INFORMATION

**Rigid Rod Model**

In order to calculate the hydrodynamic radius for a rod, we assumed it to be to be an prolate ellipsoid and used following relation for calculation

$$D = \frac{k_B T}{6\pi\eta r} G(\rho) \tag{2.4}$$

$$G(\rho) = (1-\rho^2)^{-1/2} \ln\left\{\frac{1+(1-\rho^2)^{1/2}}{\rho}\right\}; \rho < 1 \tag{2.5}$$

where $G(\rho)$ is a function of axial ratio, $\rho = b/a$ (*b* being minor semiaxis and *a* being major semiaxis) and r is the radius of effective sphere. Assuming b=0.17 nm and a= 46 nm, G(ρ) was calculated to be 6.3 and thus a radius of 26 nm.

For an oblate ellipsoid model, the following relation was used

$$G(\rho) = (\rho^2 - 1)^{1/2} \arctan[(\rho^2 - 1)^{1/2}]; \rho > 1 \tag{2.6}$$

Assuming b=3.2 nm and a=0.13 nm, G(ρ) was calculated to be 39 and thus a radius of 163 nm was found.

**Two state Model**

The observed absorption spectrum for **PP2** was fit to a sum of two spectra to obtain the relative amounts of the aggregate species and to get the equilibrium constants. Figure 1.11 gives an example of the fitting results for **PP2** in NaCl solutions. Figure 1.11A shows the theoretical absorption spectra for each of two species in the equilibrium reaction, and Figure 1.11B shows the change in concentration of the two species with increasing ionic strength.

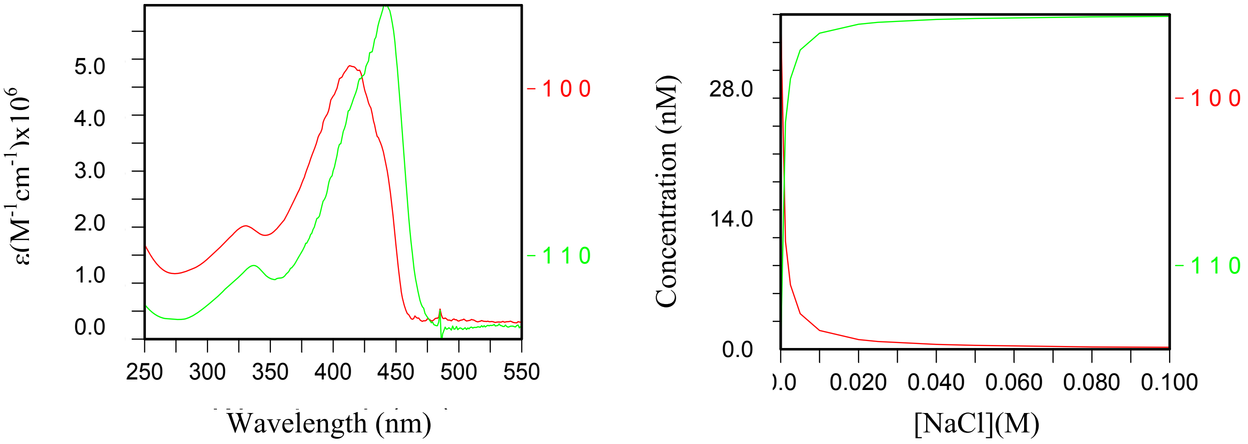

***Figure 2. 11*** *Theoretical fit to a two states model for the absorption spectrum of* ***PP2*** *in NaCl solutions. A) extinction coefficient versus absorption wavelength; B) change of concentration versus ionic strength. The molecular weight was averaged as 38,100. Red line represents the* ***PP2*** *aggregate species and green line represents the* ***PP2****:$Na^+$ aggregate.*

**Ionic Strength Dependence**

Figure 1.12 shows the fluorescence intensity ratio plot for **PP2** with LiCl, NaCl and KCl in water versus the ionic strength. The fluorescence quenching is found to be similar for all the cations.

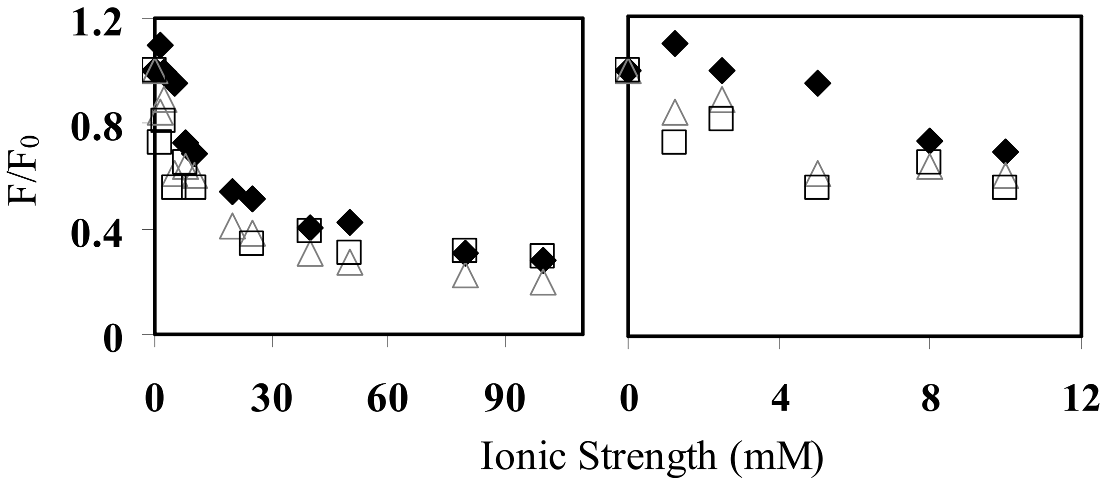

***Figure 2. 12** Fluorescence intensity ratio of **PP2** LiCl (diamonds),NaCl (Squares) and KCl (triangles) to **PP2** in water versus the ionic strength.*

The effect of different anions was studied by performing experiments with sodium iodide and sodium phosphate (figure 1.13). The trend was similar, but comparatively more quenching was observed for NaCl than NaI and sodium phosphate.

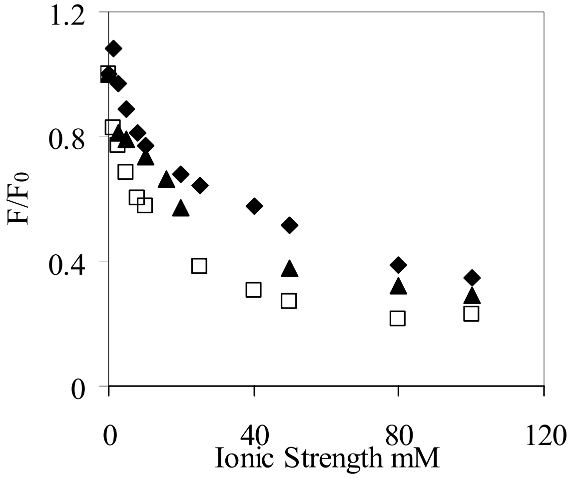

***Figure 2.11** Fluorescence intensity ratio of **PP2** in NaCl (square), sodium phosphate buffer at pH = 7 (triangle) and NaI (diamond) versus **PP2** in water.*

The ionic strength dependence for TBAF, TEAF and AF is shown in figure 1.14. The quenching was less pronounced in these cases as compared to NaCl.

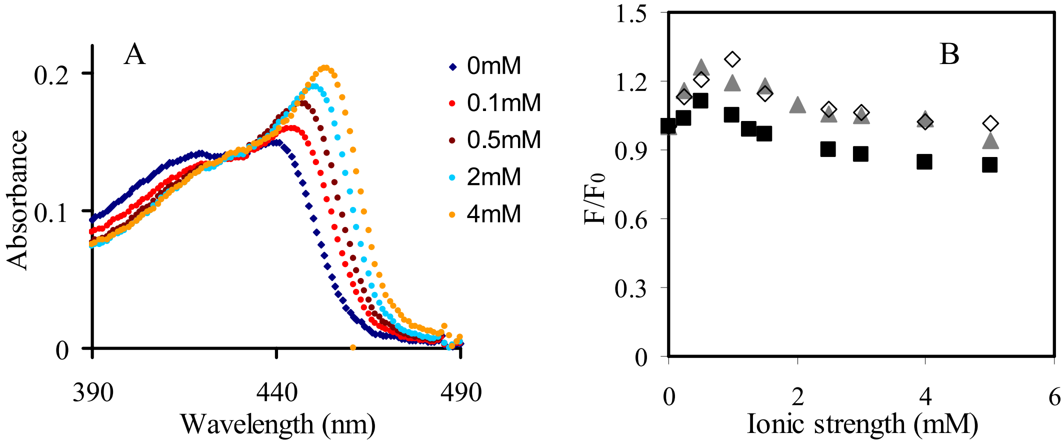

***Figure 2.12 A)*** *The absorption spectra of* ***PP2*** *for aqueous solutions with different TBAF concentrations.* ***B)*** *Fluorescence intensity ratio of* ***PP2*** *in AF (diamond), TEAF (triangle) and TBAF (square) to* ***PP2*** *in water as a function of the ionic strength.*

# CHAPTER 3 IONIC STRENGTH EFFECTS ON THE AGGREGATION OF A POLYPHENYLPHENYLENE BASED CONJUGATED POLYELECTROLYTE IN AQUEOUS SOLUTIONS

Palwinder Kaur, M. Wu, D. Tapriyal, H. Yue, Min Liu, David H. Waldeck,*
*Chemistry Department, University of Pittsburgh, Pittsburgh PA 15260*
Cuihua Xue, and Haiying Liu*
*Chemistry Department, Michigan Technical University, Houghton MI 49931*

The affects of ionic strength on the fluorescence and absorption properties of a polyphenylene based polyelectrolyte and oligomer are reported. The fluorescence of **PP1** is strongly enhanced on addition of counterions such as $Na^+$, $K^+$, $Li^+$ $TBA^+$ and $ODTMA^+$, an effect which arises from the creation of salt stabilized aggregates. The observed fluorescence and absorption spectra indicate that the conjugated polyphenylene chain forms aggregates upon increase in the ionic strength and these aggregates have a higher radiative rate than do the individual polymer strands. The increase in the radiative rate depends on the nature of the counterion and is higher for aggregates formed in the presence of counterions containing an alkyl chain.

## 3.1 INTRODUCTION

Considerable interest in conjugated polyelectrolytes has been driven by the exceptional properties they exhibit in aqueous solution, for example, high fluorescence quantum yields[1-3], the ability to interact electrostatically with other charged species[4], and an extraordinary high sensitivity to fluorescence quenchers[5-7]. As a result of these properties, this class of materials has found potential utility in light-emitting diodes[8], lasers[9], chemical and biological sensors[6,10-13] and solar cells.[14] Hence, it is important to understand how their photophysical properties are affected by their physical and chemical environment. Much work has been performed to understand the photophysical properties of polyphenylethynylene and polyphenylvinyl based conjugated polyelectrolyte solutions and solid state materials, however polyphenylphenylene based conjugated polyelectrolytes are less widely studied.[15] The restricted rotation of phenyl rings in these systems (a rotation barrier of 6.5 kJ/mol)[16] provide an interesting contrast for polyphenylethynylene conjugated polyelectrolytes, where the rotation barrier is less than 2.1 kJ/mol.[17]

Most of the work on polyphenylphenylene based conjugated polymers has used X-ray diffraction and light scattering with only a little work available on optical properties of these systems. Liu et al[18] performed light scattering studies of poly(p-phenylene) with sulfonate and dodecyl side chains at 1 mg/ml concentrations. They found that these solutions exhibit single polymer molecule properties at low ionic strength but at higher salt concentrations both single polymer molecules and aggregates coexist in solution. They further demonstrated that the amount of aggregation depends on the polymer concentration and the nature of the counterions but no explanation of types of aggregates was provided. Rulkens et al[19] provided insight into the type of aggregates that are formed in polyphenylene based systems using small angle X-ray scattering (SAXS) . The SAXS data of aqueous solutions of sulfonated poly(p-phenylenes) showed aggregated polymer chains in the form of cylindrical micelles, in which the phenylene backbone is oriented parallel to the long axis of the micelle. The charge density and the length of the alkyl side chains were shown to influence the diameter and aggregation number of the micelles. Later Bockstaller et al[20,21] studied the dependence of such aggregates on the polymer concentration using static and dynamic light scattering, small angle X-ray scattering and electron microscopy. In contrast, they found that even at their lowest concentrations of 0.001 mg/ml, individual polymer chains could not be observed, only aggregates. With further increase in the concentration, they found that these polymers first form ellipsoidal clusters with internal lyotropic ordering, then a nematic phase, and finally a columnar phase of cylindrical micelles. Recently Valiyaveettil et al[22-25] have investigated the affects of solvent on the optical properties of sulfonate and alkyl substituted phenylene conjugated polymers. They showed that the fluorescence intensity of an aqueous polymer solution initially increased on addition of the non-solvent, THF, but that on further increase in the percentage of THF beyond 65% by volume, the emission intensity decreased. They attributed this phenomenon to the formation of polymer aggregates and their subsequent precipitation from the solution. These studies were corroborated by dynamic light scattering which showed an increase in the size of the aggregates from 80-800 nm with an increase in the amount of THF in the polymer solution.  These studies provide important structural information about the aggregation of polyphenyl based conjugated systems and its dependence on solution properties.

This work reports how the fluorescence properties of a polyphenylphenylene based polyelectrolyte changes with solution conditions and demonstrates its link to the polymer aggregation. The influence of addition of simple ionic salts and ionic surfactants on the optical properties of poly[2,5-bis(3-sulfonatopropoxy)-1,4-phenylene-alt-1,4-phenylene)] (identified as **PP1**) and the oligomer **OPP1** are investigated. These studies show that the **PP1's** fluorescence is initially enhanced on addition of ionic salts but that further increase in the ionic strength causes the emission intensity to decrease. These changes in fluorescence intensity are attributed to the formation of polymer aggregates that result because of charge neutralization on the polymer strands by the counter ions. These polymer aggregates have higher fluorescence quantum yields than the unaggregated polymer chains. These studies show that the solution properties (solvent, ionic strength and surfactant) control the spectral properties of the conjugated polyelectrolyte by changing the equilibria between aggregated and unaggregated forms of the polymer

## 3.2 EXPERIMENTAL

Poly[2,5-bis(3-sulfonatopropoxy)-1,4-phenylene-alt-1,4-phenylene)] (identified as **PP1**) and the oligomer **OPP1** were prepared in a manner similar to that reported in the literature.[26] ODTMA (octadecyltrimethyl ammonium bromide), PEG (polyethylene glycol), TBAF (tetra butyl ammonium fluoroborate), TEAF (tetraethyl ammonium fluoroborate) and AF (ammonium fluoroborate) were bought from Sigma-Aldrich. The molecular weight of **PP1** was found to be 38.6 kDa and the polydispersity was 2.44 as determined by size exclusion chromatography.[17]The **OPP1** was characterized using NMR.

Both the **PP1** and **OPP1** have negative charges on the side chains, which are located on every other phenyl ring. In order to avoid intermolecular interactions between polymer strands, the experimental concentration was dilute, for example, the concentration of **PP1** was prepared at $3.3 \times 10^{-3}$ mg/ml, ~ $7.1 \times 10^{-6}$ M in terms of polymer repeat unit (assuming 38600 g/mol molecular weight) and the concentration of **OPP1** was prepared at $3.7 \times 10^{-3}$ mg/ml or ~ $7.0 \times 10^{-6}$ M in terms of polymer repeat unit. At these concentrations the effect of the polymer on solution properties, such as viscosity, can be neglected. For studies in electrolyte solutions, the concentration of background electrolyte was always much higher than the concentration of polyelectrolyte so that the solution ionic strength was determined by the added salt concentration. The current experiments varied the nature of the electrolyte and its ionic strength of electrolyte from $5 \times 10^{-4}$ M to 0.1 M.

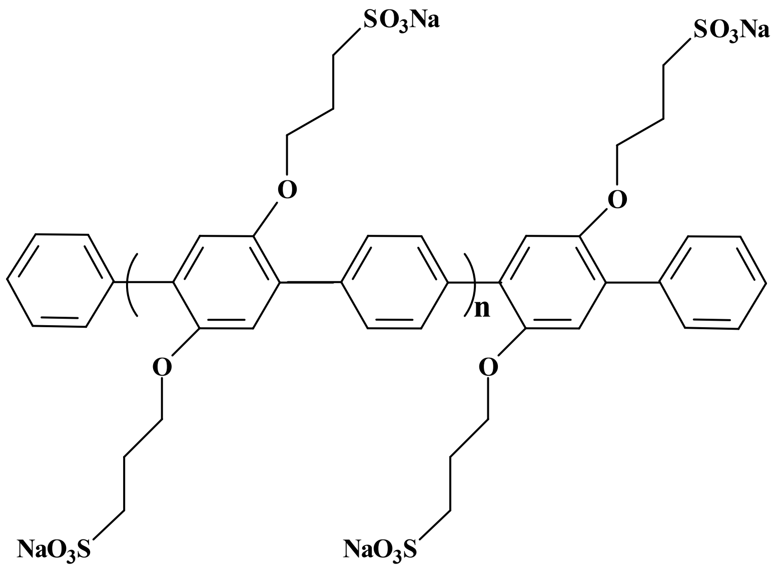

**PP1**

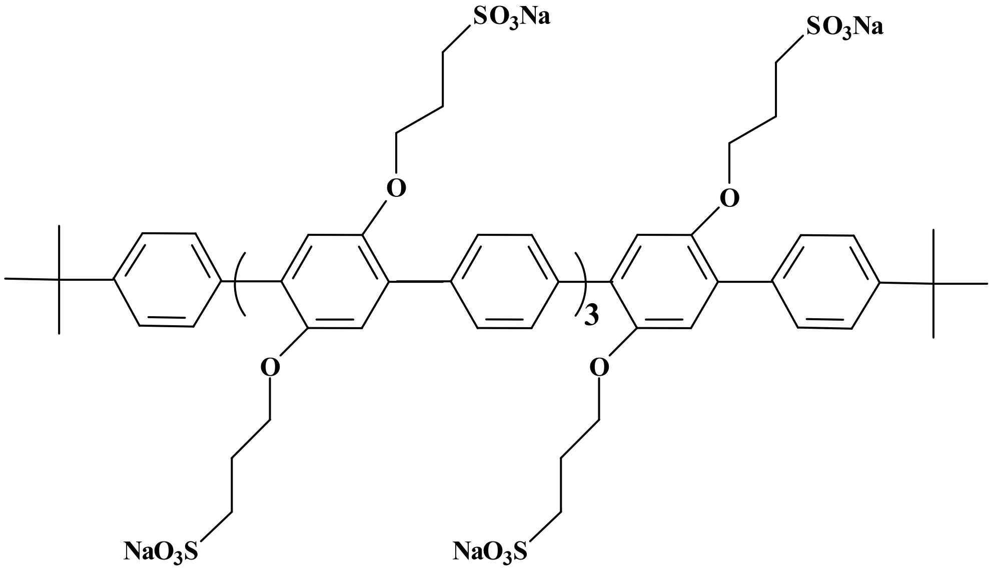

**OPP1**

***Scheme 3.1*** *Structure of* ***PP1*** *and* ***OPP1****.*

*Steady state spectroscopy:* Steady-state absorption spectra were measured on an Agilent 8453 spectrometer and the steady-state emission spectra were measured on a Spex Fluorolog 0.22 m double spectrometer.

*Time dependent fluorescence spectroscopy:* The time-resolved fluorescence data were collected using the time-correlated single photon counting method.[27] The instrument response function was measured using a sample of colloidal $BaSO_4$. The samples were excited at 330 by the frequency-doubled output of a cavity-dumped Coherent CR599-01 dye laser, using DCM (4-dicyanomethylene-2-methyl-6-*p*-dimethylamino-styryl-4H-pyran) dye, which was pumped by a mode-locked Vanguard 2000-HM532 Nd:YAG laser purchased from Spectra-Physics. The dye laser pulse train had a repetition rate of 300 kHz. Pulse energies were kept below 1 nJ, and the count rates were kept below 3 kHz to prevent pile up effects. All fluorescence measurements were made at the magic angle, and data were collected until a standard maximum count of 10,000 was observed at the peak channel. The fluorescence decay curves were fit by a convolution and compare method using IBH-DAS6 analysis software. Other details of the TCSPC apparatus can be found in reference 28.

*Fluorescence Quantum Yield calculations:* The fluorescence quantum yield was measured using the standards 9,10-diphenylanthracene (DPA) in benzene ($\Phi_{DPA}$= 0.82)[29] and quinine sulfate dihydrate (QS)[30] in 0.5 M $H_2SO_4$ ($\Phi_{QS}$= 0.546). The **PP1** was excited at 380 nm and the **OPP1** samples were excited at 321 nm. The fluorescence quantum yields for the polymer and the oligomer were calculated using the following formula

$$\phi_{sample} = \phi_{stndrd} \frac{Abs_{stndrd}}{Abs_{sample}} \times \frac{Flu_{sample}}{Flu_{stndrd}} \tag{3.1}$$

where, $Abs_{sample}$ and $Abs_{stndrd}$ are the absorbances for the sample and the standard, $Flu_{sample}$ and $Flu_{stndrd}$ are the area under the emission spectra for sample and standard. $\phi_{stndrd}$ is the fluorescence quantum yield for the standard.

The radiative rates were calculated using the following relation

$$k_r = \frac{\phi_{sample}}{\tau_F} \tag{3.2}$$

where, $\tau_F$ is the characteristic lifetime of the sample (**PP1** or **OPP1**) using the fluorescence lifetime measurements. An attempt was made to fit the data to a single exponentialdecay law but the fits were not very good indicating that the distribution of aggregates may be inhomogeneous. The correlation time[1] was used as $\tau_F$ for **PP1** and **OPP1**. The correlation time was obtained by fiting the fluorescence decays for **PP1** and **OPP1** were fit to double exponential.

*Fluorescence Correlation Spectroscopy (FCS):* FCS is a non-invasive single molecule method which provides dynamic and kinetic information about a fluorophore by following the fluctuation trajectory of fluorescence about the equilibrium state.[31-35] FCS was performed using a homemade FCS instrument based on a Zeiss IM35 inverted microscope. Details of the instrumentation will be provided elsewhere.[36] The sample was excited at 375 nm through an objective lens (Olympus UPlanfluor 40X/1.30 Oil) and the fluorescence was collected by the same lens. The concentrations of the polymer solutions were controlled to be $5.6 \times 10^{-7}$ M in polymer repeat unit. To avoid photobleaching and optical trapping, the laser power was kept low, 20 μW, as measured at the front of the objective lens. Fluorescence trajectories were collected for about 45 min; from which an autocorrelation function, G(t), was computed. The corresponding autocorrelation function G(t) was fit by equation (3) ,

$$G(t) = \frac{1}{\overline{N}}\left(1+\frac{t}{\tau_D}\right)^{-1}\left(1+\frac{\omega_{xy}^2\, t}{\omega_z^{\,2}\, \tau_D}\right)^{-1/2} \tag{3.3}$$

---

[1] The time constant $\tau_F$ is the correlation time obtained from the best fit of a double exponential model, namely $I(t) = A_1 \exp(-t/\tau_1) + (1-A_1)\exp(-t/\tau_2)$. For this model the correlation time is given by $\tau_F = A_1\,\tau_1 + (1-A_1)\,\tau_2$.

to extract the correlation time $\tau_D$. $\overline{N}$ is the average number of fluorescent molecules in the focal volume; $\omega_{xy}$ is the radius of the focal spot in the transverse direction, and $\omega_z$ is the Rayleigh range of the excitation beam (see reference [37] for details relating to equation 1). The correlation time $\tau_D$ is related to the translational diffusion coefficient $D$ of the fluorophore by

$$\tau_D = \frac{\omega_{xy}^2}{4D} \tag{3.4}$$

The apparatus was calibrated and tested using a 10 nM Rhodamine 6G aqueous solution, assuming the diffusion coefficient $D = 4.17\times10^{-6}$ cm$^2$ s$^{-1}$. The Stokes-Einstein approximation, equation (5) for a spherical model, was used to extract a hydrodynamic radius $R_H$ from the measured diffusion coefficient

$$D = \frac{k_B T}{6\pi\eta R_H} \tag{3.5}$$

where $\eta$ is the shear viscosity, $T$ is the temperature and $k_B$ is Boltzmann's constant. To obtain a characteristci radius r from for a rigid rod model, the following relation

$$D = \frac{k_B T}{6\pi\eta r} G(\rho) \tag{3.6}$$

was used, where

$$G(\rho) = (\rho^2 - 1)^{1/2} \arctan[(\rho^2 - 1)^{1/2}]; \rho > 1 \tag{3.7}$$

$G(\rho)$ is a function of axial ratio, $\rho = b/a$ ($b$ being minor semiaxis and $a$ being major semiaxis) and r is the radius determined for an effective sphere with a volume of rigid rod. Comparison of equations (5) and (6) shows that

$$R_H = \frac{r}{G(\rho)} \tag{3.8}$$

## 3.3 RESULTS

### 3.3.1 Ionic Strength Dependence of PP1 spectra

Absorption and fluorescence spectra of **PP1** ($7.1 \times 10^{-6}$ M in polymer repeat unit) were measured in different ionic strength solutions. Figure 3.1 shows the absorption and emission spectra of **PP1** in NaCl solutions for ionic strengths ranging from 1 mM to 8 mM. The absorption spectrum of **PP1** in water has an absorption peak $\lambda_{max}$ at 338 nm. When the ionic strength is less than 1.25 mM, the absorption peak is close to the 338 nm value measured for **PP1** in water and it has a similar absorbance. Upon further increasing the ionic strength, the absorbance increases and an isosbestic point is observed at 340 nm. As the ionic strength increases above 8 mM, the absorbance peak shifts slightly to a redder wavelength, but the absorbance is nearly constant, even with further increase of the ionic strength by up to ten times.

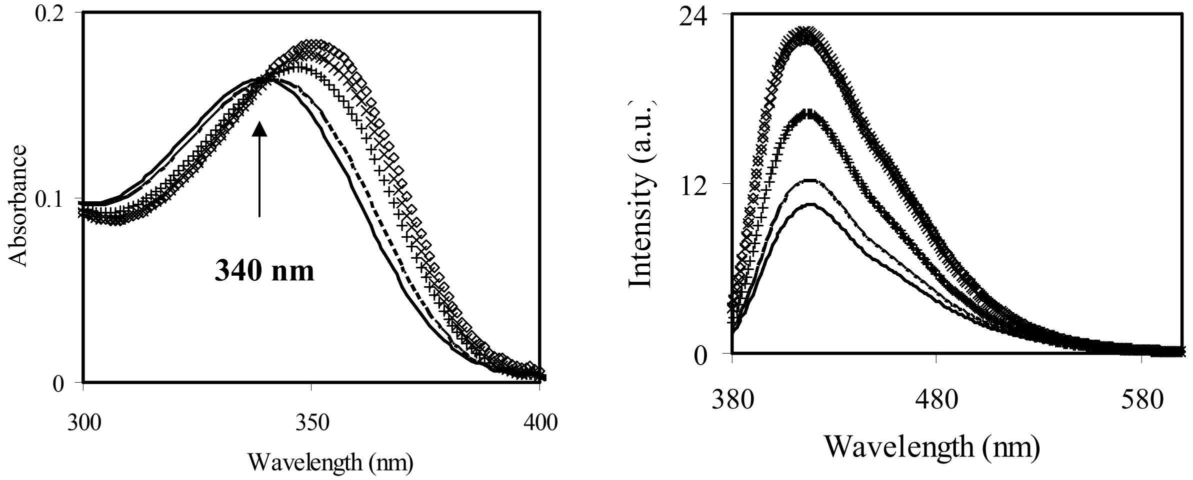

***Figure 3.1*** *Absorption (**A**) and emission (**B**) spectra of **PP1** in NaCl solutions. The ionic strength varies from 0 mM to 8 mM[0 mM (—), 1 mM (---), 2 mM (+), 4 mM (×), 8 mM (◊)]. The arrow marks the isosbestic point.*

The spectroscopic behavior of **PP1** in LiCl and KCl electrolyte solutions is similar to that in NaCl. The observed isosbestic points for **PP1** lie at 339 nm in NaCl and 341 nm in KCl. The wavelength of the isosbestic point red shifts as the radius of the cation increases [$Li^+$ (0.59 Å), $Na^+$ (1.02 Å) to $K^+$ (1.33 Å)]. The absorption spectrum changes strongly at low ionic strength and stops changing at higher ionic strength.

**Table 3.1 Parameters for fit of PP1 absorption spectrum in MCl, by a model with two species (A and B) in equilibrium (with constant K).**

| Salt | **A**<br>$\lambda_{max}$ (nm) | **B**<br>$\lambda_{max}$ (nm) | ln $K^a$ | Percentage of **A** in<br>0.01 M Salt (%) |
|---|---|---|---|---|
| LiCl | 334 | 352 | 3.2 | 9 |
| NaCl | 338 | 354 | 2.6 | 20 |
| KCl | 334 | 352 | 3.2 | 7 |

By assuming a two species equilibrium reaction containing a blue component A and a red component B, the absorption spectrum was fit to obtain an equilibrium constant, K. Figure 3.8 in the supplemental information section gives an example of the fitting results for **PP1**. Table 3.1 summarizes the fitting results: equilibrium constant K and the absorption maxima of the two 'species'. The concentration of the species A varies from 85% in solution with no extra salt added to 7% in 0.01 M salt solution.

Figure 3.1B show how the fluorescence spectrum of **PP1** changes with increasing ionic strength in NaCl solution. The emission peak for **PP1** remains at 420 nm, however the fluorescence intensity in electrolyte solution increases with ionic strength. The quantum yield of **PP1** increases by 3.7 times in 10 mM NaCl solution ($\Phi_{\mathbf{PP1},NaCl} = 0.46$, $\tau_F = 900$ ps), as compared to that in water ($\Phi_{\mathbf{PP1},H2O}$ = 0.12, $\tau_F$ = 340 ps). The radiative rate, calculated using equation 2, increased by 30 % on addition of 10 mM NaCl. Figure 3.2 plots the fluorescence intensity ratio of **PP1** in NaCl solution to its intensity in deionized water as a function of the solution's ionic strength. The fluorescence intensity ratio curves in Figure 3.2 are shown for three excitation wavelengths: the peak absorption wavelength, a wavelength 20 nm shorter than the peak wavelength, and a wavelength 20 nm longer than the peak wavelength. Each data set shows that the fluorescence intensity of **PP1** increases rapidly at low ionic strength (below 2 mM), and then stops increasing before it starts to weakly decrease. For the spectrum collected at a 20 nm shorter excitation wavelength than the peak wavelength, the fluorescence intensity is the highest; for excitation at the peak wavelength and at a 20 nm longer wavelength, the fluorescence intensities are similar. The wavelength dependence can be explained by the two state model. (See Figure 3.8 in the supplemental section). In this model the two species have different absorbances at a given wavelength, hence different excitation wavelengths cause different percentages of the two species to be excited.

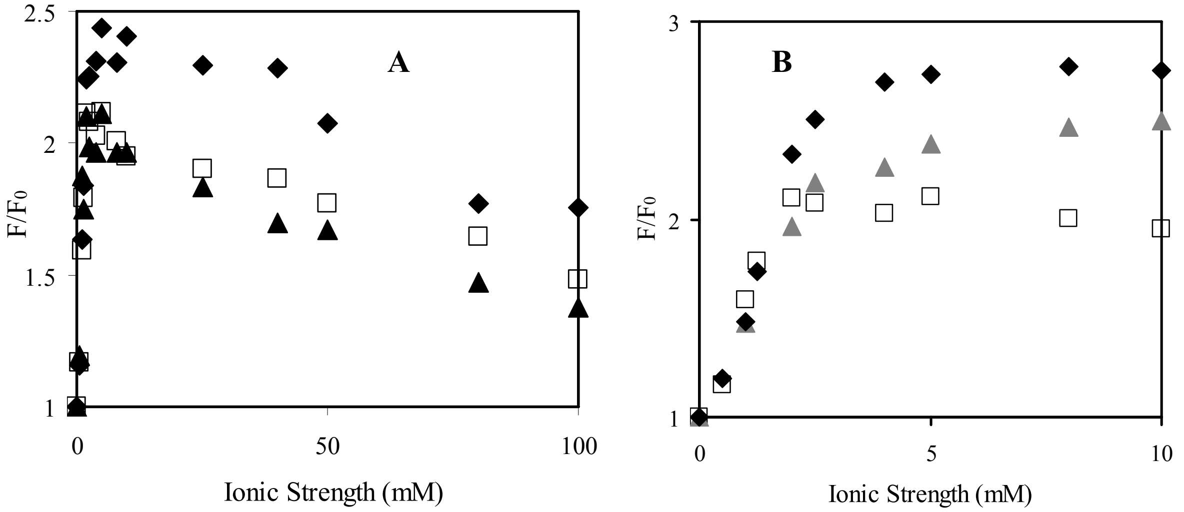

***Figure 3.2*** *Fluorescence intensity ratio of* ***PP1*** *in NaCl solutions (F) to that in water ($F_0$) versus the ionic strength. The fluorescence intensity was integrated over the whole spectrum and corresponds to the relative change in fluorescence quantum yield. The spectrum was obtained at three excitation wavelengths: the peak absorption wavelength (□), 20 nm shorter than the peak wavelength (♦) and 20 nm longer than the peak wavelength (▲). (**B**) Shows the expanded plot from 0 to 10 mM ionic strength.*

The fluorescence of **PP1** was studied in different 1:1 electrolyte solutions. The ionic strength dependence of the **PP1** fluorescence yield in KCl and LiCl solutions was similar to that observed for NaCl solutions (See Figure 3.9 in the supplemental section). Experiments were done with different sodium salts also. Like NaCl, addition of NaI and $NaH_2PO_3$ red shifted the absorption spectra and caused the fluorescence intensity to increase and then plateau at higher ionic strength before decreasing again (See Figure III in the supplemental section). These data show that the intensity increases with the charge to size ratio of the anions. In particular, $I^-$ has the smallest charge to size ratio and the largest fluorescence yield, whereas $Cl^-$ has the largest charge to size ratio and the smallest fluorescence yield. Although the charge to size ratio of the cationic counter ions also affects the fluorescence yield, the effect is less dramatic than that found for the anions. Qualitatively, all of these inorganic salts changed the polymer's optical properties in a similar manner.

Studies in solutions of TBAF, TEAF and AF were used to investigate the affect of organic cations (alkyl chain lengths) on the spectra. Compared to the inorganic ions, the organic ions are sterically large. The addition of TBAF to **PP1** solution causes the absorption spectrum to red-shift, to increase its absorbance, and to display an isosbestic point at 351 nm. The absorption spectral shift was larger than that observed for NaCl. The relative fluorescence intensity also increased with increasing ionic strength of TBAF and plateaued at high ionic strength before decreasing on further increase in ionic strength. The quantum yield of **PP1** in the presence of 4 mM TBAF increased by a factor of six ($\Phi_{\mathbf{PP1},\mathrm{TBAF}} = 0.76$) and the radiative rate increased by a factor of three (using $\tau_F = 727$ ps in equation 2) as compared to **PP1** in water only. The spectra for **PP1** in TEAF and AF behaved similarly; the wavelengths of the isosbestic point in TEAF and AF were 345 nm and 339 nm, respectively (see Table 3.2). The fluorescence intensity increased with increase in the ionic strength but the increase in the fluorescence intensity was different as compared to TBAF (Figure 3.3A) e.g. the increase in fluorescence intensity is higher in TBAF at low ionic strength than it is in AF solutions, and it correlates with the size of the cation, TBAF > TEAF > AF.

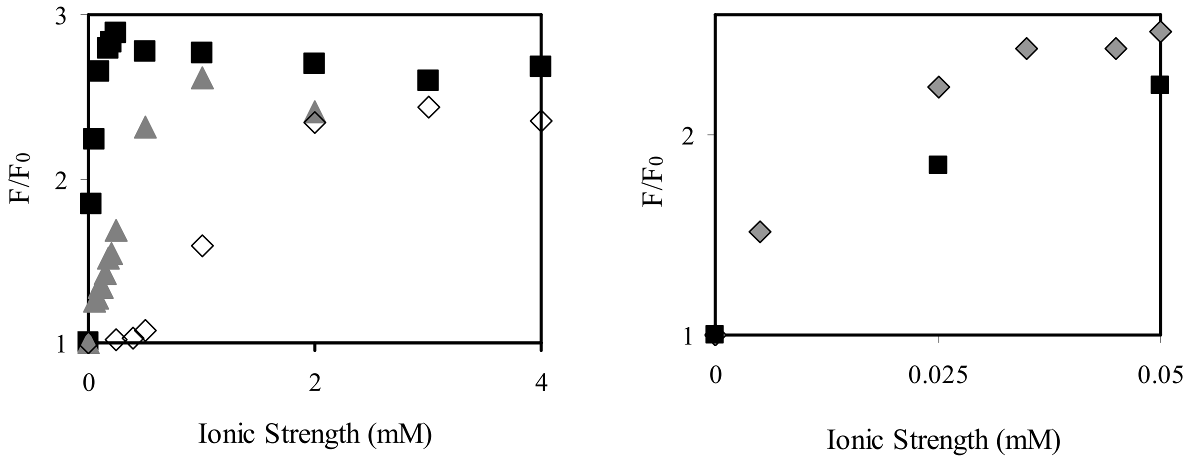

***Figure 3.3A)*** *Fluorescence intensity ratio of* ***PP1*** *in AF (◊), TEAF (▲) and TBAF (■) to* ***PP1*** *in water as a function of the ionic strength.* ***(B)*** *Fluorescence intensity ratio plot for* ***PP1*** *as a function of ODTMA (♦) and TBAF (■) concentration.*

**Table 3.2 Parameters for fit of PP1 absorption spectrum in TABF, TEAF, and AF; by a model with two species (A and B) in equilibrium (with constant K).**

| Salt | **A** | **B** | ln K | Percentage of A in 0.2 mM Salt (%) |
|---|---|---|---|---|
| TBAF | 351 | 366 | 4.0 | 37 |
| TEAF | 345 | 359 | 2.9 | 85 |
| AF | 339 | 356 | 2.7 | 90 |

These ionic strength dependence studies indicate that the fluorescence quantum yield and the radiative rate increases are larger for organic counterions such as TBAF, than the inorganic ones. To assess further how the alkyl part of the cation affects the spectral properties, experiments were done with ODTMA. On addition of a 50μM ODTMA to the **PP1** solution, the absorption red shifted by 13 nm. No isosbestic point was observed but the fluorescence was enhanced and the emission spectrum became narrow. Although only 50μM ODTMA is added to the **PP1** solution, the fluorescence intensity increase is comparable to that observed for TBAF at 2 mM. The quantum yield increased by a factor of four ($\Phi_{\mathbf{PP1},\mathrm{ODTMA}}$= 0.49) in the presence of 50μM ODTMA and the radiative rate increased by a factor of about two. Figure 3B shows the fluorescence intensity ratio plot for **PP1** in the presence of different concentrations of ODTMA.

### 3.3.2 Ionic Strength Dependence of OPP1 solution

Experiments were performed with **OPP1**(~ 7.0 x $10^{-6}$ M per repeat unit) in the presence of different ionic strengths. Unlike **PP1**, the absorption and emission spectrum of **OPP1** does not change with increase in the ionic strength up to 100 mM. The quantum yield remains similar before and after addition of 100 mM NaCl ($\Phi_{\mathbf{OPP1},\mathrm{H2O}}$= 0.32, $\Phi_{\mathbf{OPP1},\mathrm{NaCl}}$= 0.32) and no increase in the radiative rate is observed. But on further increase in the ionic strength up to 1000 mM the fluorescence intensity increases by 10-15 %. Hence, it appears that NaCl solutions have little effect on **OPP1** spectra.

The absorbance and fluorescence characteristics of **OPP1** do change in TBAF solutions. Figure 3.4A shows three absorption spectra for **OPP1** that display a red shift of the absorption maximum by 11 nm with increasing TBAF concentration. Figure 3.4B shows that the relative fluorescence intensity increases by almost two times upon increase of TBAF concentrations to 10 mM. At 4 mM $\Phi_{\mathbf{OPP1},\mathrm{TBAF}}$= 0.54 and the radiative rate increases by 38 %, as compared to water. Addition of ODTMA has the most dramatic affect on the spectral properties of **OPP1**. The absorption spectrum red shifts by 17 nm and the fluorescence quantum yield is enhanced by a factor of ~ 3 ($\Phi_{\mathrm{ODTMA}}$= 1.0), with an increase in the radiative rate by a factor of ~10. The ionic strength dependence of **OPP1** indicates that simple inorganic cations have little or not effect on the spectra, whereas organic cations and ODTMA surfactant causes changes similar to that found for **PP1** solutions.

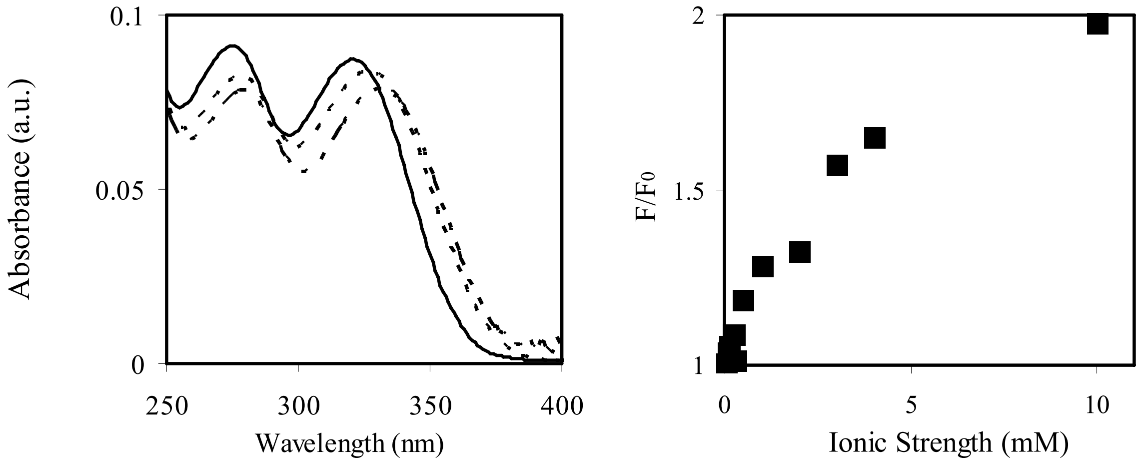

***Figure 3.4(A)*** *Absorption spectra of* ***OPP1*** *with and without TBAF, 0 mM (— ) 4 mM ( - - - - ) and 10 mM TBAF ( —--— ).****(B)*** *Fluorescence intensity ratio of* ***OPP1*** *in ionic TBAF solutions (F) to that in water ($F_0$) versus the ionic strength.*

### 3.3.3 Aggregation Studies

In order to probe whether aggregates form upon addition of ionic salts, filtration experiments were performed and fluorescence correlation spectroscopy was used to measure the diffusion constant of the fluorescent moiety.

The absorption and emission spectra of **PP1** (7.1 x $10^{-6}$ M per repeat unit) in water and in NaCl solutions were recorded before and after passing through 0.25 µm filter. On passing the **PP1** solution in water through the filter, no change in the absorbance and emission intensity was observed. In contrast, the filtration of a 100 mM NaCl solution of **PP1** caused a decrease in absorbance and a corresponding decrease in fluorescence by 25 %. Similar filtration experiments were performed with **PP1** in the presence of 10 mM TBAF. Figure 3.5A shows the absorption spectra of **PP1** in the presence of 10 mM TBAF before and after filtration. The absorbance decreased by a factor of two after passing a 10 mM TBAF solution of **PP1** through the 0.25 μm filter. Figure 3.5B shows that the fluorescence intensity decreases by 50 %. These data corroborate the hypothesis that aggregates are formed (or already existent aggregates grow in size) upon addition of inorganic and organic salts to aqueous solutions of **PP1**.

These filtration studies strongly indicate that the addition of salt induces aggregation of the polymer chains. One may infer that the aggregates are bigger or more numerous for cations containing alkyl chains as compared to those for inorganic ions, such as NaCl, because the fluorescence is attenuated more for **PP1** with 10 mM TBAF as compared to **PP1** with 100 mM NaCl when passed through a filter.

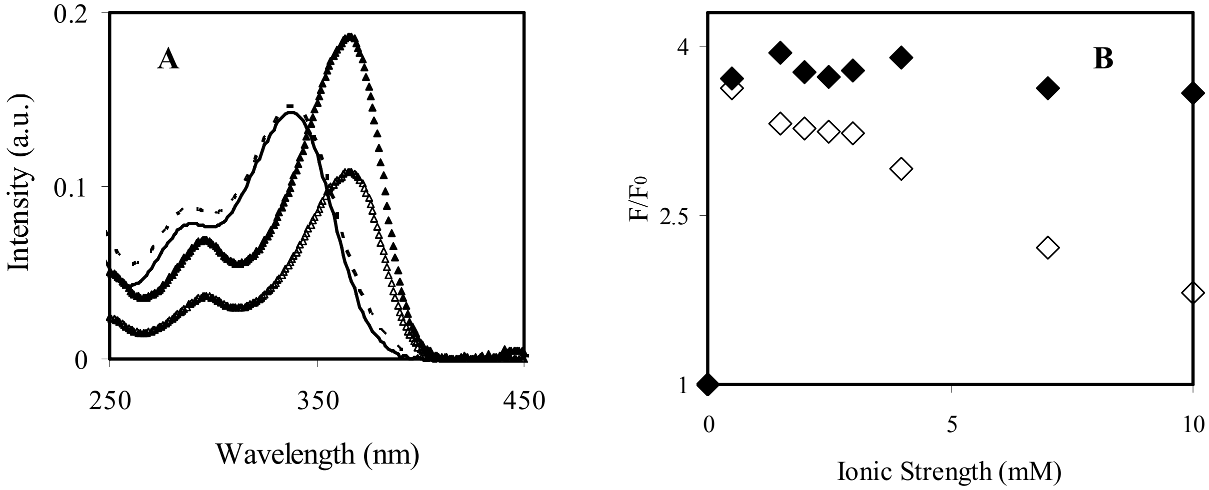

***Figure 3.5(A)*** *Absorption spectra of* ***PP1*** *in water before (——) and after (----) filtration,* ***PP1*** *with 10 mM TBAF before (▲) and after (∆) filtration.* ***(B)*** *Fluorescence intensity ratio of* ***PP1*** *in ionic TBAF solutions (F) to that in water ($F_0$) versus the ionic strength before (♦) and after (◊) filtration.*

Similarly filtration experiments were performed on **OPP1** in water and in NaCl solution. On passing **OPP1** in water solution through 0.25 μm filter, no changes in the absorption and emission spectra were observed. In contrast, passing a 1 M NaCl solution of **OPP1** through the filter, attenuated the absorbance highly and decreased the emission intensity by 55%. Also, on passing a 10 mM TBAF solution of **OPP1** through the filter, the absorbance was attenuated by a factor of three and the fluorescence decreased by 58%. These data corroborate the finding in **PP1** solution, namely that bigger aggregates are formed in the presence of inorganic and organic salts.

To further corroborate the hypothesis of aggregate formation and estimate the aggregate size, FCS studies were performed. Because the FCS experiments need to be performed at low concentration, about ten times lower ($5.7 \times 10^{-7}$ M) than those used for the spectral studies, the affect of ionic strength at this concentration was also recorded. It was observed that the absorption shifted red and the fluorescence was enhanced on increasing the ionic strength, an effect similar to that observed for **PP1** at $7.1 \times 10^{-6}$ M. Figure 3.6 shows the measured autocorrelation functions for **PP1** under different solution conditions at a constant **PP1** concentration ($5.8 \times 10^{-7}$ M) and fits of the data by equation (1). For **PP1** in water, $\tau_D$=139 μs, so that D=$1.86\times10^{-6}$cm$^2$/s and using a spherical model one gets a hydrodynamic radius of $R_H$ = 1.3 nm (using equation 1 with $\eta$= 0.89 cP and $\omega_{xy}$= 0.32 μm). As the ionic strength was increased the hydrodynamic radius also increased. For **PP1** in the presence of 10 mM NaCl, $\tau_D$=246 μs (D=1.05 $\times10^{-6}$cm$^2$/s) and $R_H$ = 2.3 nm, which is 1.8 times higher than for **PP1** in water. On further increase in the NaCl concentration to 100 mM, the hydrodynamic radius increased by a factor of nearly 4 times ($\tau_D$=566 μs, $R_H$ = 5.3 nm).

More dramatic affects were seen for **PP1** in the presence of TBAF and ODTMA. On addition of 4 mM TBAF the size increased by a factor of 8 times to that in water ($\tau_D$=1070 μs, $R_H$ = 10 nm) and by a factor of ~ 11 in the presence of 50 μM ODTMA ($\tau_D$=1502 μs, $R_H$ = 14.1 nm). These hydrodynamic radii are smaller than the characteristic size inferred from the filtration experiment (> 0.25 mm). In part this results because the FCS experiments were done at nearly ten times lower concentrations of **PP1,** however it is also caused by limitation of the spherical model for the aggregates shape, *vide infra.*

Attempts were made to perform FCS experiments on **OPP1**, however the absorbance of **OPP1** at the 375 nm laser wavelength was too weak to give a fluorescence signal that was useful.

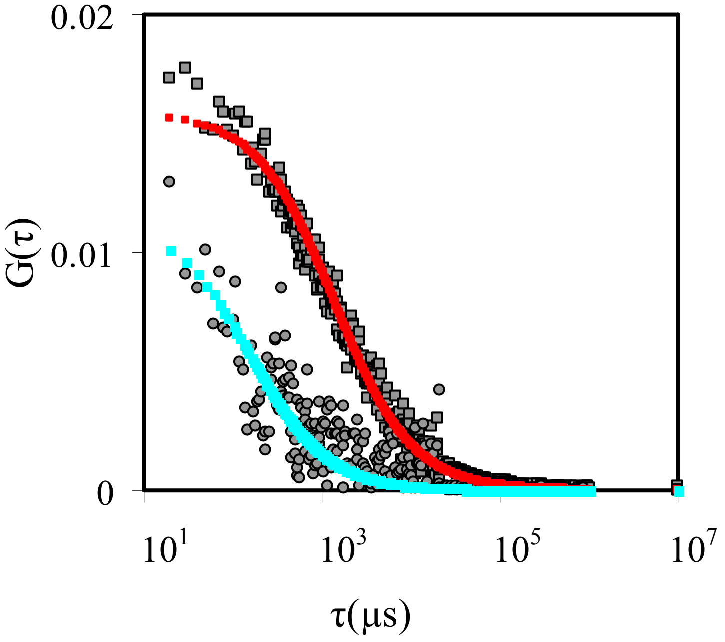

***Figure 3.6** Autocorrelation function for **PP1** in water ($5.6\times10^{-7}$ M )(○) , in the presence of 4mM TBAF (■).*

### 3.3.4 Solvent Dependence

The aggregation of **PP1** was studied in water/methanol mixtures also. The absorption and emission spectra for **PP1** were recorded in a solvent mixture of water and methanol. Figure 3.7 shows the fluorescence intensity changes when the percentage of methanol is changed in the solvent mixture. It is clear from the figure that the fluorescence intensity increases until there is

40% by volume methanol in the solution mixture. Further increase in the methanol decreases the fluorescence intensity. FCS studies were performed on **PP1** in 80 % by volume methanol to see if aggregates are formed. Figure 3.7B shows the autocorrelation function and compares it to that of water. The autocorrelation function could not be fit very well due to the presence of very large paticles. The fit gives an $R_H = 2.2$ μm ($\tau_D$=6000), further strengthening the hypothesis that these polymer chains interact hydrophobically with each other under 'bad' solvent conditions and in the presence of salts.

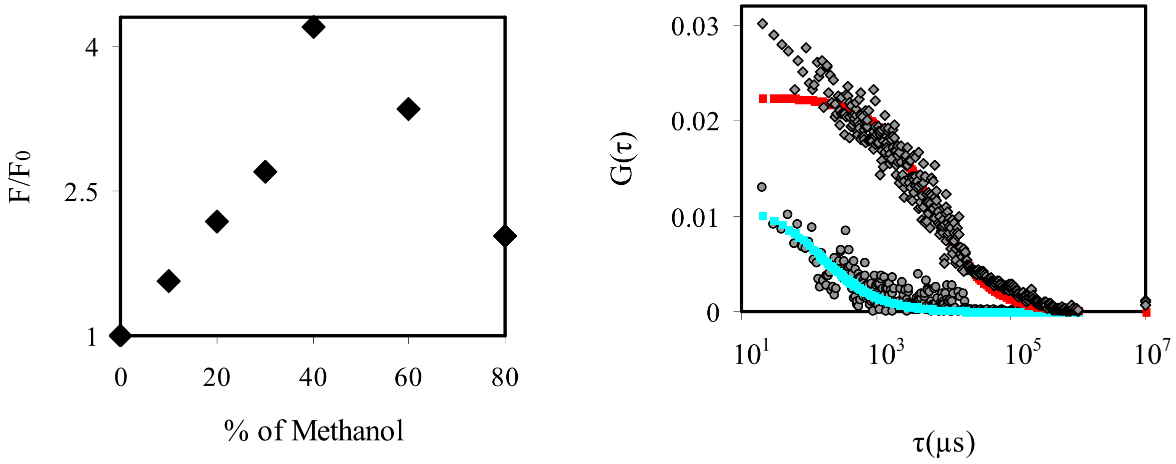

***Figure 3.7 A** Fluorescence intensity ratio of **PP1** with increasing amount of methanol in solvent mixture.(**B**) Autocorrelation function for **PP1** in water ($5.6\times1^{-7}$ M )(○) and in 80 % by volume methanol (◊)*

## 3.4 DISCUSSION AND CONCLUSION

The current work explores how the absorption and fluorescence properties of **PP1** change with ionic strength. By changing the size of the electrolyte ions (singly charged inorganic ions and organic ions), different spectroscopic behaviors were observed and studied. The absorption spectrum shows an isosbestic point for simple salt solutions but not for the surfactant ODTMA.

The wavelength of the isosbestic point shifts red with increase in the size and charge of the counterions. This observation indicates that the counterion complexes with the polyelectrolyte, forming a distinct spectroscopic signature/species.

A two state model was applied to simulate the absorption spectra of **PP1** in these solutions. This model assumes that equilibrium exists between one form, e.g. the free **PP1,** and a second form, e.g., the aggregated **PP1.** The two state model oversimplifies the actual case, i.e., it is likely that a distributions of aggregates exist at every ionic strength. Filtration and FCS studies showed that these new species formed are the aggregates of **PP1**. Nevertheless, it appears that the system can be divided into two subpopulations based on their absorption spectra.

The ionic strength affects the fluorescence of **PP1** also. At low ionic strength the fluorescence intensity of **PP1** increases with increasing ionic strength but eventually starts to decrease with further increase in the ionic strength. The aggregate species formed in the presence of inorganic and organic salt have higher quantum yields and higher radiative rates than **PP1** in water. As the ionic strength increases beyond a certain concentration the fluorescence decreases (figure 3.1), presumably because the large aggregates which form have poor solubility and precipitate from solution.

The ionic strength dependence of **OPP1** is qualitatively similar to **PP1**. In the presence of 1 M NaCl, no changes in the absorption and only a 15 % increase in the fluorescence intensity was observed. Filtration studies imply that aggregates of **OPP1** form in NaCl solution, however. In the presence of TBAF and ODTMA, the absorption spectrum of **OPP1** shifted red and its fluorescence increased by factor of 2 or 3. Further the species formed on addition of TBAF and ODTMA had higher radiative rates, trend similar for **PP1** observed in the presence of TBAF and

ODTMA. These observations suggest that the NaCl induced aggregates have weaker interchain attractions for **OPP1** than for **PP1**.

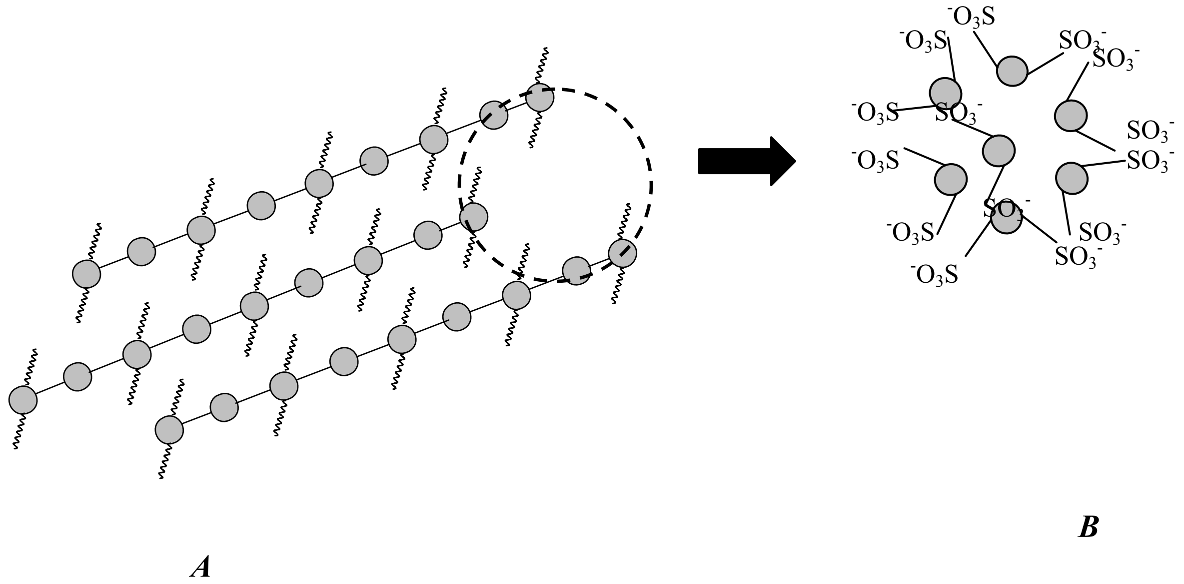

***Scheme 3.2*** *Representation of the type of aggregates of* ***PP1*** *in water (A). A projection along the columnar axis is depicted for* ***PP2*** *in water(B)*

Scheme 3.2 shows a model for the type of aggregates that might be formed in solutions of **PP1** and **OPP1**, by drawing from the structural work of Rulkens et al.[19] Based on the calculation performed using FCS data and the models proposed by Rulkens et al we believe that **PP1** forms cylindrical miceller aggregates in the presence of inorganic and organic salts and surfactants. In the absence of salt, the electrostatic repulsions of the polyelectrolytes inhibit aggregation in aqueous solutions at low concentration of the polymer. An increase in the ionic strength provides additional counter ions, such as $Na^+$, which screen the electrostatic repulsion between the polymer chains and the hydrophobic backbones tend to minimize the interaction with water molecules and therefore favor aggregation.

It has been reported in the literature that the PPP based polymers have rigid rod structure. In order to explore the affect of geometry on diffusion coefficient, three different shapes of polymer were assumed. The diffusion coefficient was calculated in the approximation that the polymer is a sphere, prolate ellipsoid or oblate ellipsoid. For oblate ellipsoid, the polymer of 58 nm length and width of 1.8 nm was used to calculate the area in the plane; this area was then used to find a radius for a circle of equivalent area to the ellipse. This radius (2.5 nm) and the thickness of the polymer strand (0.31nm) were used to calculate the geometric factor G(ρ); see equation 7. In addition, the volume of the oblate ellipsoid was calculated, and the parameter r was determined from the volume of the equivalent sphere (r=1.5 nm). With r and G(ρ) in hand, the diffusion coefficient was calculates to be D=7.2 x $10^{-5}$ $cm^2$/s. This value compares poorly with the experimental D=1.86x$10^{-6}$$cm^2$/s under dilute conditions obtained experimentally. Similar kind of analysis was done by approximating that the polymer is prolate ellipsoid. The diffusion coefficient was calculated to be 7.2 x $10^{-6}$ $cm^2$/s. This value also agrees poorly with the experimental value suggesting that polymer does not exist as a single strand species even in dilute solutions. For sphere, the volume the volume of the ellipsoid was calculated, and the parameter r was determined from the volume of the equivalent sphere (r=1.58 nm). Using this the diffusion coefficient of D=1.55x$10^{-6}$$cm^2$/s was computed which agrees very well with the experimental value.

If **PP2** forms cylindrical micelles, both the shape (axial ratio) and volume of the aggregates should be considered in modeling the diffusion coefficient. The volume factor is determined by the number of polymer strands in the aggregates. Assuming there are four strands in the aggregate and it behaves like prolate ellipsoid, the geometric factor is calculated by using b=1.2 nm (From studies by Rulken et al) and a=29.0 nm (length of the fully extended **PP2** is 58 nm). In addition, the volume of the prolate ellipsoid was calculated, and the parameter r was determined from the volume of the equivalent sphere (r=4.7 nm). Using this geometric factor and the effective radius of sphere diffusion coefficient is calculated using equation 6. Diffusion coefficient of 2.04 x $10^{-6}$ $cm^2/s$ is obtained which is very similar to what is obtained experimentally using FCS ($D=1.86x10^{-6}cm^2/s$) suggesting that **PP2** forms aggregate with at least four strands in it.

The optical changes in solutions of **PP1** and **OPP1** can be explained by the formation of aggregates with higher radiative rates, shown in Scheme 3.2. In the case of **PP1**, as the ionic strength increase the charge is screened more effectively, more and more strands come together and the effective conjugation length increases. This change causes the observed increase in the absorbance, the red shift in absorption spectrum, and the increase in the fluorescence intensity via the increased radiative rate. As the ionic strength further increases, very big aggregates are formed which can not stay in solution any longer because of their hydrophobic nature and the fluorescence intensity decreases. The effects in **OPP1** can be explained in a similar fashion; the only difference is that no downward trend is observed in the fluorescence even at 1 M NaCl indicating much higher ionic strength is required to precipitate out the **OPP1**.

## 3.5 ACKNOWLEDGEMENT

We acknowledge support from the U.S. National Science Foundation (CHE-0415457). We would like to thank Subhasis Chakrabarti for his help with lifetime measurements

## 3.6 REFERENCES

(1) Kim, S.; Jackiw, J.; Robinson, E.; Schanze, K. S.; Reynolds, J. R.; Baur, J.; Rubner, M. F.; Boils, D. *Macromolecules* **1998**, *31*, 964.

(2) Tan, C.; Pinto, M. R.; Schanze, K. S. *Chem.Comm.* **2002**, 446.

(3) Liu, B.; Yu, W.-L.; Lai, Y.-H.; Huang, W. *Chem. Commun.* **2000**, 551

(4) Thunemann, A. F.; Ruppelt, D. *Langmuir* **2001**, *17*, 5098.

(5) Chen, L.; McBranch, D. W.; Wang, H.-L.; Helgeson, R.; Wudl, F.; Whitten, D. G. *Proc. Natl. Acad. Sci. U.S.A.* **1999**, *96*, 12287.

(6) DiCesare, N.; Pinto, M. R.; Schanze, K. S.; Lakowicz, J. R. *Langmuir* **2002**, *18*, 7785.

(7) Harrison, B. S.; Ramey, M. B.; Reynolds, J. R.; Schanze, K. S. *J. Am. Chem. Soc.* **2000**, *122*, 8561.

(8) Zhang, C.; Braun, D.; Heeger, A. J. *J. Appl. Physics* **1993**, *73* 5177.

(9) Hide, F.; Diaz-Garcia, M. A.; Shwartz, B. J.; Anderson, M. R.; Pei, Q.; Heeger, A. J. *Science* **1996**, *273*, 1833.

(10) Chen, L.; McBranch, D. W.; Wang, R.; Whitten, D. *Chem Phys. Lett.* **2000**, *330*, 27.

(11) Heeger, P. S.; Heeger, A. J. *Proc. Natl. Acad. Sci. U.S.A.* **1999**, *96*, 12219.

(12) McQuade, D. T.; Pullen, A. E.; Swager, T. M. *Chem Rev* **2000**, *100*, 2537-74.

(13) Tan, C.; Pinto, M. R.; Schanze, K. S. *Chem. Commun.* **2002**, 446.

(14) Yu, G.; Gao, J.; Hummelen, J.; Wudl, F.; Heeger, A. J. *Science* **1995**, *270*, 1789.

(15) Bunz, U. H. F. *Chem. Rev.* **2000**, *100*, 1605-1644.

(16) Bastiansen, O.; Samdal, S. *J. Mol. Struct.* **1985**, *128*, 115.

(17) Halkyard, C. E.; Rampey, M. E.; Kloppenburg, L.; Studer-Martinez, S. L.; Bunz, U. H. F. *Macromolecules* **1998**, *31*, 8655-8659.

(18) Liu, T.; Rulkens, R.; Wegner, G.; Chu, B. *Macromolecules* **1998**, *31*, 6119.

(19) Rulkens, R.; Wegner, G.; Albrecht-Thurn, T. *Langmuir* **1999**, *15*, 4022.

(20) Bockstaller, M.; Kohler, W.; Wegner, G.; Fytas, G. *Macromolecules* **2001**, *34*, 6353.

(21) Bockstaller, M.; Kohler, W.; Wegner, G.; Vlassopoulos, D.; Fytas, G. *Macromolecules* **2001**, *34*, 6359

(22) Bhaskar, C.; Lai, Y.-H.; Valiyaveettil, S. *Macromolecules* **2001**, *34*, 6255

(23) Vetrichelvan, M.; Hairong, L.; Ravindranath, R.; Valiyaveettil, S. *J. Poly. Sci. Part. A* **2006**, *44*, 3763.

(24) Ravindranath, R.; Ajikumar, P. K.; Advincula, R. C.; Knoll, W.; Valiyaveettil, S. *Langmuir* **2006**, *22*, 9002

(25) Ravindranath, R.; Vijila, C.; Ajikumar, P. K.; Hussain, F. S. J.; Ng, K. L.; Wang, H.; Jin, C. S.; Knoll, W.; Valiyaveettil, S. *J. Phys. Chem. B* **2006**, *110*, 25958

(26) Kim, S.; Jackiw, J.; Robinson, E.; Schanze, K. S.; Reynolds, J. R.; Baur, J.; Rubner, M. F.; Boils, D.; *Macromolecules* **1998**, *31*, 964.

(27) Liu, M.; Kaur, P.; Waldeck, D. H.; Xue, C.; Liu, H. *Langmuir* **2005**, *21*, 1687.

(28) Liu, M.; Waldeck, D. H.; Oliver, A. M.; Head, N. J.; Paddon-Row, M. N. *Journal of the American Chemical Society* **2004**, *126*, 10778-10786.

(29) Morris, J. V.; Mahaney, M. A.; Hube, J. R. *J Phys Chem* **1976**, *80*, 969.

(30) Lakowicz, J. R. *Principles of Fluorescence Spectroscopy, 2nd Edition, Kluwer Academic/Plenum Publishers, NY* **1999**.

(31) Koppel, D. E. *Physical Review A* **1974**, *10*, 1938-1945.

(32) Leng, X. S., K.; Buffle, J. *J.Coll. Inter. Sci.* **2002**, *251*, 64.

(33) Magde, D.; Elson, E.; Webb, W. W. *Physical Review Letters* **1972**, *29*, 705-708.

(34) Pristinski, D.; Kozlovskaya, V.; Sukhishvili, S. A. *Journal of Chemical Physics* **2004**, *122*, 14907-14907.

(35) Van Rompaey, E.; Sanders, N.; Van Craenenbroeck, E.; Engelborghs, Y.; De Smedt, S. C.; Demeester, J. *Macromolecules* **2000**, *33*, 8280-8288.

(36) Yue, H.; Waldeck, D. H.; Xue, C.; Liu, H. *Manuscript in preparation*.

(37) Krichenvsky, O.; Bonnet, B. *Rep.Prog.Phys.* **2002**, *65*, 251-297.

## 3.7 SUPPLEMENTAL INFORMATION

### Two state Model

The observed absorption spectrum for **PP1** was fit to a sum of two spectra to obtain the relative amounts of the aggregate species and the equilibrium constants. Figure 3.8 gives an example of the fitting results for **PP1** in NaCl solutions. Figure 3.8A shows the theoretical absorption spectra for each of two species in the equilibrium reaction, and Figure 3.8B shows the change in concentration of the two species with increasing ionic strength.

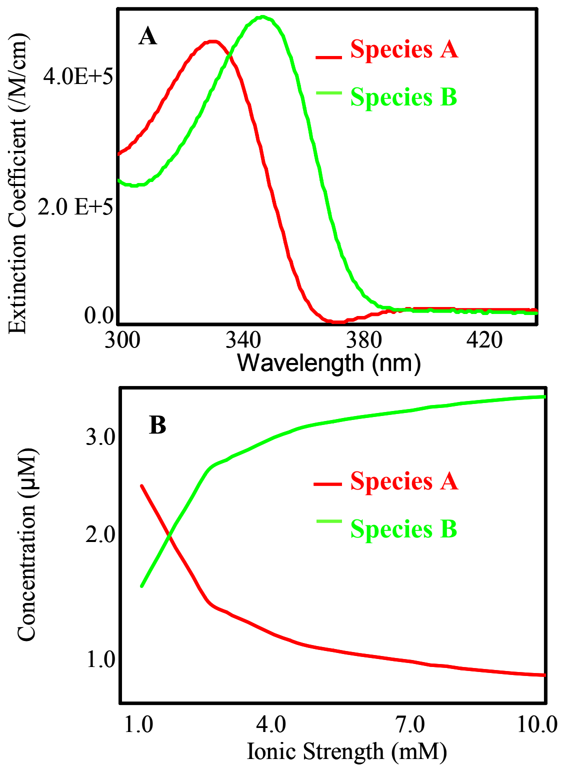

***Figure 3.8*** *Theoretical fit to a two state model for the absorption spectrum of **PP1** in LiCl solutions. **A**) Extinction coefficient (per repeat unit in the polymer) versus wavelength; **(B)** change of concentration versus ionic strength. Red line represents the species A and green line represents species B.*

### Ionic Strength Dependence

Figure 3.9 shows the fluorescence intensity ratio plot for **PP1** with LiCl, NaCl and KCl in water versus the ionic strength. The fluorescence quenching is found to be similar for all the cations.

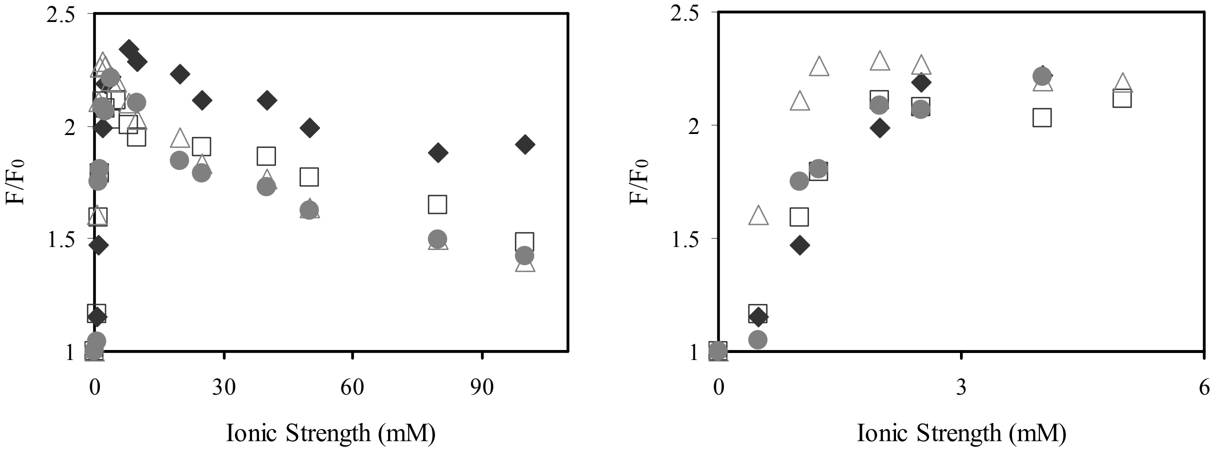

***Figure 3.9** **A** Fluorescence intensity ratio of **PP1** in LiCl (♦), NaCl (□), KCl (Δ) and CsCl (●) to **PP1** in water versus the ionic strength.(B) Expanded Fluorescence intensity ratio of **PP1** in the presence of different salts.*

The effect of different anions was studied by performing experiments with sodium iodide and sodium phosphate (figure 3.10). The trend was similar, but comparatively more quenching was observed for NaCl than NaI and sodium phosphate.

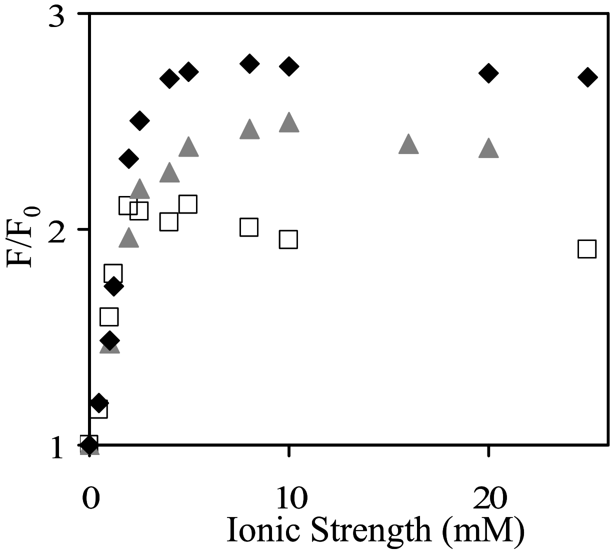

***Figure 3.10** Fluorescence intensity ratio of **PP1** in NaCl (□), sodium phosphate buffer at pH = 7 (▲) and NaI (♦) verse **PP1** in water.*

The ionic strength dependence of the fluorescence lifetime on TBAF concentration for two emission wavelengths is shown in figure 3.11. The trend was found to be similar to $F/F_0$ versus ionic strength.

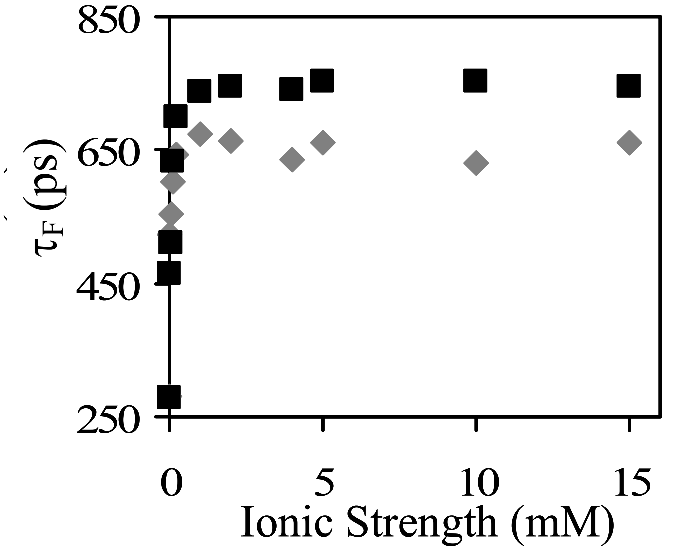

***Figure 3.11*** *The average lifetime $\tau_F$ of* ***PP1*** *as a function of TBAF ionic strengths. The fluorescence decay was excited at 326 nm and the emission was collected at 420 nm (♦) and 500 nm (■).*

**Table 3.3 Fluorescence quantum yields ($\phi$) and correlation times ($\tau_F$) for PP1 in different solution conditions**

| Sample | $\phi$ | $\tau_F$ (ps) | $R_H$ (nm) |
|---|---|---|---|
| **PP1** | 0.11 | 340 | 1.3 |
| **PP1**+10 mM NaCl | 0.38 | 839 | 2.3 |
| **PP1**+4 mM TBAF | 0.65 | 727 | 10.1 |
| **PP1**+50mM ODTMA | 0.42 | 583 | 14.2 |
| **PP1** in 80 % Methanol | 0.28 | 432 | 56.6 |

The time constant $\tau_F$ is the correlation time obtained from the best fit of a double exponential model, namely $I(t) = A_1 \exp(-t/\tau_1) + (1-A_1) \exp(-t/\tau_2)$. For this model the correlation time is given by $\tau_F = A_1 \tau_1 + (1-A_1) \tau_2$.

# CHAPTER 4 THE FLUORESCENCE QUENCHING MECHANISM OF A POLYPHENYLENE POLYELECTROLYTE WITH OTHER MACROMOLECULES: CYTOCHROME C AND DENDRIMERS.

*This work has been published as M. Liu, P. Kaur, D. H. Waldeck, C. Xue, H. Liu, Langmuir, 21, 1687, (2005).*

This study investigates the fluorescence quenching of a polyphenyl based polyelectrolyte by positively charged macromolecules (proteins and dendrimers). This work shows that the fluorescence quenching of the dendrimer materials does not involve energy transfer or electron transfer, but is correlated to the overall charge on the dendrimer and its size. The quenching is hypothesized to result from conformational changes that occur upon binding the polyelectrolyte to the protein, or dendrimer. This mechanism is qualitatively different from that invoked for small molecule analytes.

## 4.1 INTRODUCTION

Conjugated polyelectrolytes offer great possibilities as water soluble fluorescent materials[1-3] and sensors,[4-9] especially for small molecule analytes.[10] A number of groups are active in using conjugated polymers as fluorescence probes and this field has been reviewed recently.[11,12] Typically, a trap-site is created when an analyte molecule binds to the polymer, sometimes via a receptor, and quenches the emission by electron transfer or energy transfer. The sensitivity of these materials arises from the presence of many binding sites, of which only one or a few need to be occupied to quench the polymer's intrinsic fluorescence. More recently, conjugated polyelectrolytes are being used for the detection of proteins[7] and oligonucleotides,[8,9] however the mechanism of fluorescence quenching has not been as thoroughly studied.

Fluorescence quenching of a polyelectrolyte by binding with another macromolecule can occur from a number of different processes, but three are likely to dominate. These are electron transfer, energy transfer, and enhancement of the polymer's self-quenching, *eg.* internal conversion. Electron transfer quenching is often invoked with these sensor materials and can be controlled by changing the analyte's redox characteristics. Energy transfer quenching should depend strongly on the polyelectrolyte and the analyte's spectral characteristics, whether it is a Förster mechanism or a Dexter mechanism.[13] A third possibility for the quenching mechanism is a binding event that induces a conformational change in the polymer which enhances its intrinsic nonradiative rate constant.[14-16] In this case the quenching would not depend on the redox and spectral properties of the analyte, but would depend on conformational features of the binding. Lastly, these mechanisms are not exclusive; they could operate simultaneously.

This study compares the quenching mechanism for the protein cytochrome *c* with a polyphenylene polyelectrolyte to that observed for similarly sized dendrimers with the same polyelectrolyte. The fluorescence of poly[sodium 2,5-(3-sulfopropoxy)-1,4-phenylphenylene] (identified as **PP1**) is quenched by positively charged dendrimers and the protein cytochrome *c*. Cytochrome *c* is a positively charged heme protein that acts as an electron carrier in the respiratory chain of aerobic organisms[17] and has been implicated in apoptosis.[18] A recent report by Fan[7] demonstrated the utility of using a PPV based polyelectrolyte (poly[lithium 5-methoxy-2-(4-sulfobutoxy)-1,4-phenylenevinylene) to detect cytochrome *c* and concluded that the quenching occurs by electron transfer in that case.

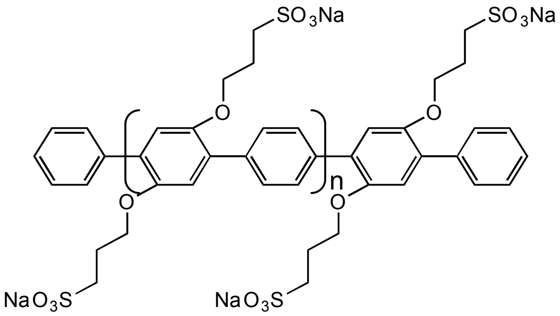

**PP1**

## 4.2 EXPERIMENTAL

Poly[2,5-bis(3-sulfonatopropoxy)-1,4-phenylene-alt-1,4-phenylene) was prepared in a manner similar to that reported in the literature (details of the preparation are given in the Supplemental Information).[1] The molecular weight was found to be 9900 and the polydispersity was 1.26, as determined by size exclusion chromatography.[10]

Both proteins and dendrimer materials were studied as analytes. The ferric cytochrome *c* was purchased from Sigma and purified in the manner described previously.[19] The ferric material was chemically reduced to ferrous with sodium dithionate.[20] The myoglobin was purchased from Sigma and used without further purification. The PAMAM (polyamidoamine) and the DAB (DAB-Am-32, Polypropylenimine dotriacontaamine Dendrimer, Generation 4.0) dendrimer materials were obtained from Dendritech and Sigma-Aldrich, respectively.

Steady-state absorption spectra were measured on an Agilent 8453 spectrometer and the steady-state emission spectra were measured on a Spex Fluorolog 0.22 m double spectrometer. The time-resolved fluorescence data were collected using the time-correlated single photon counting method; see reference [20] for details of the apparatus.

## 4.3 RESULTS

### 4.3.1 Quenching with Proteins

The steady-state electronic spectra of **PP1** and cytochrome *c* are presented in Figure 4.1. The absorption spectrum of **PP1** has a $\lambda_{max}$ at 338 nm, significantly blue of the Soret band of the cytochrome *c*. The shift in absorption wavelength of cytochrome *c* is consistent with the native state of the ferrous and ferric forms of the protein. In aqueous solution at pH=7 (20 mM phosphate buffer) **PP1** is highly fluorescent. The fluorescence spectrum in Figure 4.1 was taken with an excitation wavelength of 338 nm. The overlap of the polyelectrolyte's emission band with the absorption band of the protein shows that energy transfer quenching is possible for this system.

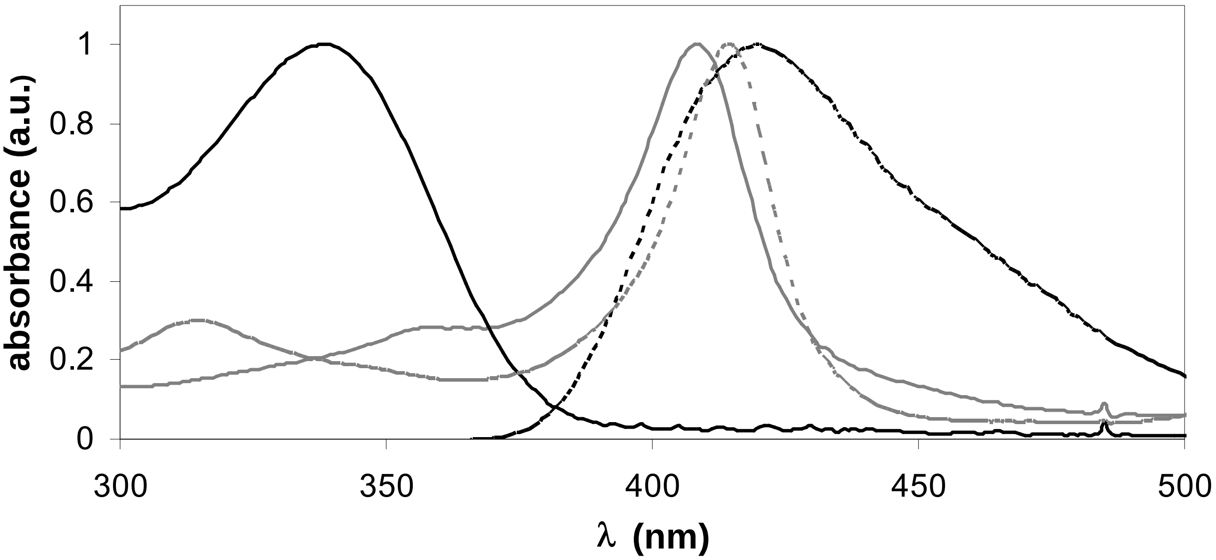

***Figure 4.1*** *The absorption spectrum (solid black line) and fluorescence spectrum (dashed black line) of the polymer are shown. The absorption spectrum of ferric (solid gray line) and ferrous (dashed gray line) are also shown.*

Upon addition of cytochrome *c* to a solution of **PP1**, the fluorescence emission intensity decreases. Figure 4.2A shows Stern-Volmer plots for a 0.3 μM solution of **PP1** with cytochrome *c* and another heme protein, myoglobin. At low concentrations of analyte good linear fits to the data are found.[21] Table 4.1 presents the Stern-Volmer constants that are obtained by analyzing these data. The quenching of the emission by ferric cytochrome *c* is greater than that by ferrous cytochrome *c*, and the quenching by cytochrome *c* is stronger than that for myoglobin; a finding that correlates with the smaller surface charge for myoglobin.

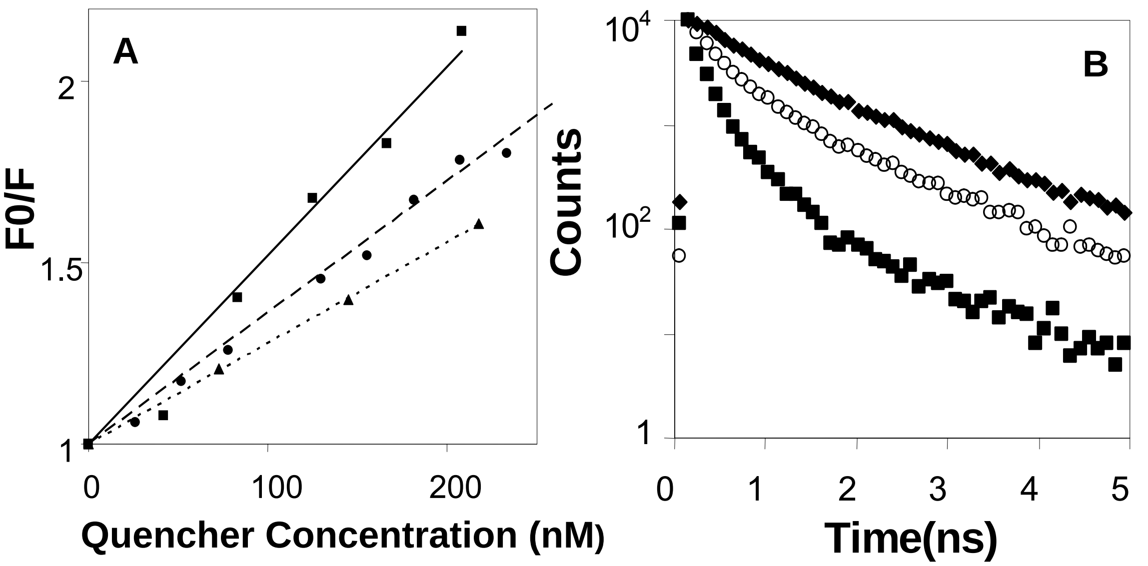

***Figure 4.2*** *Panel A shows Stern-Volmer plots for* ***PP1*** *with ferric cytochrome c (squares), ferrous cytochrome c (circles) and myoglobin (triangles). The lines show fits corresponding to the Stern-Volmer constants in Table 1. Panel B shows the fluorescence decay of* ***PP1*** *with cytochrome c at 0.0 M (diamonds), 0.46 μM (circles), and 0.92 μM (squares).*

Figure 4.2B shows the fluorescence decay curves for solutions of **PP1** with cytochrome *c*. The fluorescence decay of **PP1** in aqueous solution is nonexponential with an average fluorescence lifetime of 857 ps. In a methanol/water mixture the same polymer sample displays a single exponential fluorescence decay law (see Figure 4.3B). Because the polymer is highly soluble in both systems, the different behavior is not ascribed to fractionation of the sample, but is believed to arise from differences in **PP1**'s conformation in the two solvents. As cytochrome *c* is added to the aqueous **PP1** solution, the fluorescence decay profile becomes more highly nonexponential. A fit of the data to a sum of exponentials shows that the fast relaxation component (*ca* 100 ps lifetime) increases in amplitude as the concentration of cytochrome *c* increases. Although the lifetime distribution appears to be inhomogeneous, the short time component was ascribed to quenching of the polymer emission by static quenching.

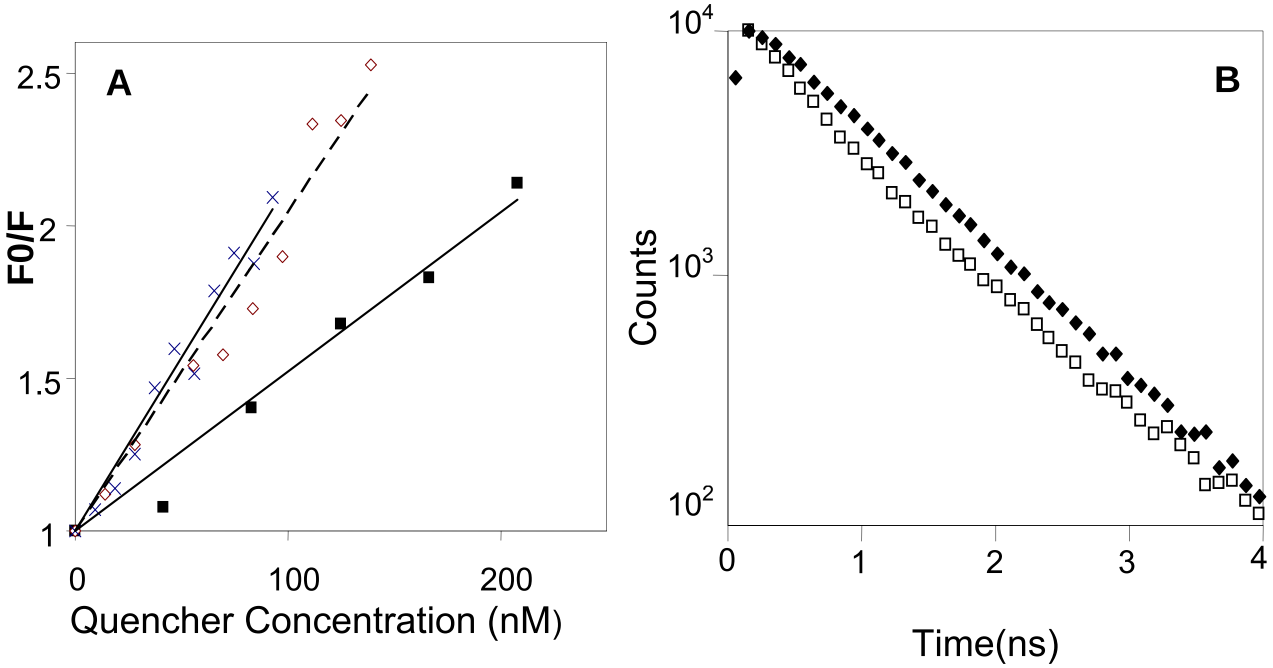

**Figure 4.3** *Panel A shows Stern-Volmer plots for* ***PP1*** *with different macromolecular quenchers: DAB 4G (X), PAMAM 3G (diamonds), and ferric cytochrome c (squares). The lines show fits corresponding to the Stern-Volmer constants in Table 1. Panel B shows the fluorescence decay law of* ***PP1*** *in water/methanol mixtures at PAMAM 3G concentrations of 0.0 M (diamonds) and 0.21μM (squares).*

The quenching mechanism for the polymer with cytochrome *c* was analyzed in several ways. Table 4.1 shows that the quenching of the ferrous and ferric forms of the protein are similar, suggesting that electron transfer quenching is not dominant. The influence of molecular geometry on the quenching was studied by denaturing the protein. The ferric form of the protein was heated to 353 K and cooled back to room temperature (denaturation was verified by measuring CD and UV/visible spectra). This form of the protein also quenched the polymer fluorescence but with about 71% the efficiency of the native protein, $K_{SV} = 3.7 \times 10^6\ M^{-1}$. In a second experiment, apocytochrome *c* was prepared.[22] The CD spectrum for this form of the protein was similar to that reported earlier, and it did not display any heme features, as expected. The $K_{SV}$ for the apocytochrome c was $6.3 \times 10^5\ M^{-1}$, which is about six times smaller than that for the denatured protein and eight times smaller than that for the native protein. Assuming that the **PP1**'s self-quenching and energy transfer quenching are independent relaxation processes, comparison of these two $K_{SV}$ values suggest that the energy transfer quenching mechanism is more important than the conformational quenching mechanism for the denatured cytochrome *c*.[23]

**Table 4.1 The Stern-Volmer constants for PP1 with some different macromolecules.**

| **Protein Analyte** | **$K_{SV}$ ($M^{-1}$)** | **Net Charge** | **Size** |
|---|---|---|---|
| $Fe^{2+}$- cytochrome c | $0.36 \times 10^7$ | +5e | 14 $nm^3$ |
| $Fe^{3+}$- cytochrome c | $0.52 \times 10^7$ | +6e | 14 $nm^3$ |
| $Fe^{3+}$- myoglobin | $0.28 \times 10^7$ | 0 | 20 $nm^3$ |
| PAMAM 3G | $1.0 \times 10^7$ | +32e | 24 $nm^3$ |
| DAB 4G | $1.1 \times 10^7$ | +32e | 5.0 $nm^3$ |

### 4.3.2 Quenching with Dendrimers

Figure 4.3A shows Stern-Volmer plots for **PP1** with PAMAM 3G and DAB 4G dendrimers. Interestingly the quenching by the dendrimers is even stronger than that of the cytochrome *c*. Each of these dendrimers contains 32 ammonium groups in its outer shell and they are expected to bind strongly to **PP1**. Figure 4.3B shows the fluorescence decay of **PP1** with PAMAM 3G in methanol/water solutions. These data reveal that the quenching mechanism is static; i.e., the unbound polyelectrolyte has a single exponential decay law with a 843 ps lifetime and the bound polyelectrolyte has a 210 ps fast component lifetime. The relative amplitude of the two components changes with PAMAM 3G concentration, but the lifetimes are the same. The change in quenching efficiency for each of the analytes correlates with the expected change in electrostatic binding for the macromolecules (see Table 4.1). Such a correlation was identified by Wang et al[24] for binding of PPV with differently charged viologens.

Although the dendrimer molecules PAMAM 3G and DAB 4G have the largest Stern Volmer constants, they do not possess visible chromophores. A Förster energy transfer quenching mechanism between **PP1** and the analyte requires an overlap of **PP1**'s emission spectrum with the analyte's absorption spectrum, and hence this mechanism is clearly not operative for the dendrimer molecules. A comparison of the absorption spectra are provided in the Supplemental Information.

An electron transfer quenching mechanism was also discounted. The dendrimers do not possess good electron acceptor groups, but possess primary and tertiary amines which might quench the fluorescence by an electron transfer mechanism. The importance of this mechanism was probed by changing the pH of the solution. A titration curve of PAMAM 3G dendrimer showed that the ammonium groups on the dendrimer are almost fully ionized at pH 7 (≥30 of the 32 groups). To assess the importance of this mechanism the pH was raised to 12 in order to reduce the surface charge and generate more amines. In this latter case, no quenching was found. At intermediate pH values, between 7 and 12, the Stern Volmer constant decreases from its value at pH=7 because the net positive charge on the dendrimer surface is decreasing. By lowering the solution pH, it is possible to fully protonate the surface amines and significantly protonate the 'interior' tertiary amines of the dendrimer. The Stern-Volmer constants do not change much, less than a factor of 2, as the pH is lowered - $K_{SV} = 6.8 \times 10^{6}\ M^{-1}$ at pH=4 and $K_{SV} = 1.8 \times 10^{7}\ M^{-1}$ at pH=2.15. These studies show that the quenching is not sensitive to amine availability (hence electron transfer quenching is not important) but is sensitive to the dendrimer charge.

The data in Table 4.1 show a correlation of the quenching efficiency with the positive charge on the analyte, however the quenching also depends on the analyte's size. This dependence is evident when comparing different generations of the same dendrimer material, for example the quenching efficiency of the PAMAM 3G dendrimer with that of the PAMAM 0G dendrimer. By increasing the PAMAM 0G dendrimer concentration to eight times that of PAMAM 3G the same equivalents of ammonium groups are made available to **PP1**, however the quenching efficiency is very low. The $K_{SV}$ for the PAMAM 0G is $<3.3x10^{3}$ $M^{-1}$. If this value is modified to account for the number of ammonium groups (multiplied by eight), it is $<2.7x10^{4}$ $M^{-1}$, more than 400 times smaller than that found for PAMAM 3G. The Stern-Volmer constant observed for PAMAM 0G is also much smaller than that obtained for the common electron transfer quencher, methylviologen (for which $K_{SV}$ was found to be $1.0x10^{6}$ $M^{-1}$), corroborating the unimportance of electron transfer quenching for PAMAM.

## 4.4 DISCUSSION AND CONCLUSION

These observations demonstrate that the fluorescence quenching of conjugated polyelectrolyte **PP1** by charged macromolecules need not involve the typically used mechanisms of electron transfer or energy transfer. The dependence of the quenching efficiency on the dendrimer size and charge suggests that the polyelectrolyte changes conformation upon binding. When the dendrimer size is small (zero or one generation) the charged units on the dendrimer probably interact with only two sequentially charged units on the polymer backbone. The larger analyte molecules allow for more interactions with the **PP1** backbone, so that the **PP1** can distort and/or 'wrap' itself onto the analyte's surface. This process should cause conformational changes in the **PP1** and create conditions for enhanced coupling between the electronically excited state and the ground state, increasing the internal conversion rate.

This work investigated the mechanism of fluorescence quenching in a conjugated polymer electrolyte when it binds with other macromolecules, in particular proteins and dendrimers. The binding constants can be quite large, supporting the promise of these materials as fluorescence sensors. A comparison of the different analytes confirms that the quenching mechanism is controlled by the electrostatic interactions between the macromolecular analytes and the polyelectrolyte. This study demonstrates that electron transfer and electronic energy transfer need not be present to cause quenching. The dependence of the quenching efficiency for a particular polyelectrolyte on the size and charge of the dendrimer analyte suggests a mechanism in which the polyelectrolyte has multiple 'contacts' with the dendrimer surface. We hypothesize that the multiple interactions between the polymer and the dendrimer changes the polymer's conformation and enhances the internal conversion, 'self-trapping'.

## 4.5 ACKNOWLEDGEMENT

D.H.W. acknowledges support from the U.S. National Science Foundation (CHE-0111435).

# 4.6 REFERENCE

(1) Kim, S.; Jackiw, J.; Robinson, E.; Schanze, K. S.; Reynolds, J. R.; Baur, J.; Rubner, M. F.; Boils, D.; *Macromolecules* 1998, *31*, 964.

(2) Tan, C.; Pinto, M. R.; Schanze, K. S. *Chem.Comm.* 2002, 446.

(3) Liu, B.; Yu, W.-L.; Lai, Y.-H.; Huang, W. *Chem. Commun.* 2000, 551

(4) Chen, L.; McBranch, D. W.; Wang, H.-L.; Helgeson, R.; Wudl, F.; Whitten, D. G. *Proc. Natl. Acad. Sci. U.S.A.* 1999, *96*, 12287.

(5) DiCesare, N.; Pinto, M. R.; Schanze, K. S.; Lakowicz, J. R. *Langmuir* 2002, *18*, 7785.

(6) Harrison, B. S.; Ramey, M. B.; Reynolds, J. R.; Schanze, K. S. *J. Am. Chem. Soc.* 2000, *122*, 8561.

(7) Fan, C.; Plaxco, K. W.; Heeger, A. J. *J Am Chem Soc.* 2002, *124*, 5642.

(8) Gaylord, B. S.; Heeger, A. J.; Bazan, G. C. *Proc. Nat. Acad. Sci.* 2002, *99*, 10954-10957.

(9) Kushon, S. A.; Ley, K. D.; Bradford, K.; Jones, R. M.; McBranch, D.; Whitten, D. *Langmuir* 2002, *18*, 7245-7249.

(10) Zhou, Q.; Swager, T. M. *J. Am. Chem. Soc.* 1995, *117*, 12593-12602.

(11) McQuade, D. T.; Pullen, A. E.; Swager, T. M. *Chem Rev* 2000, *100*, 2537-74.

(12) Swager, T. M. *Acc. Chem. Res.* 1998, *31*, 201.

(13) Lacowitz, J. R. *Principles of Fluorescence Spectroscopy,Plenum Press NY* 1983.

(14) Huser, T.; Yan, M.; Rothberg, L. *Proc. Natl. Acad. Sci. U.S.A.* 2000, *97*, 11187.

(15) Sluch, M. I.; Godt, A.; Bunz, U. H. F.; Berg, M. A. *J. Am. Chem. Soc.* 2001,, *123*, 6447.

(16) Hu, D. H.; Yu, J.; Barbara, P. F. *J. Am. Chem. Soc.* 1999, *121*, 6936.

(17) Moore, G. R.; Pettigrew, G. W. *Cytochromes c, Evolutionary, Structural and Physicochemical Aspects; Springer-Verlag: Berlin, Germany,* 1990.

(18) Dove, A. *Nature Biotech.* 2001, *19*, 615.

(19) Yamamoto, H.; Liu, H.; Waldeck, D. H. *Chem. Commun. B* 2001, 1032.

(20) Trewhella, J.; Carlson, V. A. P.; Curtis, E. H.; Heidorn, D. B. *Biochemistry* 1988, *27*, 1121.

(21) Lavigne, J. J.; Broughton D. L. ; Wilson, J. N.; Erdogan, B.; Bunz, U. H. F. *Macromolecules* 2003, *36*, 7409-7412.

(22) Fisher, W. R.; Taniuchi, H.; Anfinsen, C. B. *J. Biol. Chem.* 1973, *248*, 3188.

(23) Kim, I. B.; Dunkhorst, A.; Bunz, U., H. F. *Langmuir* 005, *21*, 7985-7989.

(24) Wang, D.; Wang, J.; Moses, D.; Bazan, G. C.; Heeger, A. J. *Langmuir* 2001, *17*, 1262.

# 4.7 SUPPLEMENTAL INFORMATION

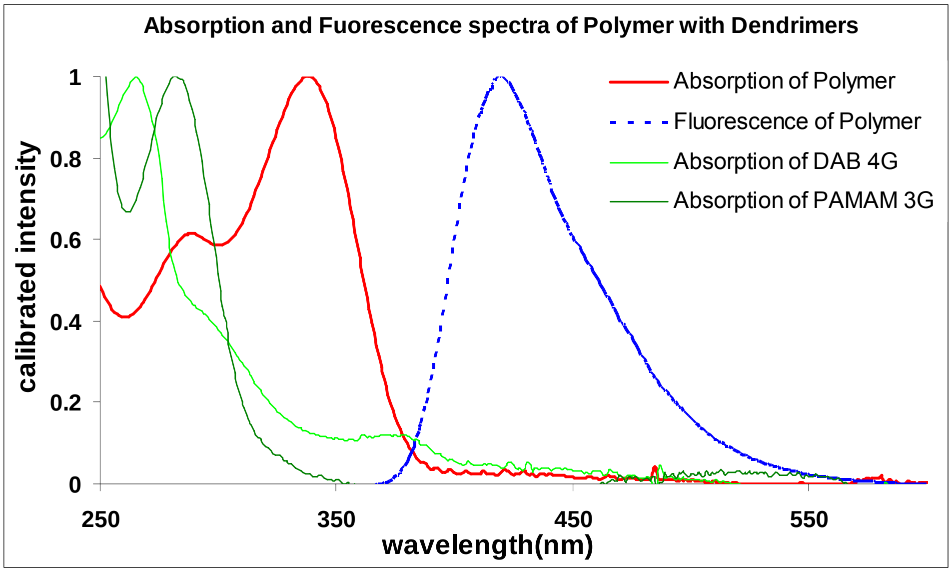

***Figure 4.4*** *The spectra shown below demonstrate that the dendrimer absorption spectrum is blue shifted from that of the* ***PP1*** *polyelectrolyte.*

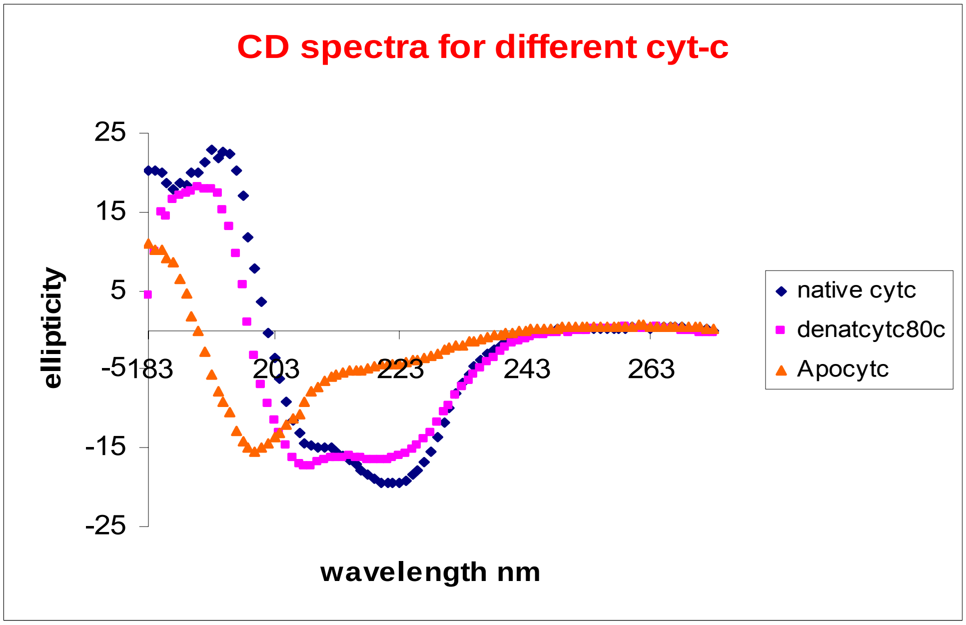

***Figure 4.5*** *Shown below are CD spectra for the native cytochrome c, denatured cytochrome c, and the apocytochrome c.*

# CHAPTER 5 DEPENDENCE OF POLYPHENYLETHYNYLENE POLYELECTROLYTE'S FLUORESCENCE QUENCHING ON THE ELECTROSTATIC AND HYDROPHOBIC PROPERTIES OF THE QUENCHER

This study investigates the changes in sensitivity and optical properties of a polyphenylethynylene (**PP2**) based polyelectrolyte by positively charged and neutral macromolecules. This work shows that the change in the fluorescence yield of **PP2** can arise from a number of factors, including electrostatic, hydrophobic and energy transfer interactions with the quencher and also changes in the solution conditions such as concentration and ionic strength. This fluorescence quenching is attributed to the formation of aggregates that form upon addition of different quenchers to **PP2** solution and/or the solution conditions. The extent of aggregation of **PP2** is shown to depend on the type of interaction between **PP2** and quencher, the concentration of **PP2** and the ionic strength of the solution.

# 5.1 INTRODUCTION

In recent years conjugated polymer materials have been exploited as enabling materials for new technologies and applications, e.g. light-emitting diodes,[1] lasers,[2] and solar cells.[3] One of these potential applications aims to exploit their fluorescence yield's sensitivity to minute quantities of a quencher to create biosensors. [4-8] The binding of quencher to the polymer creates a trap site which then quenches the fluorescence via energy transfer, electron transfer or due to conformational changes induced on binding to the quencher. This phenomenon has commonly been referred to as molecular wire effect in literature [9-11]

A number of conjugated polymer materials are fluorescent (PPV, PPP, polythiophenes, and others) and have been demonstrated to perform as sensing agents for chemical and biological molecules.[12-21] An important development is the use of anionic functionalities on the polymer backbone to make the materials water soluble and useful for biological sensing. Typically, these anionic functionalities are designed to correspond to a bound, or associated, analyte species that quenches the excitation. The bulk of the research effort on these materials has explored the ability of different polymer backbones and receptor strategies to sense the macromolecules, whereas the fluorescence quenching mechanism and the factors that affect the optical properties are still not very clear. Fan et al[22] showed that the fluorescence quenching of PPV based polyelectrolyte by the protein cytochrome-*c* arises from a combination of ultrafast photoinduced electron transfer and the formation of bound complexes between cationic and anionic polyelectrolytes. Liu et al.[19] showed that the quenching in polyphenylethynylene based polyelectrolyte results from conformational changes that occur upon binding the polyelectrolyte to the protein, dendrimer etc. and further showed that electron and energy transfer mechanism need not be present. From such studies it is clear that complex formation between the polymer and the analyte plays an important role in fluorescence quenching of the polyelectrolytes. Recently Kim et al[23] demonstrated fluorescence quenching of PPE based polyeletrolytes and oligomers by a number of analytes such as histones, lysozymes, myoglobin, hemoglobin etc. They showed that the net negative charge of the PPE plays a significant role but is not the only factor in the interaction of proteins with these polyelectrolytes. A number of factors such as electrostatic, hydrophobic interactions, electron transfer, energy transfer etc. are likely to contribute to the fluorescence quenching of these polyelectrolytes. Sometimes one factor is a dominant contributor to the fluorescence quenching and sometimes a combination of factors is important. Hence, it is important to understand how each of these factors affects the sensitivity of these polyelectrolytes towards the presence of quencher.

This work reports how the fluorescence quenching of a polyphenylethynylene based polyelectrolyte (**PP2**) changes in the presence of different macromolecules (proteins, dendrimers and surfactants) and under different solution conditions (concentration and ionic strength). The change in the optical properties and relative fluorescence quantum yield of **PP2** in the presence of different macromolecules is explained by the different kind of interactions that are present between **PP2** and macromolecules. The fluorescence quenching in the case of protein and dendrimers quencher is attributed to the formation of polymer aggregates via electrostatic and hydrophobic interactions between multiple polymer strands and the quencher molecules. The affect of solution condition on the sensitivity of **PP2** has been studied by varying the concentration of polymer and ionic strength of solution.

# 5.2 EXPERIMENTAL

Material: Poly[2,5-bis(3-sulfonatopropoxy)-1,4-phenylethynylene-alt-1,4-polyphenylene ethynylene] (identified as **PP2**) is a polyelectrolyte with two negative charges per repeat unit and was prepared in a manner similar to that reported in the literature.[24]Cytochrome-*c* was bought from Sigma and was used without further purification. PAMAM-3G was bought from Dendritech, Inc. and protonated using trifluoroacetic acid. Six-arm poly(ethylene oxide) hydroxy terminated, dipentaerythritol Core (PEG-OH), M. Wt. 12 KDa was purchased from Polymer Source Inc. DEM-3.5 G was a gift from Professor T. Chapman at University of Pittsburgh. Size exclusion chromatography[25] was used to determine the molecular weight of **PP2** in DMSO (a good solvent), 38,100 Da with a polydispersity of 3.04. The experimental polymer solution was highly diluted ($10^{-6}$~$10^{-8}$ M in terms of polymer repeat unit). All concentrations in this paper are reported in terms of polymer repeat unit. At these concentrations the effect of the polymer on solution properties, such as viscosity, can be neglected.

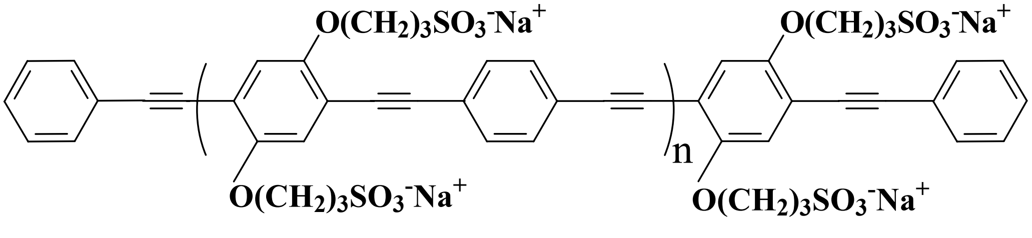

***Figure 5. 1*** *Chemical structure of PP2*

Steady state spectroscopy: Steady-state absorption spectra were measured on an Agilent 8453 spectrometer and the steady-state emission spectra were measured on a Spex Fluorolog 0.22 m double spectrometer.

*Stern-Volmer Constant:* The Stern-Volmer constants were obtained using the Stern-Volmer equation[26] described as follows.

$$\frac{F_0}{F} = 1 + K_{sv}[Q] \tag{5.1}$$

with $F_0$ being the fluorescence intensity of the conjugated polymer by itself and $F$ being the fluorescence intensity of the conjugated polymer after addition of a given concentration of quencher $[Q]$. $K_{sv}$ is the Stern-Volmer constant and can be extracted from the slope of the graph that plots $F_0/F$ versus quencher concentration with intercept 1. The Stern-Volmer constants reported in this paper were obtained by fitting the data at very low quencher concentration ranging from 0- 0.4 μM.

*Time dependent fluorescence spectroscopy:* The time-resolved fluorescence data were collected using the time-correlated single photon counting method.[19] The instrument response function was measured using a sample of colloidal $BaSO_4$. The samples were excited at 438 nm using a diode laser (PIL043, A.L.S. GmbH) and the emission was collected at different wavelengths. The fluorescence decay curves were fit by a convolution and compare method using IBH-DAS6 analysis software. Other details of the TCSPC apparatus can be found in reference 27.

*Fluorescence Correlation Spectroscopy (FCS):* FCS is a non-invasive single molecule method which obtains dynamic and kinetic information by following the fluctuation trajectory of fluorescence about the equilibrium state.[28-32] FCS was performed on a home made FCS instrument based on a Zeiss IM35 inverted microscope. Details of the instrumentation will be provided elsewhere.[33] The sample was excited at 438 nm through an objective lens (Olympus UPlanfluor 40X/1.30 Oil) and the fluorescence was collected by the same lens. The concentrations of the polymer solutions were controlled to be $5.2 \times 10^{-8}$ M and $2.5\times 10^{-6}$ M. To avoid photobleaching and optical trapping, the laser power was kept low, 24 μW, as measured at the front of the objective lens. Each measurement lasted 2 to 5 min, during which the time trajectory of fluorescence was monitored and only those having stable fluorescence intensity were kept. The corresponding autocorrelation function G(t) was fit by equation (2)

$$G(t) = \frac{1}{\overline{N}}\left(1+\frac{t}{\tau_D}\right)^{-1}\left(1+\frac{\omega_{xy}^2\, t}{\omega_z^{\,2}\,\tau_D}\right)^{-1/2} \tag{5.2}$$

to extract the correlation time $\tau_D$. $\overline{N}$ is the average number of fluorescent molecules in the focal volume; $\omega_{xy}$ is the radius of the focal spot in the transverse direction, and $\omega_z$ is the Rayleigh range of the excitation beam (see reference 34 for details relating to equation 2). The correlation time $\tau_D$ is related to the translational diffusion coefficient $D$ of the fluorophore by

$$\tau_D = \frac{\omega_{xy}^2}{4D} \tag{5.3}$$

The apparatus was calibrated and tested using a 10 nM Rhodamine 6G aqueous solution, assuming the diffusion coefficient $D = 4.14\times10^{-6}$ cm$^2$ s$^{-1}$.[35] The Stokes-Einstein approximation, equation (4) was used to extract the hydrodynamic radius $R_H$ from the measured diffusion coefficient

$$D = \frac{k_B T}{6\pi\eta R_H} \tag{5.4}$$

where $\eta$ is the shear viscosity, $T$ is the temperature and $k_B$ is Boltzmann's constant.

# 5.3 RESULTS AND DISCUSSION

It has been reported in the literature that the photophysical properties of polyphenyethynylene based conjugated polymers change with the temperature, concentration, ionic strength and solution environment.[36] The recent study by Kaur et al[36] has shown that the PPE based polyelectrolytes exist as independent strands at low concentration in good solvent and they aggregate at high concentrations and in the presence of salts, causing the fluorescence to quench. Figure 5.2 shows the variation of emission spectrum of **PP2** with concentration and ionic strength. **PP2** exists as individual polymer strands at very low concentration (~$10^{-8}$ M) and is aggregated at higher concentration (~$10^{-6}$ M). Similarly **PP2** aggregates at higher ionic strength and the fluorescence is highly quenched (Figure 5.2).

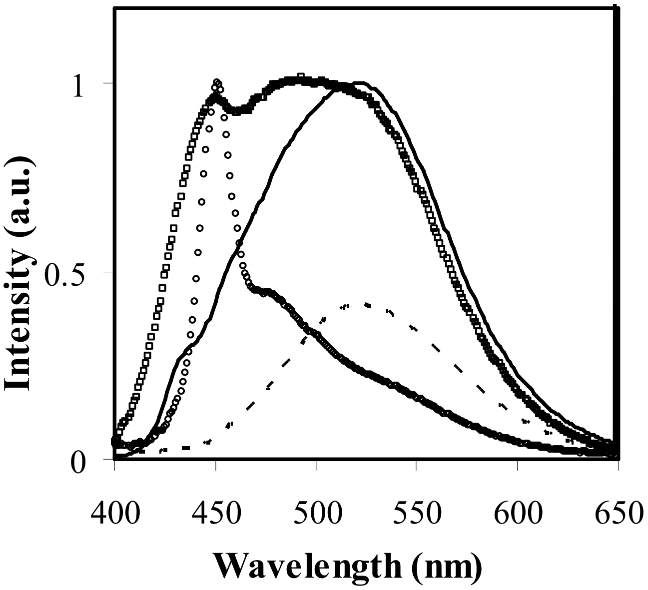

***Figure 5.2*** *Emission spectra for* ***PP2*** *in water at different concentrations (2.0×10-6(—), 8.8×10-8(□), 1.0×10-8 (○) M) and at 50 mM Na3PO4 at 2.0×10-6* ***PP2*** *concentration (----)*

### 5.3.1 Quenching of PP2 by Cytochrome-c

Fluorescence quenching experiments were done at different concentrations of **PP2** with ferric cytochrome-*c*. Figure 5.3A shows the dependence of the Stern-Volmer constant on the concentration of **PP2.** As the concentration of the **PP2** was increased the Stern-Volmer constant decreased by a factor of nearly ten and then became constant. The work of Kaur et al show that **PP2** aggregates at concentrations above $10^{-6}$ M, hence these data show that **PP2** is more sensitive in its unaggregated form. To corroborate this result further, quenching experiments were done at different ionic strengths for a **PP2** concentration of $10^{-6}$ M (Figure 5.3B). On increasing the ionic strength of the solutions, the Stern-Volmer constant decreased by a factor of nearly 2.3. Experiments at ionic strength higher than 60mM were not performed because of poor solubility of **PP2** in these higher ionic strength solutions. These results imply that when **PP2** is in a relatively unaggregated form, it is more readily quenched.

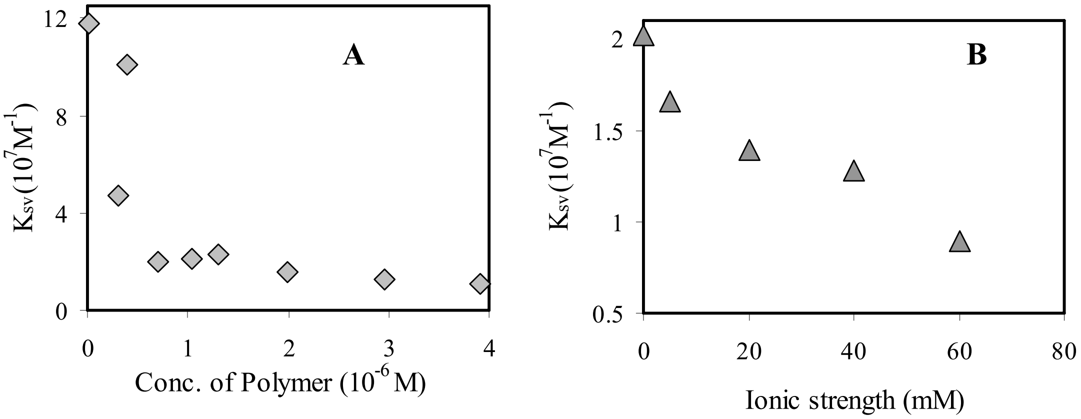

**Figure 5. 3** *Dependence of Stern-Volmer constant on concentration of **PP2** at an intrinsic ionic strength of polymer only (A). and on ionic strength at a **PP2** concentration of $10^{-6}$ M in (**B**).*

Since **PP2** is more sensitive in an unaggregated form, quenching experiments were performed for **PP2** (~ 2 x $10^{-7}$ M) in unaggregated form. To further ensure that the **PP2** exists in an unaggregated form, the **PP2** solutions were first heated to dissociate any aggregates and then cooled to room temperature; see reference 36. On addition of ferric cytochrome-*c* to the unaggregated **PP2** solution, a new red shifted peak was observed in the absorption spectrum. This red peak has been attributed to aggregate formation in the previous literature.[36,37] Figure 5.4 shows the absorption and emission spectra of the heated **PP2** before and after addition of 0.4 μM cytochrome-*c*. The addition of ferric cytochrome-*c* quenched the fluorescence of **PP2** by 98 %. Hence the protein induces polymer aggregation and it effectively quenches the fluorescence.

The fluorescence quenching mechanism of **PP2** in the presence of ferric cytochrome-*c* was elucidated by performing quenching experiments with different forms of cytochrome-*c*'s namely ferrous, and apo, denatured forms of the protein. It was found that the quenching by ferric and ferrous forms of the protein is similar; suggesting that the electron transfer quenching is not dominant. Apo cytochrome-*c* also quenched the fluorescence but with an efficiency nearly fourteen times lower than that for the native protein. Further the denatured cytochrome-*c*[2] quenched the polymer fluorescence but with 80% of the efficiency of the native protein. Comparison of these quenching efficiencies suggests that the energy transfer quenching as well as the induced aggregation upon addition of cytochrome-*c* govern the fluorescence quenching of **PP2**.

---

[2] Ferric cytochrome-*c* was heated to 353 K and then cooled back to room temperature. The denaturation was verified using CD and UV/Vis spectroscopy.

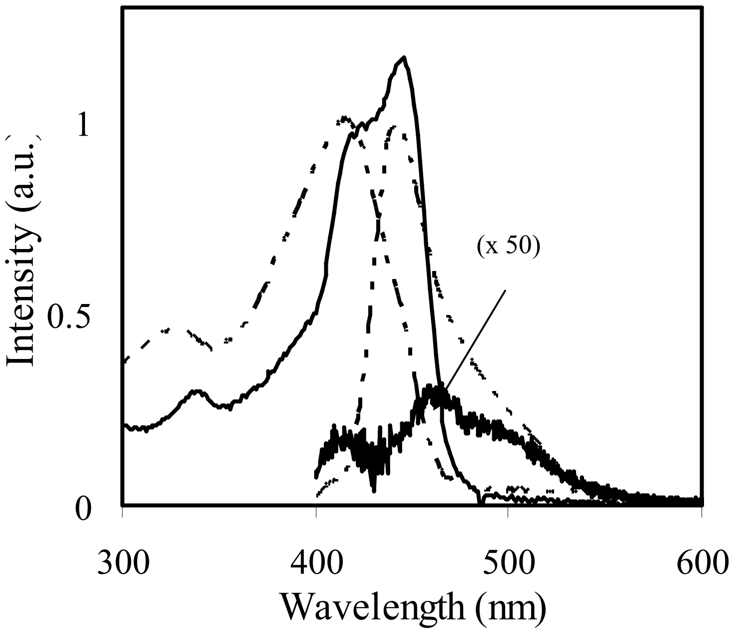

***Figure 5. 4*** *Absorption and emission spectra of unaggregated **PP2** in water without (— --—) and with 0.4 μM ferric cytochrome-c (—). The emission of **PP2** in the presence of 0.4 □M ferric cytochrome-c has been magnified 50 times for clarity.*

To further investigate the aggregation induced on addition of ferric cytochrome-*c* into **PP2** solution and to explain the appearance of a red shifted peak on addition of ferric cytochrome-*c*, the **PP2**-cytochrome-*c* solution was passed through a 0.25 μm filter and the emission and absorption were recorded again. The absorption was attenuated nearly ten times as compared to **PP2**-cytochrome-*c* solution before filtration. In order to make sure that the attenuation was not coming from **PP2** sticking to the filter, **PP2** in water was passed through 0.25 μm filter. The absorption and emission of **PP2** in water did not change. Hence the **PP2**-cytochrome-*c* solution contains aggregates that are retained by the filter, implying that aggregates > 0.25 μm are formed on addition of micromolar amounts of ferric cytochrome-*c*.

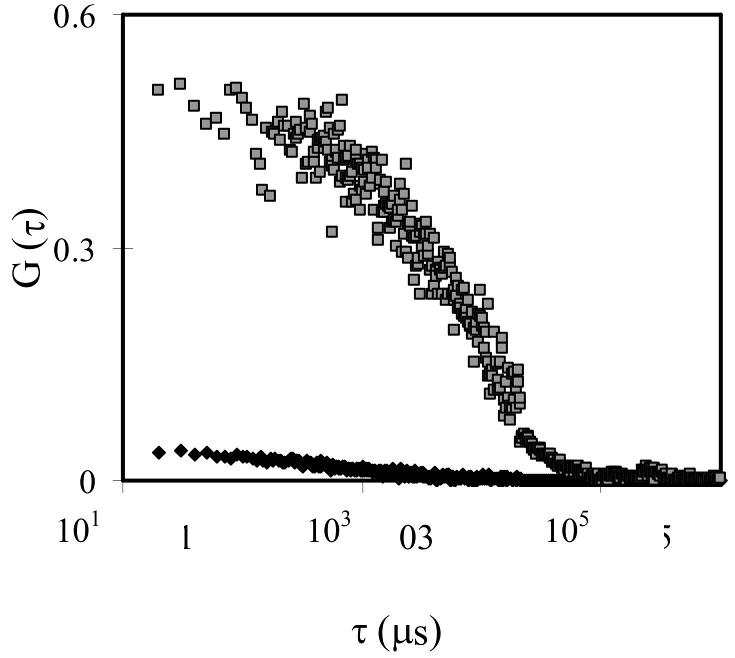

***Figure 5. 5** Autocorrelation function for **PP2** in water (♦) and with 0.4 μM cytochrome-c (■)*

To further corroborate the hypothesis of aggregate formation on addition of ferric cytochrome-*c*, FCS studies were performed. Hydrodynamic radius, $R_H$, was obtained for **PP2** in water using equation 3. In the absence of cytochrome-*c*, **PP2** had a correlation time of 686 μs and hence $R_H$ of 4.4 nm ($\eta$= 0.89 cP and $\omega_{xy}$= 0.39 μm), whereas on addition of 0.4 μM cytochrome-*c* no correlation was observed indicating the presence of very big particles (Figure 5.5). This behavior is similar to the one seen for autocorrelation function of 0.2μm fluorecein beads further corroborating the fact that very large particles are formed.

From the filtration and FCS experiments it is clear that **PP2** forms large aggregates when it interacts with the ferric cytochrome-*c*. Since **PP2** is negatively charged and ferric cytochrome-*c* is positively charged, we conclude that multiple polymer strands interact with the ferric cytochrome-*c* molecules electrostatically which leads to polymer aggregation.

### 5.3.2 Importance of Electrostatic Binding

The ionic strength dependence implies that electrostatic interactions play an important role in the quenching of the **PP2** fluorescence via aggregation of polymer strands. If this is true, than analyte with higher charge should form even bigger aggregates with **PP2** since it can bring more polymer strands together via electrostatic interaction. To test this hypothesis, quenching experiments with PAMAM 3G and **PP2** were performed. PAMAM 3G is similar in size to ferric cytochrome-*c* (diameter = 3.0 nm), however it has a charge of +32e at neutral pH. On addition of 10 μM PAMAM 3G the absorption spectrum shows a red shifted peak (see figure 5.6A), similar to that seen on addition of ferric cytochrome-*c* indicating aggregates are formed. The fluorescence was also quenched, but by only 30 %, which is smaller than that of ferric cytochrome-*c* (Figure 5.6A). On passing the **PP2**-PAMAM-3G solution through a 0.2 μm filter, the absorbance did not change and the fluorescence also did not change, indicating that any aggregates formed are smaller in size than the 200 nm filter. To further see if there is any contribution from other factors such as electron transfer since PAMAM-3G has amine groups, quenching experiments were done at pH 2 and pH 4 where even inner amines are charged. The quenching efficiency was found to be the same as that found at pH 7. The quenching experiments were also done at pH 12 where PAMAM-3G is not charged and the surface amine groups might act as electron donors. No quenching was seen at higher pH. These data indicate that the quenching occurs by electrostatic aggregation of **PP2** with PAMAM-3G and it does not involve electron transfer.

FCS experiments were performed to better quantify the s ize of the aggregates formed on addition PAMAM-3G to **PP2**. Figure 5.6B shows the autocorrelation function for **PP2** in the presence of PAMAM-3G. The correlation time increased by a factor of nearly 1.4 times ($\tau_{PAMAM\text{-}3G}$ = 850 μs, $R_H$= 6 nm) as compared to **PP2** in water ($\tau_{H2O}$ = 640 μs, $R_H$= 4.4 nm) indicating that aggregates are formed on addition of PAMAM-3G, but they are much smaller than those formed by **PP2** in the presence of cytochrome-*c* (> 0.25 μm). Two observations were made for **PP2** in the presence of 10 μM PAMAM-3G. First that small aggregates are formed and second that fluorescence quenching efficiency is weaker for PAMAM-3G than cytochrome-*c*, presumably because it does not have an energy transfer centre.

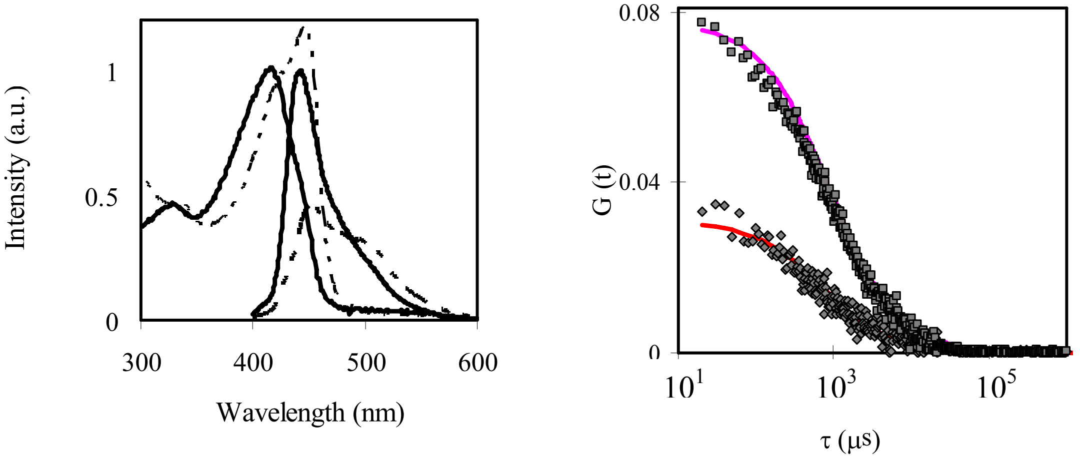

***Figure 5. 6 (A)** Absorption and emission spectra of unaggregated **PP2** in water (—) and with 10 μM PAMAM-3G (— --—). **(B)** Autocorrelation function for **PP2** in water (♦) and with 10 μM PAMAM-3G (■)*

### 5.3.3 Importance of Hydrophobic Interactions

An important difference between PAMAM-3G and ferric cytochrome-*c* is the presence of hydrophobic interactions for ferric cytochrome-*c*. The importance of hydrophobic interactions were explored by performing quenching experiments with PEG-OH which has a hydrophobic core and is neutral (Figure 5.7A). The addition of 50 μM PEG-OH to a ~2 $x10^{-7}$ M solution of

**PP2,** which **e**xists as aggregates, appears to create indepedent strands of **PP2** in solution. . On addition of 50 μM PEG-OH, the absorption spectrum red shifts but does not indicate the formation of aggregates species. Also the addition of PEG-OH enhances the fluorescence of **PP2** rather than quenching it (Figure 5.7B). This behavior is similar to what has been observed for **PP2** with octadecyl trimethylammonium bromide (ODTMA) already reported in the literature.[36] Further, FCS studies show that the correlation time increases by a factor of nearly three ($\tau_{H2O}$ = 1920 μs, $R_H$= 13.2 nm), indicating larger particles than are formed in the PAMAM-3G/**PP2** solution. Hence aggregates form but they are not the quenched red emitting homoaggregates of **PP2**. It may be that the addition of PEG-OH forms heteroaggregates between **PP2** and PEG-OH as observed for surfactant ODTMA.

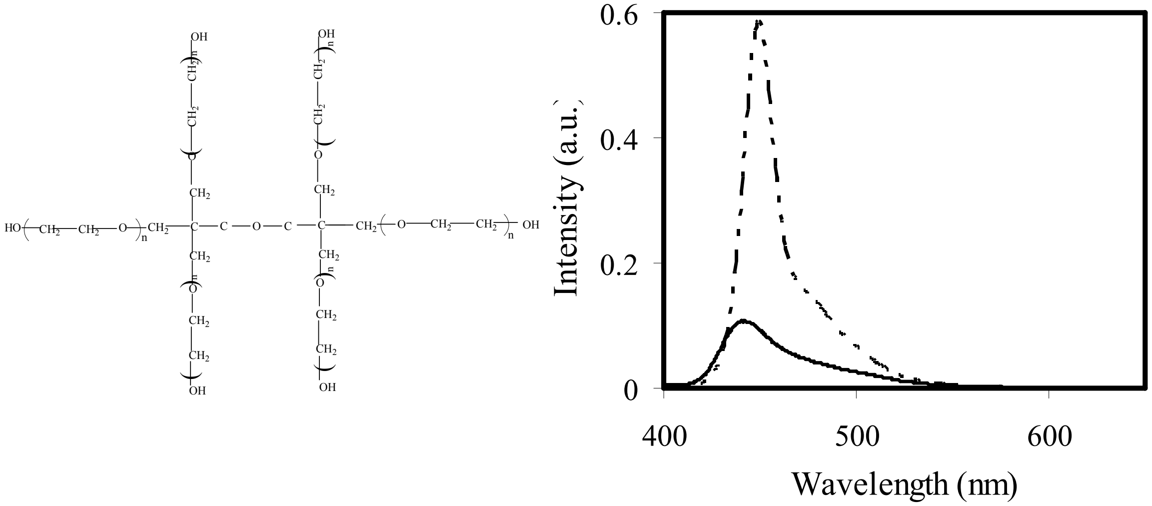

***Figure 5.****7 Chemical Strcuture of PEG-OH. (****B****) Emission spectra of* ***PP2*** *without (—) and with 50 μM PEG-OH (— -- —).*

### 5.3.4 Importance of Hydrophobic and Electrostatic Interactions

In order to probe if hydrophobic and electrostatic interactions play an important role in the interaction between polymer and the analyte, fluorescence quenching experiments were performed in the presence of DEM3.5G. Figure 5.8A shows the chemical structure of DEM-3.5G dendrimer which was used for the quenching experiments. This dendrimer has both a hydrophobic and a charged component.

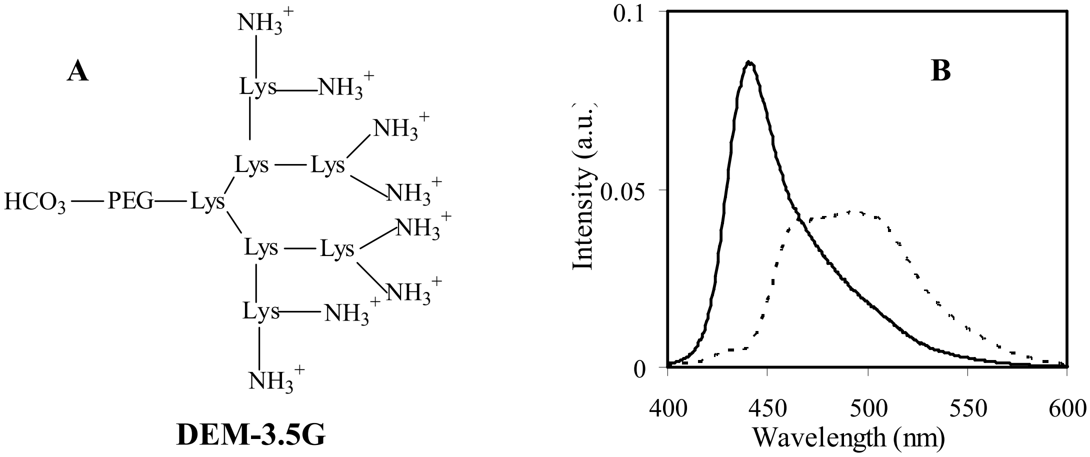

*Figure 5.8 A Structure of DEM3.5G (B) Emission spectra of **PP2** in water (—) and in the presence of 8.9 mM DEM3.5G (---).*

On addition of 8.9 mM DEM-3.5G to a ~2 x$10^{-7}$ M solution of **PP2**, the emission was quenched by only 20 % but became very broad and displayed a red emission band (Figure 5.8B). A new red-shifted peak was observed in the absorption spectrum, as well. The spectral changes indicate the formation of aggregates. Filtration of the **PP2** solution with 8.9 mM DEM-3.5G caused the fluorescence to decrease by 95 % and the absorbance to attenuate, corroborating the conclusion that large aggregates are formed. As with the ferric cytochrome-*c* system FCS experiments on the aggregates showed large particles but could not be quantified.

## 5.4 CONCLUSION

These studies show how the interaction between **PP2** and analyte change the optical properties of **PP2**. From the quenching experiments done with the macromolecules ferric cytochrome-*c*, PAMAM-3G and DEM3.5G, it is clear that interaction of these analytes induces aggregation of **PP2** in aqueous solutions. In the case of the protein ferric cytochrome-*c*, the fluorescence is quenched by 98 % and very big aggregates (>0.25 μm) are formed. The high quenching by ferric cytochrome-*c* results because it induces aggregation and it provides a chromophore that can quench the fluorescence by energy transfer. Contributions from each of these factors were studied by observing the optical properties of **PP2** in the presence of different quenching partners. Experiments with PAMAM-3G and DEM3.5G showed that both electrostactic and hydrophobic interactions are important for inducing aggregation in **PP2**, however these interactions are not sufficient to quench the fluorescence of **PP2** as effectively as ferric cytochrome-*c* where the presence of energy transfer centre makes the fluorescence quenching very efficient. Further it was shown that PEG-OH does not induce aggregatiom of multiple **PP2** strands. It appears that PEG-OH molecules hydrophobically interact with the polymer backbone, dissociating the homoaggregates and enhancing the fluorescence. These studies provide insight into the importance of different kind of interactions that might be responsible for fluorescence quenching of polymer because such multiple interactions will be present for analysis in complex biological systems.

Further these studies show that the sensitivity of **PP2** is also affected by its aggregation state. The polymer is unaggregated at low concentration (~$10^{-8}$ M) and at this concentration the highest Stern-Volmer constant is observed, suggesting that polymer is most sensitive when it is in its unaggregated form. This is further corroborated by the ionic strength dependence studies of Stern-Volmer constant. As the ionic strength increases, the polymer aggregates and the sensitivity decreases indicating polymer is not very sensitive in its aggregated state. This behavior may arise because polymer in unaggregated state can interact more effectively with the quencher i.e. it can wrap around the quencher more easily than when it is in aggregated form. Similar kinds of behavior was shown by Harrison et al[38] for PPE based conjugated polyelectrolytes but no explanation was provided.

## 5.5 ACKNOWLEDGEMENT

D.H.W. acknowledges support from the U.S. National Science Foundation (CHE-0415457)

## 5.6 REFERENCES

(1) Zhang, C.; Broun, D.; Heeger, A. J. *J. Appl. Phys.* **1993**, *73*, 5177.

(2) Hide, F.; Diaz-Garcia, M. A.; Schwartz, B. J.; Andersson, M. R.; Pei, Q.; Heeger, A. J. *Science* **1996**, *273*, 1833-1836.

(3) Yu, G.; Gao, J.; Hummelen, J.; Wudl, F.; Heeger, A. J. *Science* **1995**, *270*, 1789.

(4) Chen, L.; McBranch, D. W.; Wang, R.; Whitten, D. *Chem Phys. Lett.* **2000**, *330*, 27.

(5) DiCesare, N.; Pinto, M. R.; Schanze, K. S.; Lakowicz, J. R. *Langmuir* **2002**, *18*, 7785.

(6) Heeger, P. S.; Heeger, A. J. *Proc. Natl. Acad. Sci. U.S.A.* **1999**, *96*, 12219.

(7) McQuade, D. T.; Pullen, A. E.; Swager, T. M. *Chem Rev* **2000**, *100*, 2537-74.

(8) Tan, C.; Pinto, M. R.; Schanze, K. S. *Chem.Comm.* **2002**, 446.

(9) McQuade, D. T.; Pullen, A. E.; Swager, T. M.; Lacowitz, J. R. *Langmuir* **2002**, *18*, 7785.

(10) Swager, T. M. *Acc. Chem. Res.* **1998**, *31*, 201.

(11) Zhow, Q.; Swager, T. M. *J. Am. Chem. Soc.* **1995**, *117*, 12593.

(12) Pinto, M. R.; Scahnze, K. S. *Proc. Nat. Aca. Sci.* **2004**, *101*, 7505.

(13) Rininsland, F.; Xia, W.; Wittenburg, S.; Shi, X.; Stankewicz, C.; Achyuthan, K.; McBranch, D.; Whitten, D. *Proc. Nat. Acad. Sci.* **2004**, *101*, 15295-15300.

(14) Kim, I. B.; Dunkhorst, A.; Gilbert, J.; Bunz, U. H. F. *Macromolecules* **2005**, *38*, 4560-4562.

(15) Liu, B.; Bazan, G. C. *Chem. Mater.* **2004**, *16*, 4467.

(16) Kumaraswamy, S.; Bergstedt, T. S.; Shi, X.; Rininsland, F.; Kushon, S. A.; Xia, W.; Achyuthan, K.; McBranch, D. W.; Whitten, D. *Proc. Nat. Aca. Sci.* **2004**, *101*, 7511.

(17) Disney, M. D.; Zheng, J.; Swager, T. M.; Seeberger, P. H. *J Am Chem Soc* **2004**, *16*, 13343.

(18) Wosnick, J. H.; Mello, C. M.; Swager, T. M. *J Am Chem Soc* **2005**, *127*, 3400.

(19) Liu, M.; Kaur, P.; Waldeck, D. H.; Xue, C.; Liu, H. *Langmuir* **2005**, *21*, 1687-1690.

(20) Thomas III, S. W.; Joly, G. D.; Swager, T. M. *Chem. Rev.* **2007**, *107*, 1339.

(21) Zhang, T.; Fan, H.; Zhou, J.; Liu, G.; Feng, G.; Jin, Q. *Macromolecules* **2006**, *39*, 7839.

(22) Fan, C.; Plaxco, K. W.; Heeger, A. J. *J Am Chem Soc.* **2002**, *124*, 5642.

(23) Kim, I. B.; Dunkhorst, A.; Bunz, U., H. F. *Langmuir* **2005**, *21*, 7985.

(24) Kim, S.; Jackiw, J.; Robinson, E.; Schanze, K. S.; Reynolds, J. R.; Baur, J.; Rubner, M. F.; Boils, D. *Macromolecules* **1998**, *31*, 964-974.

(25) Kim, I. B.; Dunkhorst, A.; Bunz, U., H. F. *Langmuir* **005**, *21*, 7985-7989.

(26) Lacowitz, J. R. *Principles of Fluorescence Spectroscopy,Plenum Press NY* **1983**.

(27) Liu, M.; Waldeck, D. H.; Oliver, A. M.; Head, N. J.; Paddon-Row, M. N. *Journal of the American Chemical Society* **2004**, *126*, 10778-10786.

(28) Koppel, D. E. *Physical Review A* **1974**, *10*, 1938-1945.

(29) Magde, D.; Elson, E.; Webb, W. W. *Physical Review Letters* **1972**, *29*, 705-708.

(30) Pristinski, D.; Kozlovskaya, V.; Sukhishvili, S. A. *Journal of Chemical Physics* **2004**, *122*, 14907-14907.

(31) Van Rompaey, E.; Sanders, N.; Van Craenenbroeck, E.; Engelborghs, Y.; De Smedt, S. C.; Demeester, J. *Macromolecules* **2000**, *33*, 8280-8288.

(32) Leng, X. S., K.; Buffle, J. *J.Coll. Inter. Sci.* **2002**, *251*, 64.

(33) Yue, H.; Waldeck, D. H.; Xue, C.; Liu, H. *Manuscript in preparation*.

(34) Krichenvsky, O.; Bonnet, B. *Rep.Prog.Phys.* **2002**, *65*, 251-297.

(35) Culbertson, C. T.; Jacobsen, C. S.; Ramsey, J. M. *Talanta* **2002**, *56*, 365-373.

(36) Kaur, P.; Yue, H.; Wu, M.; Liu, M.; Treece, J.; Waldeck, D. H. *J. Phys. Chem. B* **2007**, *DOI: 10.1021/jp071307o*.

(37) Bunz, U. H. F. *Chem. Rev.* **2000**, *100*, 1605-1644.

# CHAPTER 6 INTRODUCTION TO NANOAPERTURE ARRAYS AND PLASMONIC SENSOR STUDIES

## 6.1 CHEMICAL MODIFICATION OF METALLIC NANOAPERTURE ARRAYS AND THEIR POTENTIAL FOR BIOCHEMICAL SENSING USING SURFACE PLASMON RESONANCE

Surface plasmon resonance (SPR) spectroscopy is widely used in chemical and biological sensing.[1] In the commonly used Kretschmann configuration, a light incident through a prism coupler reflects back at the interface with a thin metal layer. For certain incident angles and wavelengths, part of the incident energy reaches the other side of the metal layer, exciting surface plasmon waves that can interact with adjacent analytes. The loss of this energy is observed as a sharp attenuation of reflectivity, known as the surface plasmon resonance effect. The SPR technique senses the integral changes in the dielectric ambient in the vicinity of the metal surface that supports the surface plasmon waves. At a planar metal/dielectric interface, the plasmon fields evanescently extend into the dielectric with 200-300 nm depth and into the metal with 20-30 nm depth.[2]

## 6.2 SURFACE PLASMONS AND SURFACE PLASMON RESONANCE

“Surface plasmons (SP) are those plasmons that are confined to surfaces and that interact strongly with light. They occur at the interface of a vacuum or material with a positive dielectric constant with that of a negative dielectric constant. These are light waves that are trapped on the surface because of their interaction with the free electrons of the conductor. In this interaction, the free electrons respond collectively by oscillating in resonance with the light wave. The resonant interaction between the surface charge oscillation and the electromagnetic field of the light constitutes the surface plasmon and gives rise to its unique properties.”[2]

“The interaction between the surface charge density and the electromagnetic field results in the momentum of the SP mode, $\hbar k_{SP}$, being greater than that of a free-space photon of the same frequency, $\hbar k_0$. ($k_0 = \omega/c$ is the free-space wavevector.) Solving Maxwell's equations under the appropriate boundary conditions yields the SP dispersion relation, that is, the frequency-dependent SP wave-vector, $k_{SP}$,

$$k_{SP}=k_0\sqrt{\frac{\varepsilon_d\varepsilon_m}{\varepsilon_d+\varepsilon_m}} \tag{1}$$

The frequency-dependent permittivity of the metal, $\varepsilon_m$, and the dielectric material, $\varepsilon_d$, must have opposite signs if SPs are to be possible at such an interface. In order to excite surface plasmons in a resonant manner, one can use an electron or light beam (visible and infrared are typical). An incident electromagnetic wave can couple and thus excite the surface plasmons only if its angular frequency and momentum match that of the surface plasmons. However, the momentum of a free photon propagating in a dielectric medium is always smaller than the momentum of a surface plasmon propagating at the interface of the same medium and a metal. There is thus no angle of incidence for which the horizontal component of the incident photon wave matches the surface plasmon. There are three main techniques by which the missing momentum can be provided. The first makes use of prism coupling to enhance the momentum of the incident light.[3,4] The second involves scattering from a topological defect on the surface, such as a subwavelength protrusion or hole, which provides a convenient way to generate SPs locally.[5,6] The third makes use of a periodic corrugation[7] in the metal's surface"[8]

Typical metals that support surface plasmons are silver and gold, but metals such as copper, titanium, or chromium can also support surface plasmon generation. At a planar metal/dielectric interface, the plasmon fields evanescently extend into the dielectric with 200–300 nm depth and into the metal with 20–30 nm depth[8] (Figure 6.1). Since the field is on the interface of the metal and the external medium (air or dielectric for example), these oscillations are very sensitive to any change in the refractive index of this interface. These changes can be easily caused by the adsorption of molecules to the metal surface.

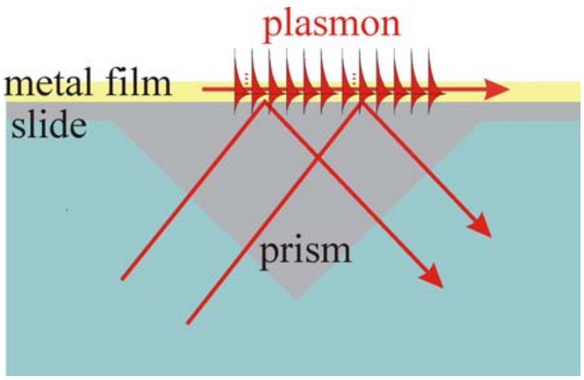

***Figure 6.1*** *Schematic representation of surface plasmon on metal films.Figure taken from internet.*

Salamon et al[9] provided both the theoretical and experimental understanding of the surface plasmons propagating along a metal-dielectric interface in surface plasmon resonance spectroscopy. They demonstrated the dependence of surface plasmon resonance on the refractive index, n, the thickness, t, and the extinction coefficient, k of thin film. They showed that the position of the resonance is largely a function of the extinction coefficient, k; the width of the resonance is mainly determined by the value of the refractive index, n; and the depth of the resonance is predominantly controlled by the thickness, t, of thin film (Figure 6.2).

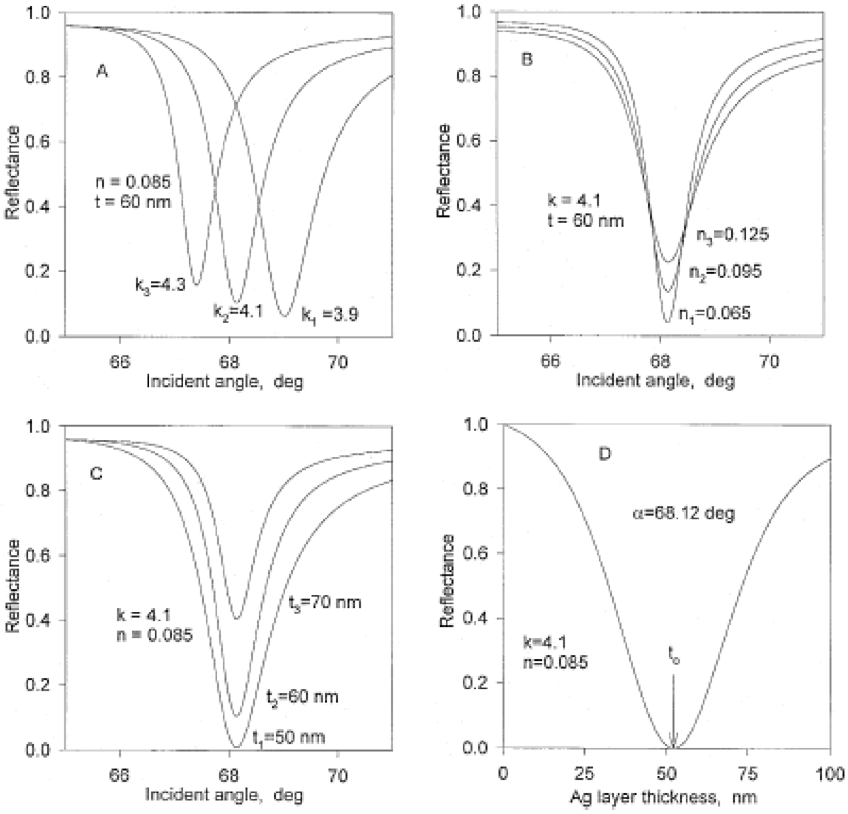

***Figure 6.2*** *Influence of extinction coefficient (panel A), of refractive index (panel B), and of thickness (panels C) and ( D) of a silver film (thicknesses noted in panels A, B, and C) on the theoretical SPR spectra obtained with an excitation wavelength λ=632.8 nm, and a glass prism (n=1.515), with water (n=1.33) as an emergent medium. The figure is taken from the reference 9.*

## 6.3 METALLIC NANOAPERTURE ARRAYS

Although a lot of techniques are available which exploit surface plasmon resonance, the desire to use and control photons in a manner analogous to the control of electrons in solids has inspired great interest in topics such as "localization or confinement of light".[11] Strong confinement of plasmonic fields near the metal surface can be utilized for the benefit of enhancing plasmonic interactions with an analyte layer and thus for efficient transduction and sensing of surface binding events. In the case of metal particles or thin metal island films, the plasmonic fields can be more narrowly confined to the metal surface with 10–30 nm penetration depth to adjacent dielectric. Recently there has been a growing interest in SPR sensing of biochemicals using a nanostructured metal layer, such as nanoparticle or nanohole arrays.[10-12]

Optical transmission through metal nanoapertures has recently been a subject of great interest, primarily because of the plasmonic phenomena that result in strong confinement of light and its funneling into subwavelength channels.[13,14] It has been shown in the literature that periodic arrangement of holes can drastically enhance the transmission. This effect has been attributed to the increases in the energy density on the surface of the metal screen through the creation of standing waves.[13]

Ebbesen et al[13] were among the first to show that the transmission of light through arrays of cylindrical holes of diameter varying from 150 nm to 1 μm with the spacing between the holes to range from 0.6 to 1.8 μm. They made many important observations. "First that the shape and intensity of the transmission peak is dependent on the hole diameter, periodicity, thickness and type of metal and secondly it changes with the type of lattice, whether it is a square or a triangular lattice. They further showed that this phenomenon of enhanced transmission arises from surface plasmon resonance by demonstrating the absence of enhanced transmission in hole arrays fabricated in Ge films and through the angular dependence of the spectra in nanohole array samples. They hypothesized that this enhancement of transmitted light occurs because of coupling of the light with the surface plasmons of the two-dimensional array of sub-wavelength holes. Numbers of unique features, such as surface plasmon modes on the metal–air interface are distinctly different from those at the metal–quartz interface, were observed by then however, could not be explained with existing theories."[13]

Besides nanoholes, nanoslit arrays have also been extensively studied by many groups[15-22].The Main research effort using these nanoslit arryas has been towards the fundamental understanding of transmission through these arrays. Sun et al[15] investigated the dynamic evolution of surface plasmon resonances in metallic nanoslit arrays. They proposed that "the optical transmission through a metallic nanoslit array can be understood in terms of polarizability of the medium and the periodic arrangement of nanoslits which serve as energy flow channels with the funneling effect. They showed that in shorter wavelength region, the transmission is governed by the surface plasmon resonances occurring at the top or bottom side of the metal surfaces and that the transmission sensitivity depend on the slit width at longer trnamission wavelength. In the intermediate wavelength regions, the surface plasmons reveal a quadrupolar distribution along the periphery of each metal island."[16] Jansenn et al[17] showed that "the plasmons are launched by a slit in antiphase with the incident field. This phase difference of π was used to explain enhanced and reduced transmission for a two slit system. They showed that the slit distance for constructive interference is a multiple of the plasmon wavelength and that the constructive interference captures a lot of energy on the metal surface and scattered laterally."[18] Later Ung et al[16] investigated the interference of the surface plasmons with an incident beam on a metallic slit using the FDTD calculations. They showed that "the bulk waves radiated at the slit edge by scattering of the surface plasmons leak into the slit and induce accumulated charges within the skin depth, which excites new surface plasmons on the slit side walls. These excited new surface plasmons on the slits walls create the Fabry-Perot resonantor modes along the slit axis".[17]

Because of these unique optical properties these nanoaperture arrays offer several advantages for SPR based sensing. One main advantage is that the transmission mode allows for a simpler collinear optical arrangement and provides a smaller area than the typical Kretschmann configuration. Hence it should be possible to miniaturize these arrays. The first steps in this direction were reported by Brolo et al.[23] They used arrays of nanoholes in a gold film to monitor the binding of organic and biological molecules to the metallic surface. The sensitivity was shown to be 400 nm per refractive index unit, which is comparable to other grating-based surface plasmon resonance (SPR) devices (Figure 6.3)

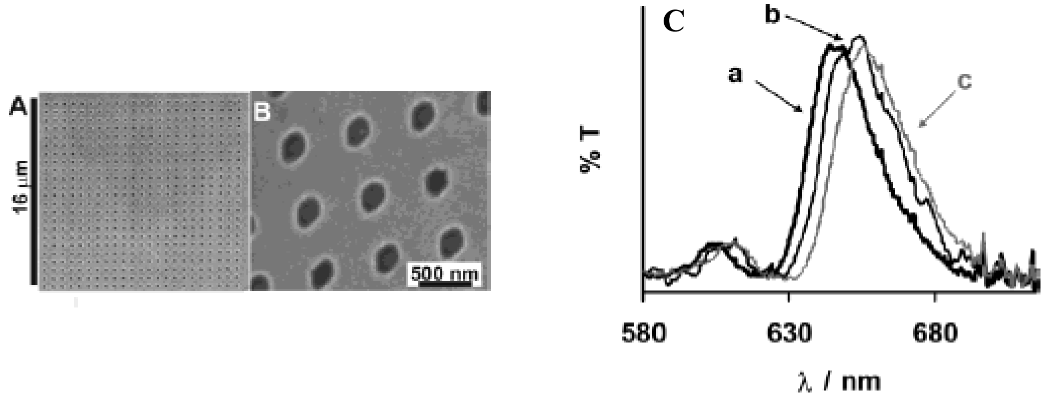

***Figure 6.3(A,B)*** *Scanning electron microscopy images of a typical array of sub-wavelength holes. The image in part B is an enlargement of the array presented in part A.* ***(C)*** *Normalized transmission spectra of normally incident white light through an array of sub-wavelength (200 nm diameter) holes on a 100-nm-thick gold substrate deposited on a glass slide. (a) Bare (clean) Au surface; (b) Au modified with a monolayer of MUA; (c) Au-MUA modified with BSA. Figure taken from reference 23.*

In the same year as Brolo, Lahav et al[24] used ultrathin gold island films evaporated on transparent substrates for chemical and biological sensing in the transmission surface plasmon resonance (T-SPR) mode. "The biotin-derivatized Au island film were used as a biological recognition surface for selective sensing of avidin binding and to distinguish between specific and nonspecific binding to the substrate. Transduction of the binding event into an optical signal was achieved by T-SPR spectroscopy, using plasmon intensity measurements, rather than wavelength change, for maximal sensitivity and convenience."[24]

Modulation of the nanoaperture array's optical response by adsorbed analytes may offer improved sensitivity and selectivity over conventional surface plasmon resonance methods, which are widely used and commercialized for analysis in detecting biological and chemical agents. The surface plasmons resonance in nanoaperture arrays involves funneling of light along the metal surface or strong optical confinement in the aperture region. The surface plasmon waves propagating along the aperture surfaces experience an accumulated effect in optical absorption along the resonance path, and this can result in a strong attenuation of the optical transmission. Utilizing the lateral (in-plane) interaction should increase the length of plasmonic interaction far beyond the vertical scale of the adsorbed analytes. In addition, a dielectric constant change in the aperture area will sensitively modulate the near-field coupling between metal islands and thus the optical transmission. In conventional SPR, the index change at the planar metal/dielectric interfaces (air or substrate side) has a relatively minor effect on the spectral shift and intensity. In contrast, the nanostructured arrays can be designed to operate in the strong near-field coupling regime and could be highly sensitive to refractive index changes.

Chapter 7 and 8 explore the nano-slit-array-based SPR sensing. Chapter 7 explores the optical transmission through metal nanoslit arrays with characteristic spectra involving surface plasmon resonances that occur at various sections of the metal surfaces. Chemical modification of these metal surfaces with alkanethiol self-assembled monolayers, results in the spectral shift of optical transmission. Adsorption of a self-assembled monolayer (1.5-nm thick) on a silver nanoslit array (slit width of 30-50 nm and grating period of 360 nm) is found to cause an 11 nm red-shift of the main transmission peak. Analysis of the plasmonic fields and charge distributions shows that the strong confinement of optical fields in the narrow slit region allows sensitive transduction of surface modification into a shift of surface plasmon resonance wavelength. Chapter 8 describes the initial steps toward the sensing of cancer cells using surface plasmon resonance based on metal nanoslit arrays. Analysis of the preliminary data obtained using fluorescence microscopy and Surface Plasmon Resonance Spectroscopy has shown that these nanoslit arrays have a potential for biological and chemical sensing.

## 6.4 REFERENCES

(1) J. Homola; Yee, S. S.; Gauglitz, G. *Sensors and Actuators B* **1999**, *54*, 3.

(2) Raether, H. *Surface plasmons on smooth and rough surfaces and on gratings ,Springer-Verlag, Berlin* **1988. (b)** Barnes, W. L., Dereux, A , Ebbesen, T. W. *Nature*, **2003**, 424, 824. **(c)** www.wikipedia.org

(3) Kretschmann, E.; Raether, H. *Z. Naturforsch. A* **1968**, *23*, 2135−2136.

(4) Otto, A. *Z. Phys.* **1968**, *216*, 398.

(5) Ditlbacher, H. *Appl. Phys. Lett.* **2002**, *80*, 404−406.

(6) Hecht, B.; Bielefeldt, H.; Novotny, L.; Inouye, Y.; Pohl, D. W. *Phys. Rev. Lett.* **1996**, *77*, 1889−1892.

(7) Ritchie, R. H.; Arakawa, E. T.; Cowan, J. J.; Hamm, R. N. *Phys. Rev. Lett.* **1968**, *21*, 1530−1533.

(8) Malinsky, M. D.; Kelly, K. L.; Schatz, G. C.; Van Duyne, R. P. *J. Am. Chem. Soc.* **2001**, *123*, 1471.

(9) Salamon, Z.; Macleod, H. A.; Tollin, G. *Biochimica et Biophysica Acta* **1997**, *1331*, 117

(10) Riboh, J. C.; Haes, A. J.; McFarland, A. D.; Yonzon, C. R.; Van Duyne, R. P. *J. Phys. Chem. B* **2003**, *107*, 1772.

(11) Williams, S. M.; Stafford, A. D.; Rodriguez, K. R.; Rogers, T. M.; Coe, J. V. *J. Phys. Chem. B* **2003**, *107*, 11871.

(12) Barnes, W. L.; Dereus, A.; Ebbesen, T. W. *Nature* **2003**, *424*, 824.

(13) Ebbesen, T. W.; Lezec, H. J.; Ghaemi, H. F.; Thio, T.; Wolff, P. A. *Nature* **1998**, *391*, 667.

(14) Lahav, M.; Vaskevich, A.; Rubinstein, I. *Langmuir* **2004**, *20*, 7365.

(15) Sun, Z.; Jung, Y. S.; Kim, H. K. *Appl. Phys Lett* **2005**, *86*, 23111

(16) Ung, B.; Sheng, Y. *Optics Express* **2007**, *15*, 1182.

(17) Janssen, O. T. A.; Urbach, H. P.; ' t Hooft, G. W. *Optics Express* **2006**, *14*, 11823.

(18) Kim, J. E.; Park, Y. C.; Park, D. J.; Ahn, Y. H.; Ropers, C.; Lienau, C.; Kim, J.; Park, Q. H.; Kim, D. S. *Phys. Rev. B* **2007**, *75*, 35414.

(19) Sun, Z.; Jung, Y. S.; Kim, H. K. *Appl. Phys Lett* **2003**, *83*, 3021

(20) Wuenschell, J.; Kim, H. K. *Optics Express* **006**, *14*, 10000.

(21) Ropers, C.; Park, D. J.; Stibenz, G.; Steinmeyer, G.; Kim, J.; Kim, D. S.; Lienau, C. *Phys. Rev. Lett.* **2005**, *94*, 113901.

(22) Jung, Y. S.; Sun, Z.; Kim, H. K. *Appl. Phys Lett* **2005**, *87*, 263116.

(23) Brolo, A. G.; Gordon, R.; Leathem, B.; Kavanagh, K. L. *Langmuir* **2004**, *20*, 4813.

(24) Lahav, M.; Vaskevich, A.; Rubinstein, I. *Langmuir* **2004**
*20*, 7365

# CHAPTER 7 HIGH-SENSITIVITY SURFACE PLASMON RESONANCE SPECTROSCOPY BASED ON METAL NANOSLIT ARRAYS

*This work has been published as Yun Suk Jung, Zhijun Sun, Jeff Wuenschell, Hong Koo Kim, Palwinder Kaur, Lei Wang, David Waldeck, App. Phys. Lett.* ***88****, 243105 (2006)*

Optical transmission through metal nanoslit arrays shows characteristic spectra involving surface plasmon resonances that occur at various sections of the metal surfaces. We have chemically modified the metal surfaces with alkanethiol self-assembled monolayers, and have characterized the resulting spectral shift of optical transmission. Adsorption of a self-assembled monolayer (1.5-nm thick) on a silver nanoslit array (slit width of 30-50 nm and grating period of 360 nm) is found to cause a 11 nm red-shift of the main transmission peak. Analysis of the plasmonic fields and charge distributions shows that the strong confinement of optical fields in the narrow slit region allows sensitive transduction of surface modification into a shift of surface plasmon resonance wavelength. The nano-slit-array-based surface plasmon spectroscopy is amenable to ultracompact miniaturization of instruments for biochemical sensing.

Surface plasmon resonance (SPR) spectroscopy is widely used in chemical and biological sensing.[1] In the commonly used Kretschmann configuration, a light incident through a prism coupler reflects back at the interface with a thin metal layer. For certain incident angles and wavelengths, part of the incident energy reaches the other side of the metal layer, exciting surface plasmon waves that can interact with adjacent analytes. The loss of this energy is observed as a sharp attenuation of reflectivity, known as the surface plasmon resonance effect. The SPR technique senses the integral changes in the dielectric ambient in the vicinity of the metal surface that supports the surface plasmon waves. At a planar metal/dielectric interface, the plasmon fields evanescently extend into the dielectric with 200-300 nm depth and into the metal with 20-30 nm depth.[2] In the case of metal particles or thin metal island films, the plasmonic fields can be more narrowly confined to the metal surface with a spatial extension of 10-30 nm to dielectric.[3] Strong confinement of plasmonic fields near the metal surface can be utilized for the benefit of enhancing plasmonic interactions with an analyte layer and thus for efficient transduction and sensing of surface binding events. Recently there has been a growing interest in SPR sensing of biochemicals using a nanostructured metal layer, such as nanoparticle or nanohole arrays.[3-7] Nanostructure-based SPR sensing can also operate in the transmission configuration, thereby simplifying the optical arrangement and requiring small amounts of analyte.

In this Letter we report a transmission SPR sensor based on a metal nanoslit array structure. Optical transmission through metal nanoapertures has recently been a subject of great interest, primarily because of the plasmonic phenomena that result in strong confinement of light and its funneling into subwavelength channels.[8] Biochemical sensing based on an array of subwavelength holes has been reported, demonstrating a beneficial use of strong confinement of light in nanoapertures.[5,6] Despite the simple geometry, a nanoslit array offers unique properties that cannot be attained with nanohole arrays.[9-11] A metal nanoslit, for example, supports guided modes without cutoff wavelength, whereas optical transmission through a metal nanohole array is critically limited by the hole size and metal thickness. This feature suggests that metal nanoslit arrays may be intrinsically more suitable for transmission-mode SPR sensing.

In this work, we have used a 190-nm-thick silver slit array. The slit width is designed to be in the range of 30-50 nm, and the grating period is 360 nm. Details of fabrication of a silver nanoslit array structure of the same geometry have been described elsewhere.[11] The sample was then chemically treated to coat the metal surface with an alkanethiol self-assembled monolayer (SAM) [$HS(CH_2)_7COOH$]. Alkanethiols on Ag is one of the most widely-used SAMs with well-established chemistry. They form dense, well-ordered, tightly-bonded films on Ag, and the SAM can be easily tailored to incorporate a variety of molecular recognition elements designed for specific binding.[12]

Optical transmission through the Ag nanoslit array was then characterized in the spectral range of 350-1750 nm, using unpolarized light that strikes the nanoslit array at normal incidence. Figure 7.1 shows the transmission spectra measured before and after chemical modification of the exposed metal surface. The as-deposited nanoslit array shows a characteristic transmission spectrum with clear peaks defined by transmission minima (black curve). Light which is incident on the nanoslit array excites surface plasmons (SPs) on the nanoapertured metal surface, and the SP waves are funneled into and propagate through each slit. Part of the SPs emerging from the slits couples into the SP waves propagating laterally towards the neighboring slits, while some decouples into radiation modes. The laterally propagating SPs encounter a periodic perturbation introduced by the slit array, and form Bloch waves. The SPs' periodic interaction with the media results in formation of plasmonic bandgap around the resonance point, similar to the dielectric-based photonic crystal's case.[13,14] The transmission dip at 400 nm corresponds to the in-plane SP resonance at the metal/air interface and the transmission dip at 600 nm corresponds to the metal/quartz interface.[11] The dip at 800 nm corresponds to the surface plasmon resonance localized around each metal island.

Adsorption of a SAM causes a red-shift of the transmission spectrum (the red curve in Figure 1). The amount of red-shift measured with the main transmission peak at around 690 nm is 11 nm. The thickness of the SAM is estimated to be 1.5 nm. The sensitivity of this response, defined as the ratio of the transmission spectral shift to the adsorbed analyte layer thickness, is calculated to be 7. In the case of nano-hole-array-based SPR sensing, a sensitivity of 2.5 was reported: 4-nm spectral shift for adsorption of a 1.7-nm-thick SAM on Ag nanoholes, measured with similar analyte/ambient dielectric contrast, i.e., $\varepsilon_a/\varepsilon_d$ = 2.1/1.0.[6] In order to better understand this nano-slit-array-based SPR sensor's response to analyte coverage, we have analyzed the plasmonic interaction of an incident light wave with an adsorbed analyte layer.

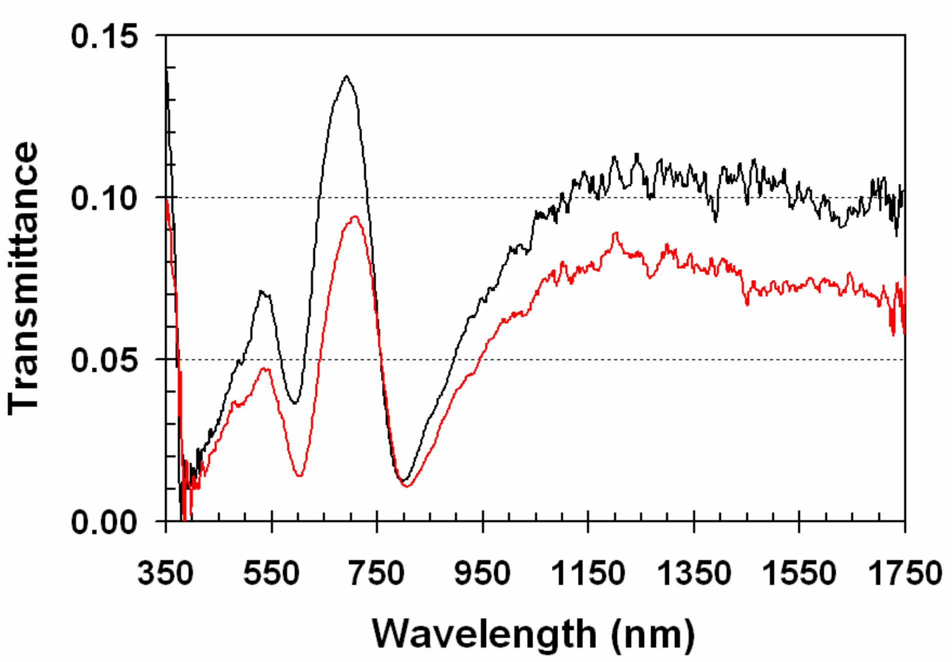

***Figure 7.1*** *Optical transmission through the Au-coated Ag nanoslit array: before chemical modification of metal surface (black), and after adsorption of an alkanethol SAM (red).*

Figure 7.2 shows the finite-difference time-domain (FDTD) analysis of the SP polarization charge distribution on a metal surface calculated at 650 nm wavelength, which is close to the peak transmission point. The blue and red colors represent negative and positive polarity of the charges, respectively.[15] The polarization charges show a quadrupolar distribution along the periphery of each metal island separated by slits. A single period of charge oscillation spans one plasmonic wavelength, and the plasmon wavelength depends on the nature of metal/dielectric interface. From the quadrupolar resonance condition, the optical wavelength at the transmission peak can be expressed as follows.[11]

$$\lambda = \frac{1}{2} L_1 \operatorname{Re}(n_{e1}) + \frac{1}{2} L_2 \operatorname{Re}(n_{e2}) + L_3 \operatorname{Re}(n_{e3}) \tag{7.1}$$

Here $L_1$ is the length of the top surface section (air side) of a metal island, $L_2$ the length of the bottom surface (substrate side), and $L_3$ the height of metal side-walls, i.e., slit depth. $n_{ei}$ ($i$ =1, 2, or 3) is defined as the SP wave vector normalized by the free-space propagation constant $k_0$, and corresponds to the effective index of the metal/dielectric interface being considered. The effective index $n_e$ is, in general, a complex number, having both propagation and attenuation components. In the case of Ag, SP wave vectors are propagation-dominant in the visible to near-infra-red range. In this work with a submicron-period slit array, therefore, we neglect the imaginary part of the effective indices. Along the transverse direction, the SP fields evanescently extend into both metal and dielectric regions. The effective index value reflects the integral effects resulting from interactions of a plasmon wave with the media over the entire extension of the fields. Chemical modification of each metal surface is expected to alter the effective index $n_{ei}$ in that section, by an amount commensurate with the change in the plasmonic fields in the dielectric ambient, causing a resonant wavelength shift. The dispersion property of materials (especially the wavelength dependence of metal's dielectric function) in conjunction with a spectral shift also contributes to the effective index change. Taking into account these two contributing factors and also the fact that chemical modification was made on the top surface of metal ($L_1$) and the side walls of slits ($L_3$), but not on the quartz/metal interface ($L_2$), we can express the total wavelength shift as follows.

$$\Delta\lambda = \frac{\frac{1}{2}L_1\left(\frac{dn_{e1}}{d\varepsilon_d}\right)\Delta\varepsilon_d + L_3\left(\frac{dn_{e3}}{d\varepsilon_d}\right)\Delta\varepsilon_d}{1-\frac{1}{2}L_1\left(\frac{dn_{e1}}{d\lambda}\right)-L_3\left(\frac{dn_{e3}}{d\lambda}\right)} \tag{7.2}$$

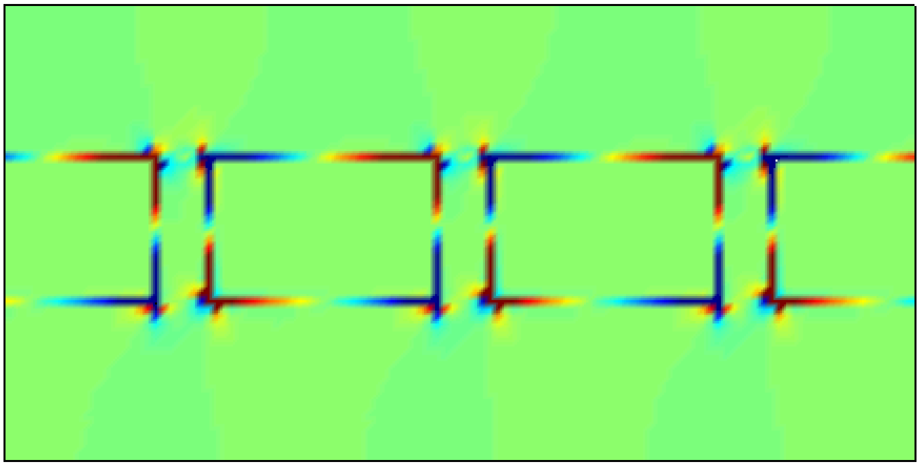

***Figure 7.2*** *SP polarization charge distribution on a silver nano-slit array (370 nm period; 180 nm thickness; 80 nm slit width) calculated with the finite-difference time-domain analysis at 650 nm wavelength, which corresponds to the peak transmission point.*

The effective index changes caused by chemical modification are expected to be different for the top surface of a metal island and the slit side walls. Hence they will show different sensitivities to an adsorbed analyte layer, because of the different distribution of plasmonic fields along the transverse direction. To find the effective index change for the top surface section, we model it as a planar metal/dielectric interface with semi-infinite extension of dielectric. The effective index for SPs on that surface can be expressed as $n_{e1} = [(\varepsilon_m\varepsilon_d)/(\varepsilon_m+\varepsilon_d)]^{1/2}$, and the dispersion term ($dn_{e1}/d\lambda$) is determined as $(1/2)n_{e1}^3\,\varepsilon_m^{-2}\,(d\varepsilon_m/d\lambda)$. Imagine that an analyte layer of thickness $d$ and dielectric constant $\varepsilon_a$ is adsorbed on the metal surface. Assume that the analyte layer thickness is much smaller than the plasmon field extension (i.e., the penetration depth in dielectric). The SP effective index change caused by analyte adsorption, $(dn_{e1}/d\varepsilon_d)\Delta\varepsilon_d$ can be expressed as follows.[16]

$$\left(\frac{dn_{e1}}{d\varepsilon_d}\right)\Delta\varepsilon_d = \frac{\pi}{\lambda}\frac{\left|\varepsilon_m\right|^{3/2}\varepsilon_d^{\;1/2}}{\left(\varepsilon_m+\varepsilon_d\right)^2}\left(1-\frac{\varepsilon_d}{\varepsilon_a}\right)d \tag{7.3}$$

The index change in the slit requires more development. In the case of a metal slit of width $w$, propagation of a plasmon wave along the slit is governed by the following dispersion relation.[17,18]

$$\frac{\gamma_m}{\varepsilon_m}+\frac{\gamma_d}{\varepsilon_d}\frac{1-e^{-\gamma_d w}}{1+e^{-\gamma_d w}}=0 \tag{7.4}$$

Here, $\gamma_d = (k_{sp}^2 - \varepsilon_d k_0^2)^{1/2} = k_0(n_{e3}^2 - \varepsilon_d)^{1/2}$ is the decay constant of plasmon fields inside the slit region, and describes the evanescent profile in the dielectric gap. The decay constant in the metal region, given by $\gamma_m = (k_{sp}^2 - \varepsilon_m k_0^2)^{1/2} = k_0(n_{e3}^2 - \varepsilon_m)^{1/2}$, determines the penetration depth in metal. Figure 7.3(a) shows the effective index $n_{e3}$ (both the real and imaginary parts) calculated for a silver nanoslit with air gap by solving the dispersion relation at three different wavelengths, 450, 650, and 800 nm. As assumed before, the imaginary part remains small compared to the real part so that SP attenuation would be insignificant for the slit dimensions being considered. The effective index monotonically increases as the slit width decreases. For the case of a 40-nm slit width, the effective index is calculated to be 1.5 at 650 nm. Figure 7.3(b) shows the $E_x$ field distribution (the $E$-field component normal to metal surface) calculated for the same slit structure. Note that the electric field at the dielectric side of the interface is $|\varepsilon_m/\varepsilon_d|$ times greater than that at the metal. The field remains nearly constant across the gap region, whereas it quickly decays in the metal with a penetration depth of ~30nm. For narrow slits ($\gamma_d\, w << 1$), the dispersion relation can be simplified as follows.

$$\frac{\gamma_m}{\varepsilon_m} + \frac{\gamma_d}{\varepsilon_d}\frac{\gamma_d w}{2} = 0 \tag{7.5}$$

By differentiation of Equation (7.5) with respect to $\lambda$, we obtain an expression for ($dn_{e3}/d\lambda$) as follows.

$$\frac{dn_{e3}}{d\lambda} = \frac{k_0^{\,2}\varepsilon_d\left(\frac{d\varepsilon_m}{d\lambda} - \frac{k_0}{\pi}\varepsilon_m\right) + \frac{d\varepsilon_m}{d\lambda}\gamma_m\gamma_d^{\,2} w - \frac{k_0^{\,3}}{\pi}\varepsilon_m\varepsilon_d\gamma_m w}{2n_{e3}k_0^{\,2}(\varepsilon_d + \varepsilon_m\gamma_m w)} + \frac{n_{e3}k_0}{2\pi} \tag{7.6}$$

The effective index change induced by analyte adsorption can be expressed as ($dn_{e3}/d\varepsilon_d$) $\Delta\varepsilon_d$. $\Delta\varepsilon_d$ represents the change of dielectric ambient in the slit region caused by adsorption of analytes on slit walls. For the case of analytes of dielectric constant $\varepsilon_a$ and thickness $d$ on each sidewall, $\Delta\varepsilon_d$ can be expressed as $2(1-\varepsilon_d/\varepsilon_a)(d/w)$.[19] $dn_{e3}/d\varepsilon_d$ can be derived from the dispersion relation, Equation (7.5), by taking differentiation of the equation with respect to $\varepsilon_d$. Combining the two, the effective index change in the slit region can be expressed as,

$$\left(\frac{dn_{e3}}{d\varepsilon_d}\right)\Delta\varepsilon_d = \frac{1}{n_{e3}}\left(\frac{\frac{1}{2}k_0\varepsilon_m w - \left(n_{e3}^{\,2} - \varepsilon_m\right)^{1/2}}{k_0\varepsilon_m w + \varepsilon_d\left(n_{e3}^{\,2} - \varepsilon_m\right)^{-1/2}}\right)\left(1 - \frac{\varepsilon_d}{\varepsilon_a}\right)\frac{2d}{w} \tag{7.7}$$

Given these expressions for the effective index changes and the dispersion effects, we can calculate the wavelength shift from the different regions. Calculation shows that the dispersion effect on the top surface of metal is negligible, i.e., $L_1(dn_{e1}/d\lambda)$ <<1 in the first term of the denominator of Equation (2). Substituting ($dn_{e1}/d\varepsilon_d$)$\Delta\varepsilon_d$ in Equation (2) with the expression in Equation (3), and ($dn_{e3}/d\lambda$) in Equation (2) with Equation (6), we can calculate the wavelength shift of the transmission peak caused by analyte adsorption on the top surface of the metal. Similarly substituting $(dn_{e3}/d\varepsilon_d)\Delta\varepsilon_d$ in Equation (2) with Equation (7), we can calculate the wavelength shift caused by adsorption in the slit region. Equations (6) and (7) involve the effective index in the slit region, $n_{e3}$, and we obtain its value referring to Figure 3(a), which shows $n_{e3}$ values calculated for a broad range of slit width. For the given structure and materials system characterized in this work, we assume $L_1$ = 300 nm, $L_3$ = 150 nm, $w$ = 40 nm, $\lambda$ = 680 nm, $d$ = 1.5 nm, $\varepsilon_a = 2.1$, $\varepsilon_d = 1.0$, $\varepsilon_m = -19.1 + i1.2$, and $d\varepsilon_m/d\lambda = -0.068$.[20] Calculation shows that the slit region contributes 13 nm to the wavelength shift of the transmission peak while the top surface contributes 0.3 nm to the shift. The total shift of 13.3 nm calculated from this formula is in reasonable agreement with the measurement (11 nm) shown in Figure 1. The analysis clearly reveals that the slit region provides efficient transduction of ambient index change into a spectral shift of optical transmission, while the planar top surface of metal makes a very minor contribution. Sensitivity of this nano-slit-based SPR sensing can be further enhanced by reducing the slit width (Equation (7)) and/or by increasing the slit depth (Equation (2)). Figure 7.4 shows the sensitivity calculated at 680 nm wavelength for different slit width of a Ag nanoslit array (with grating period of 360 nm and slit depth of 190 nm). Here the sensitivity is defined as the ratio of the wavelength shift to the analyte layer thickness. In this calculation, the analyte layer's dielectric constant is assumed to be 2.1, and the gap ambient is either air ($\varepsilon_d$ = 1.0) or water ($\varepsilon_d$ = 1.77).

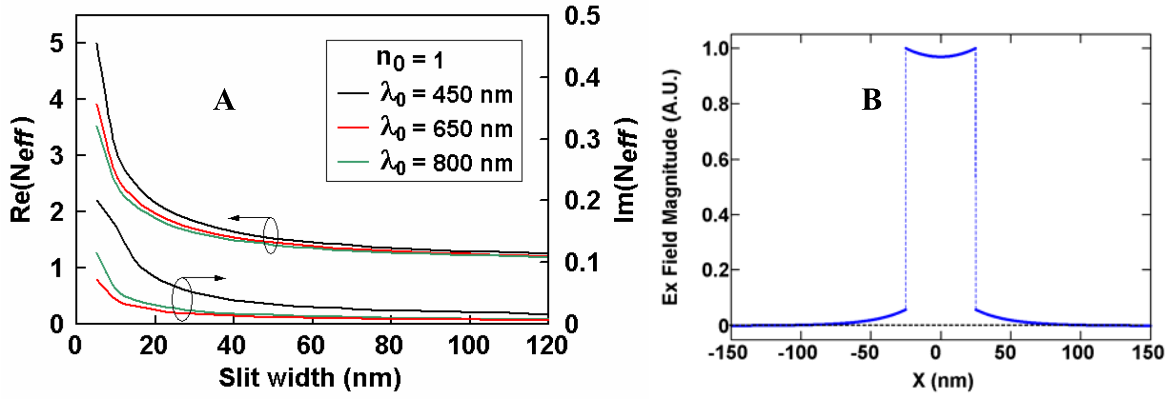

***Figure 7.3(A)*** *SP effective index $n_e$ in a silver nanoslit with air gap: calculated at 450, 650, and 800 nm wavelength for various different slit widths.* ***(B)*** *$E_x$ field distribution (the E-field component normal to metal surface) calculated for a Ag slit with 50-nm air gap.*

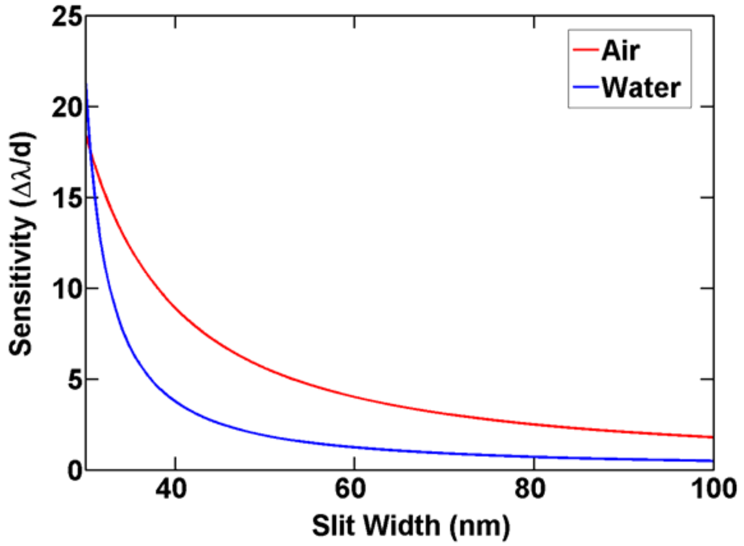

***Figure 7.4*** *Sensitivity calculated at 680 nm wavelength for different slit width of a silver nanoslit array (grating period of 360 nm and slit depth of 190nm). The gap ambient is assumed to be either air ($\varepsilon_d$ = 1.0) or water ($\varepsilon_d$ = 1.77). The sensitivity is defined as a ratio of the wavelength shift to the analyte layer thickness ($\varepsilon_a$ = 2.1).*

Nano-slit-array-based SPR sensing offers greater flexibility than nano-hole-array-based SPR sensing.[6] In the latter case, the hole diameter cannot be designed too small and/or the hole depth cannot be increased too high, otherwise an extremely poor transmission will result because of cutoff wavelength of waveguide modes. A related and alternative approach to utilizing highly confined plasmonic fields for SPR sensing has also been reported.[3] Instead of confining plasmonic fields into a physically defined region (i.e., the narrow slits), nano-particles are used to confine the evanescent field region in the dielectric. Depending on the particle size, the field extension can be made as small as 10-20 nm, and high sensitivity SPR sensing has been reported with nano-particle-based structures. In summary, chemical modification of nanostructured metal surfaces that allow nanoscale confinement of plasmonic fields is a promising approach to developing a new class of SPR sensors that will enable high sensitivity sensing and extremely small miniaturization of SPR devices.

## 7.1 ACKNOWLEDGEMENT.

This work has been supported by the NSF NIRT ECS-0403865.

## 7.2 REFERENCES

1. J. Homola, S. S. Yee, and G. Gauglitz, Sensors and Actuators B **54**, 3 (1999).
2. H. Raether, *Surface plasmons on smooth and rough surfaces and on gratings* (Springer-Verlag, Berlin, 1988).
3. M. D. Malinsky, K. L. Kelly, G. C. Schatz, and R. P. Van Duyne, J. Am. Chem. Soc. **123**, 1471 (2001).
4. J. C. Riboh, A. J. Haes, A. D. McFarland, C. R. Yonzon, and R. P. Van Duyne, J. Phys. Chem. B **107**, 1772 (2003).
5. S. M. Williams, A. D. Stafford, K. R. Rodriguez, T. M. Rogers, and J. V. Coe, J. Phys. Chem. B **107**, 11871 (2003).
6. A. G. Brolo, R. Gordon, B. Leathem, and K. L. Kavanagh, Langmuir **20**, 4813 (2004).
7. M. Lahav, A. Vaskevich, and I. Rubinstein, Langmuir **20**, 7365 (2004).
8. W. L. Barnes, A. Dereus, and T. W. Ebbesen, Nature **424**, 824 (2003).
9. J. A. Porto, F. J. Garcia-Vidal, and J. B. Pendry, Phys. Rev. Lett. **83**, 2845 (1999).
10. A. Degiron and H. J. Lezec, W. L. Barnes, and T. W. Ebbesen, Appl. Phys. Lett. **81**, 4327 (2002).
11. Z. Sun, Y. S. Jung and H. K. Kim, Appl. Phys. Lett. **83**, 3021 (2003).
12. C. J. Love, L. A. Estroft, J. K. Kriebel, R. G. Nuzzo, and G. M. Whitesides, Chem. Rev. **105**, 1103 (2005).
13. W. L. Barnes, T. W. Priest, S. C. Kitson, and J. R. Sambles, Phys. Rev. B **54**, 6227 (1996).

14. Y. S. Jung, Z. Sun, H. K. Kim, Appl. Phys. Lett. **87**, 263116 (2005).

15. Z. Sun, Y. S. Jung, and H. K. Kim, Appl. Phys. Lett. **68**, 023111 (2005).

16. $\Delta\varepsilon_d$ is determined from a formula that equates the total amount of polarization charge change induced by analyte adsorption to that with a uniform increment of ambient dielectric constant: $\int_0^\infty \varepsilon_0(\widetilde{E} - E)dz = \int_0^\infty \Delta\varepsilon_d \varepsilon_0 E dz$. $\varepsilon_0$ is the free-space permittivity. $\widetilde{E}$ and $E$ are the electric fields (the normal component to the metal surface) in the dielectric region before and after analyte adsorption, respectively. The electric field in the analyte layer is $(\varepsilon_d/\varepsilon_a)$ times the electric field in the ambient dielectric and assumed to be constant across the analyte layer thickness, d. Assuming negligible perturbation of the fields outside the analyte region, $\Delta\varepsilon_d$ is calculated as $d\gamma_d(1-\varepsilon_d)/\varepsilon_a$. $\gamma_d$ is the decay constant in the ambient dielectric and is expressed as $k_0 n_{e1} \varepsilon_d^{1/2}|\varepsilon_m|^{-1/2}$.

17. Z. Sun and H. K. Kim, Appl. Phys. Lett. **85**, 642 (2004).

18. I. P. Kaminow, W. L. Mammel, and H. P. Weber, Appl. Opt. **13**, 396 (1974).

19. $\Delta\varepsilon_d$ is determined by equating the total amount of polarization charge change induced by analyte adsorption to that with a uniform increment of ambient dielectric constant in the gap region: $\int_0^w \varepsilon_0(\widetilde{E} - E)dx = \int_0^w \Delta\varepsilon_d \varepsilon_0 E dx$. The electric field is assumed to be constant in the gap region.

20. *Handbook of Optical Constants of Solids*, edited by E. D. Palik, (Academic, New York, 1998).

# CHAPTER 8 DETECTING CANCER CELLS USING SURFACE PLASMON RESONANCE SPECTROSCOPY AND FLUORESCENCE MICROSCOPY ON METAL FILMS AND METAL NANOSLIT ARRAYS

This chapter describes our preliminary results toward sensing cancer cells by using surface plasmon resonance based on metal nanoslit arrays. We have chemically modified the metal films and metal nanoslit arrays with DNA based aptamers. These modified metal films and nanoslit arrays are further shown to bind a specific kind of cancer cells. Analysis of the preliminary data obtained using fluorescence microscopy and surface plasmon resonance spectroscopy has shown that these nanoslit arrays have the potential for biological and chemical sensing.

## 8.1 INTRODUCTION

SPR is widely used in affinity biosensors for real-time analysis of biological agents.[1] The major developments in this technology have focused on improving its sensitivity and selectivity through chemical and biological modification of the metal films whose SPR is monitored.[2-8] SPR is used to measure competitive protein adsorption on biomaterials, the relative concentrations of blood proteins, for oligonucleotide based assays, and antibody-antigen assays, among others.[9-11] The SPR measurement usually involves bulky optics and high-precision mechanics for angular or wavelength interrogation of metal films in contact with analytes. As such, it is difficult to implement and automate the conventional SPR technique in compact instrumentation. But the recent breakthroughs in plasmonics that involve metallic nanostructures promise a better method for SPR sensing of biochemical agents. Plasmonic interactions in nanoaperture arrays offer new, rich phenomena that cannot be observed in microscale or macroscale metallic structures. The strong confinement and transmission of light in these subwavelength aperture arrays depend strongly on analyte species bound on the structures and provide high sensitivity detection of biological and chemical agents.[12-14] Modulation of the nanoaperture array's optical response by adsorbed analytes may offer improved sensitivity and selectivity over conventional surface plasmon resonance methods, which are widely used and commercialized for analysis in detecting biological and chemical agents.

The surface plasmons resonance in nanoaperture arrays involves funneling of light along the metal surface or strong optical confinement in the aperture region. The surface plasmon waves propagating along the aperture surfaces experience an accumulated effect in optical absorption along the resonance path, and these results in a strong attenuation of the optical transmission. Utilizing the lateral (in-plane) interaction has the effect of increasing the length of plasmonic interaction far beyond the thickness (normal to plane) of the adsorbed analytes. In addition, the dielectric constant change in the aperture area should sensitively modulate the near-field coupling between metal structures and thus the optical transmission. In conventional SPR, the index change at the planar metal/dielectric interfaces (air or substrate side) has a relatively minor effect on the spectral shift and intensity. In contrast, nanostructured arrays can be designed to operate in the strong near-field coupling regime and should be highly sensitive to refractive index changes. Further, the nanoaperture arrays are amenable to miniaturization and the development of centimeter scale devices that contain more than a million sensing elements. Therefore, there has been a growing interest in SPR sensing of biochemicals using a nanostructured metal layer, such as nanoparticle or nanohole arrays.[11,13,15-17,18]

We are interested in exploiting these gold and silver nano-slit arrays for biosensing purposes. The chemical modification of metal and semiconductor interfaces by self-assembled monolayers of organic molecules is an established method for controlling the chemical nature of a surface and adsorbing biological agents. A number of strategies for chemical modification are available, but the most common uses thiol bonds between the molecules and the substrate. Organic thiol molecules have been shown to spontaneously form compact molecular monolayers on metals (Au, Ag, Cu, stainless steel).We have used thiol chemistry for the chemical modification of these nano-slit arrays and shown that the transmission peak shifts on modification with alkanethiol due to change in the dielectric constant.[19] In this chapter I describe our initial efforts toward sensing of cancer cells on nano-slit arrays, by using similar chemistry as used by Herr et al[20] used on nanoparticles.

## 8.2 EXPERIMENTAL

_Materials_: Thin gold films were made using mica substrates as a template. Freshly cleaved ultrapure mica was placed into a thermal evaporation chamber. 99.99% pure gold foil was placed into a tungsten wire evaporation basket. The evaporation chamber pressure was reduced to 5 x

$10^{-6}$ Torr and 10 Amps of current was passed through the tungsten basket. When an optically opaque gold film was observed on the mica sheets, the current was turned off. Glass microscope cover slips were attached to the freshly deposited gold surface using epoxy (Expoy Technology # 337). The mica/gold/epoxy/glass sandwich structure was stored in a vacuum oven at $50^0$ C. Immediately before the SAM preparation, the glass and gold were lifted off of the mica substrate exposing the templated gold surface.

Nanoslit arrays were provided by Professor H.K. Kim's group at University of Pittsburgh.

DNA was bought from integrated DNA technologies, Inc. in a dithiol form(5'-/5ThiolMC6-D/TTT AAA ATA CCA GCT TAT TCA ATT AGT CAC ACT TAG AGT TCT AGC TGC TGC GCC GCC GGG AAA ATA CTG TAC GGA TAG ATA GTA AGT GCA ATC T-3'). Since the DNA sequences were received as disulfides, they were cleaved before using, resulting in a single thiol moiety terminating the sequence. To cleave the disulfide, the DNA was first dissolved in a 100 mM solution of DTT (dithioreitol) in 1 ml of 0.1 M $Na_3PO_4$ buffer (pH 8.3) for half an hour and then the small thiol fragments were removed by passing the solution through a sephadex G-50 column. The cell lines CCL-119 (acute lymphoblastic) and CRL-1596 (Burkitt's lymphoma) were bought from ATCC. The growth medium RPMI 1640 with 2 mM L-glutamine adjusted to contain 1.5 g/L sodium bicarbonate, 4.5 g/L glucose, 10 mM HEPES, and 1.0 mM sodium pyruvate, 90%; fetal bovine serum, 10% was used for cell culture. For cell culture the cells were suspended in flask and incubated, horitzontally, at $37^0$ C in a 5 % $CO_2$ in air atmosphere. The cell density was maintained at 2-3 x $10^5$ viable cells/ml. Calcein AM and ethidium bromide were purchased from Invitrogen for live-dead cell analysis and were used without further purification.

*Fluorescence Imaging:* An upright fluorescence microscope was used for fluorescence imaging (Model No. Olympus BX51W1). The upright fluorescence microscope is equipped with a vertical illuminator that contains a turret of absorption and emission filter cubes, and a mercury or xenon arc lamp housing. Light passes from the lamp through field and aperture diaphragms and into a cube that contains both excitation and emission filters and a dichroic mirror. After passing through the objective and being focused onto the specimen, the reflected excitation and secondary fluorescence are filtered upon return through the cube. The light is then routed to the eyepieces or detector.

*Transmission Spectroscopy:* Figure 8.1 shows the setup for collinear transmission spectrometer that was used for measurements. The sample is illuminated with white light source using multimode fiber (MMF) with 60 μm diameter. The transmitted signal is then collected using another multimode fiber (60 μm diameter) at the other end of the sample. The signal is then detected using an optical spectrum analyzer.

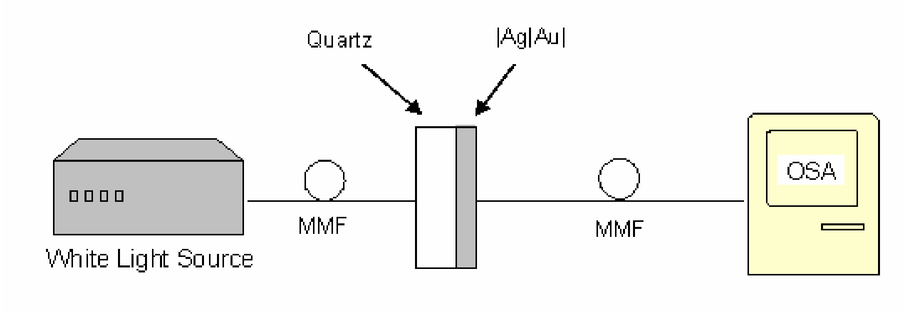

**Figure 8. 1** *Schematic representation of collinear transmission spectrometer.*

## 8.3 RESULTS AND DISCUSSION

Cell binding experiments were first done on thin gold films to develop the chemistry of cell binding before performing experiments with nanogratings. Thin Au films were incubated in 10 mM TRIS buffer solution of 88- base oligonucleotide for 5-6 hours. It has been shown by the tumor cell SELEX technique that this particular oligonucleotide/aptamer has very high specificity towards our leukemia cell line CCL-119. The aptamer folds into a unique three dimensional conformation with distinct biomolecular binding properties. The Au-films were then washed with 10 mM Tris(hydroxymethyl) amino methane (TRIS) buffer to remove any unbound oligonucleotide. In the meantime the CCRF-CEM cells were labeled with calcein-AM dye. Calcein AM dye (Calcein acetoxymethylester) is a non-fluorescent, cell permeant compound that is hydrolyzed by intracellular esterases into the fluorescent anion calcein and hence makes the cells fluorescent. The oligonucleotide coated Au films were then incubated with labeled CCL-119 cell for 30 minutes, and the samples were washed again with cell media to remove any kind of unbound cell. Fluorescence imaging was done to see the bound cells. Figure 8.2A shows a cartoon of the chemistry of cell binding and figure 8.2B shows the dye labeled CCL-119 cells bound to oligonucleotide coated Au films.

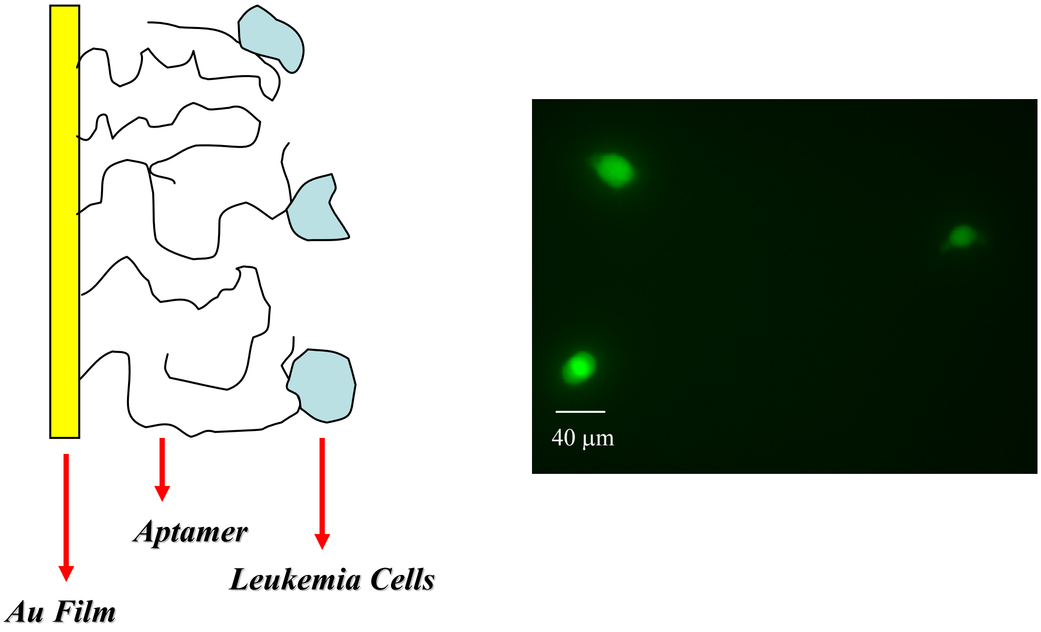

***Figure 8. 2 (A)*** Schematic representation of chemistry of cell binding on Au films. **(B)** Fluorescence image of calcein-AM labeled CCL-119 cells bound to DNA modified Au films.

In order to show that the binding between the CCL-119 cells and oligonucleotide is very specific, control experiments were done with CRL-1596. The same incubation procedure was used for CRL-1596 cells. Fluorescence imaging was done to seeny binding. Figure 8.3 shows the fluorescence imaging for CRL-1596 cells. No cells were seen under the fluorescence microscope indicating that CCRF-CEM bind specifically to the oligonucleotide.

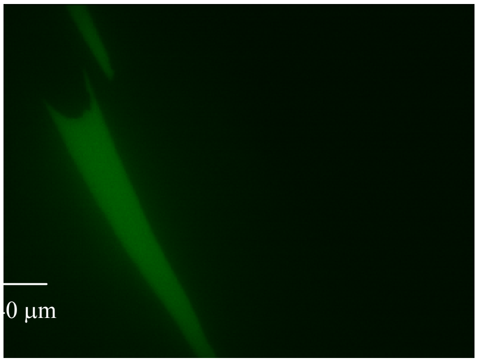

***Figure 8. 3*** *Fluorescence image of DNA coated Au films after 30 minute incubation with CRL-1596 cells.*

After establishing the chemistry on thin Au films experiments were done on nano-slit arrays. Since the thiol chemistry for Au and Ag is similar, Ag nano-slit arrays were used as they are easier to make. Figure 8.4 shows the SEM image of Ag nano-slit array structures which are supported on a quartz substrate. A holographic lithography technique was used to define the 1D grating patterns on Cr-coated quartz substrates. These nano-slit arrays were incubated in 10 mM TRIS buffer solution of 88- base oligonucleotide for 5-6 hours. The nano-slit arrays were then washed with 10 mM TRIS buffer to remove any unbound oligonucleotide. The transmission measurements' for nano-slit arrays were done both with and without the oligonucleotide bound to it. Figure 8.5 shows the transmission spectra of nano-slit array in the absence and presence of DNA. In the presence of 10 mM TRIS buffer the shape of transmission spectrum changes and shifts red; an effect that we attribute to a change in the dielectric constant above the film. The spectrum changed shape on further binding of the DNA oligonucleotide to the surface; it became slightly narrower and the bluer peak at 652 nm attenuated in intensity.

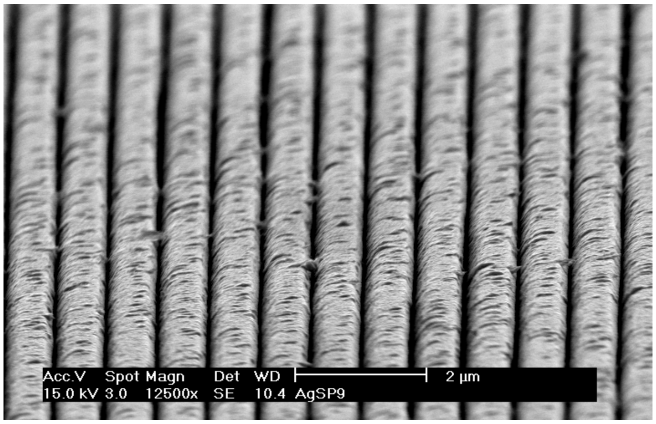

**Figure 8. 4** SEM image of Ag nano-slit arrya structures which are supported on a quartz substrate

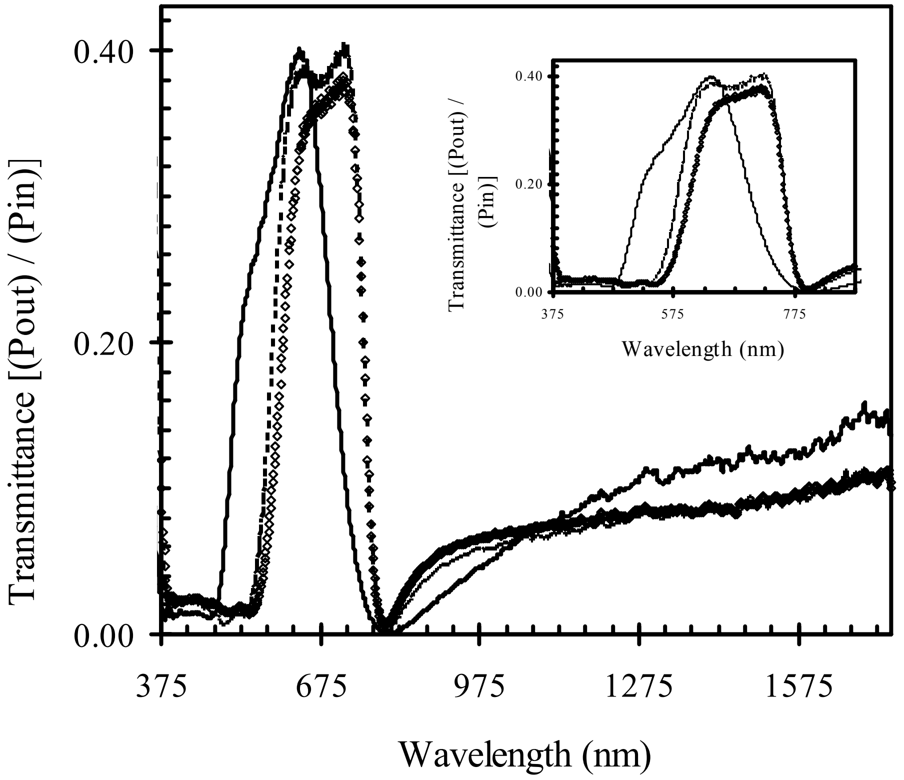

**Figure 8. 5** *Transmission spectra of Ag nano-slit array (—), in the presence of 10 mM TRIS buffer (----) and in the presence of DNA oligonucleotide (Δ).Inset shows the expanded transmission spectrum from 375 nm to 800 nm.*

A transmission spectrum was also measured on binding cells to the DNA modified nano-slit arrays. CCL-119 cells were used for binding since CRL-1596 cells do not bind to this particular DNA sequence as shown by fluorescence imaging studies discussed earlier. The transmission spectrum intensity decreased by nearly 50 % and the transmission maximum shifted by 6 nm indicating changes in the dielectric constant on incubating in cell medium (Figure 8.6). Control experiments were done where nano-slit arrays without DNA were incubated with CCl-119 cells, no changes in the transmission spectrum were seen for nano-slit arrays before and after incubating with cells indicating that cells bind to the DNA specifically.

Although these fluorescence microscopy and transmission spectroscopy provide some insight into the use of these nano-slit arrays for biosensing experimetns, a number of questions need to be answered. From the above studies the changes in the transmission spectrum on binding the CCL-119 cells are very small and the reason behind this is not clear. Therefore, a number of other experiments need to be performed to test the chemistry of cell binding. One such experiment is to have the incubating medium to be same at each step so that the effect on the transmission spectrum due to the incubating medium can be subtracted at each step. Right now we are using TRIS buffer as an incubating medium for oligonucleotide binding and RPMI-1640 for cell binding. We need to find a common medium for these two incubations. Another reason to get rid of RPMI-1640 medium is that it contains lot of other materials such as L-glutamine, sodium bicarbonate, glucose, HEPES, sodium pyruvate, fetal bovine serum etc. There might be some non-specific interactions that might change the transmission spectrum. But we need to be careful in choosing a medium for incubation so that it does not affect oligonucleotide and cell viability. Also we need to check the reproducibility of this chemistry by performing more experiments/trials few more times.

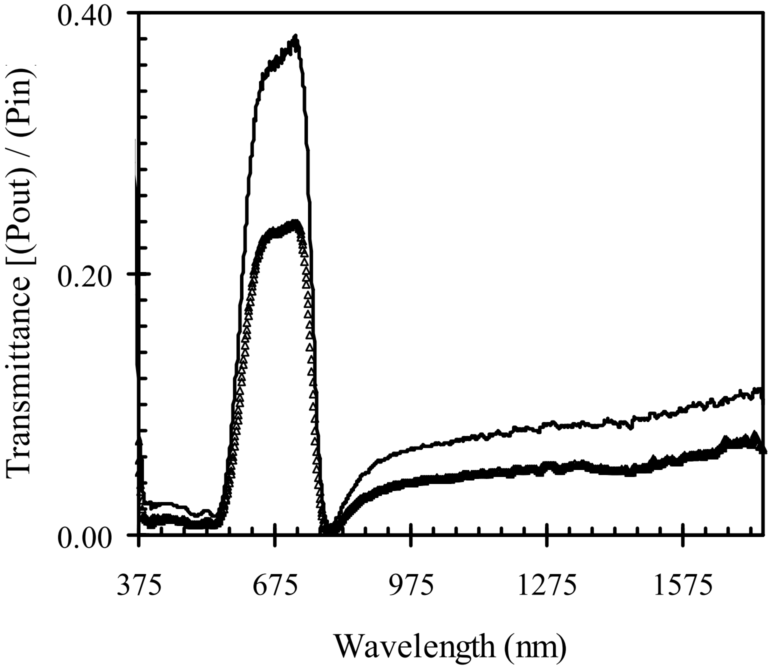

***Figure 8. 6*** *Transmission spectra of DNA coated Ag nano-slit array (----) and in the presence of CCL-119 cells (Δ).*

Studies are in progress and number of control experiments will be performed in near future to answer these questions. Further studies will be done with different systems such as antigen antibody interactions.

## 8.4 REFERENCES

(1) Homola, J.; Yee, S. S.; Gauglitz, G. *Sensors and Actuators B* **1999**, *3*, 54.

(2) Mu, Y.; Zhang, H.; Zhao, X.; Song, D.; Wang, Z.; Sun, J.; Li, M.; Jin, Q. *Sensors* **2001**, *1*, 91

(3) Su, X.; Wu, Y.-J.; Robelek, R.; Knoll, W. *Langmuir* **2005**, *21*, 348

(4) MVareiro, M. M. L. M.; Liu, J.; Knoll, W.; Zak, K.; Williams, D.; Jenkins, A. T. A. *Analytical Chemisrty* **2005**, *77*.

(5) Shumaker-Parry, J. S.; Zareie, M. H.; Aebersold, R.; Campbell, C. T. *Analytical Chemisrty* **2004**, *76*, 918

(6) Zhang, J.; Malicka, J.; Gryczynski, I.; Lakowicz, J. R. *J. Phys. Chem. B* **2005**, *109*, 7643.

(7) Ekgasit, S.; Stengel, G.; Knoll, W. *Analytical Chemisrty* **2004**, *76*, 4747.

(8) Potyrailo, R. A.; Conrad, R. C.; Ellington, A. D.; Hieftje, G. M. *Analytical Chemisrty* **1998**, *70*, 3419

(9) Haes, A. J.; Hall, W. P.; Chang, L.; Klein, W. L.; Van Duyne, R. P. *Nano Lett.* **2004**, *4*, 1029

(10) Alivisatos, P. *Nature Biotechnology* **2004**, *22*, 47.

(11) Malinsky, M. D.; Kelly, K. L.; Schatz, G. C.; Van Duyne, R. P. *J. Am. Chem. Soc.* **2001**, *13*, 1471.

(12) Bishop, Y. L.; Williams, L.; Blair, S.; Herron, J. *Nanotechnology* **2004**, *15*, 1368.

(13) Lahav, M.; Vaskevich, A.; Rubinstein, I. **Lahav, M.**

.

(14) barnes, W. L.; Dereux, A.; Ebbesen, T. W. *Nature* **2003**, *424*, 824.

(15) Riboh, J. C.; Haes, A. J.; McFarland, A. D.; Yonzon, C. R.; Van Duyne, R. P. *J. Phys. Chem. B* **2003**, *107*, 1772.

(16) Williams, S. M.; Stafford, A. D.; Rodriguez, K. R.; Rogers, T. M.; Coe, J. V. *J. Phys. Chem. B* **2003**, *107*, 11871.

(17) Brolo, A. G.; Gordon, R.; Leathem, B.; Kavanagh, K. L. *Langmuir* **2004**, *20*, 4813.

(18) Lahav, M.; Vaskevich, A.; Rubinstein, I. *Langmuir* **2004**
*20*, 7365

(19) Jung, Y. S.; Sun, Z.; Wuenschell, J.; Kim, H. K.; Kaur, P.; Wang, L.; Waldeck, D. H. *Appl. Phys Lett* **2006**, *88*, 243105.

(20) Herr, J. K.; Smith, J. E.; Medley, C. D.; Shangguan, D.; Tan, W. *Analytical Chemisrty* **2006**, *78*, 2918.

# CHAPTER 9 CONCLUSION

This thesis consists of two parts. The first part describes the work done on understanding the affect of different solution conditions and association with different macromolecules on optical properties of polyphenylethynylene (**PP1**) and polyphenylphenylene (**PP2**) based conjugated polyelectrolytes. Second part of the thesis investigates the chemical modification of metallic nanoaperture arrays and their potential for biochemical sensing using surface plasmon resonance.

Conjugated polymers are of great scientific interest because of their promise for applications. The photophysical studies performed on these polyelectrolytes has provided important insight in to the structural changes in different solution conditions. These studies are useful if the potential of these polyelectroytes in complex biological fluids are to be realized as biosensors since the optical properties are greatly affected by solution conditions.

The studies of polyphenylethynylene based anionic polyelectrolytes in dilute solutions in chapter 2 discusses how solvation and aggregation affects the optical properties of PP2. The studies show that the photophysical properties of polyphenylethynylene are very sensitive to electrolyte concentration and surfactants. The fluorescence intensity of PP2 decreased with increasing ionic strength of inorganic and organic salts, because of the formation of aggregates. If the aggregates and the unaggregated form have different sensitivities for the analyte, then the aggregation will need to be controlled for sensing applications.

Chapter 3 reports on the fluorescence properties of a polyphenylphenylene based polyelectrolyte and how they change with solution conditions and demonstrate its link to the polymer aggregation. The influence of simple ionic salts and ionic surfactants on the optical properties of poly[2,5-bis(3-sulfonatopropoxy)-1,4-phenylene-alt-1,4-phenylene)] (identified as **PP1**) and the oligomer **OPP1** were investigated. These studies showed that the **PP1's** fluorescence is initially enhanced on addition of ionic salts but that further increase in the ionic strength causes the emission intensity to decrease. These changes in fluorescence intensity are attributed to the formation of polymer aggregates, which results because of charge neutralization on the polymer strands by the counter ions, that have higher fluorescence quantum yields than the unaggregated polymer chains. These studies show that the solution properties (solvent, ionic strength and surfactant) control the spectral properties of the conjugated polyelectrolyte by changing the equilibria between aggregated and unaggregated forms of the polymer. Like the studies reported for **PP2** in chapter 2, these studies also have important implications, if these polylectrolytes are to be exploited for biosensing purpose.

Chapter 4 investigates the changes in optical properties of **PP2** by association with positively charged and neutral macromolecules, i.e. quencher. The studies showed that the change in fluorescence of **PP2** arises from a number of factors such as electrostatic, hydrophobic and energy transfer interactions with the quencher and also from changes in the solution conditions such as concentration and ionic strength. Further, the variation of **PP2**'s aggregation state is shown to affect the sensitivity of **PP2**. The **PP2** is most sensitive when it is in its unaggregated form. The Stern-Volmer constant is shown to decrease by a factor of ten on changing from independent strand to multi-strand aggregate.

Chapter 5 describes the fluorescence quenching mechanism for **PP2** in the presence of macromolecules, namely cytochrome-*c* and dendrimers (PAMAM 3G and DAB-4G). These studies show that fluorescence quenching of the dendrimer materials does not involve energy transfer or electron transfer, but is correlated to the overall charge on the dendrimer and its size. The quenching is hypothesized to result from conformational changes that occur upon binding the polyelectrolyte to the protein, or dendrimer. This mechanism is qualitatively different from that invoked for small molecule analytes.

Second part of the thesis investigates the chemical modification of metallic nanoaperture arrays and their potential for biochemical sensing using surface plasmon resonance. This metallic nanostructure-based SPR sensing is interesting since it can operate in the transmission configuration, thereby simplifying the optical arrangement and requiring small amounts of analyte. Chapter 7 demonstrates the optical transmission through metal nanoslit arrays involving surface plasmon resonances that occur at various sections of nanostructured metal surfaces. The chemical modification of metal surfaces with alkanethiol self-assembled monolayers causes a spectral shift in the main transmission peak of optical transmission by 11 nm red-shift. Analysis of the plasmonic fields and charge distributions show that the strong confinement of optical fields in the narrow slit region allows sensitive transduction of surface modification into a shift of surface plasmon resonance wavelength. Further, chapter 8 focuses on the preliminary results toward sensing cancer cells using surface plasmon resonance based on metal nanoslit arrays. Analysis of the preliminary data obtained using fluorescence microscopy and surface plasmon resonance spectroscopy has shown that these nanoslit arrays have the potential for biological and chemical sensing.

In summary this thesis consists of two parts. The first part focuses on the optical properties of PPE and PPP based conjugated polelectrolytes. The detailed investigation shows that the optical properties of these polyelectrolytes are greatly affected in the presence of inorganic and organic salts, as well as surfactants. Further, the quenching studies in the presence of macromolecules have shown that the quenching mechanism is controlled by different kind of interactions between the macromolecular analytes and the polyelectrolyte. This study demonstrates that in case of **PP2** electron transfer and electronic energy transfer need not be present to cause quenching but energy transfer plays an important role in fluorescence quenching in **PP1**. The second part of this thesis explores the optical transmission through nano slit arrays and the potential of these arrays for biosensing.